HELSINKI INSTITUTE OF PHYSICS INTERNAL REPORT SERIES

HIP-2008-03

NON-GAUSSIANITIES AND PREHEATING FROM N-FLATION AND MAGNETOGENESIS VIA ROTATING COSMIC STRING LOOPS

DIANA BATTEFELD

Helsinki Institute of Physics
University of Helsinki
Helsinki, Finland

ACADEMIC DISSERTATION
To be presented, with the permission of the Faculty of Science of the University of Helsinki, for public criticism in the Auditorium (E204) of Physicum, Gustaf Hällströmin katu 2a, on the 5th of August 2008 at 12 O'Clock.

Helsinki 2008

To Willie (1917-2002) and Dennis (1947-2005)

ISBN 987-952-10-3718-4 (printed version)
ISSN 1455-0563
ISBN 987-952-10-3719-1 (pdf version)
http://ethesis.helsinki.fi
Yliopistopaino
Helsinki 2008

Acknowledgments

First and foremost, I would like to thank Kari Enqvist, who has been the best supervisor I could have wished for – I could not have landed in better hands and in a better place. Special thanks go to UniverseNet for this amazing fellowship which has given me the freedom to explore new avenues, choose my collaborators and work at my own pace.

I am also grateful to my collaborators Thorsten Battefeld, Shinsuke Kawai, Daniel Wesley, Mark Wyman, as well as the many people who provided suggestions and comments, such as Richard Easther, who advised me during the early stages of my project on Preheating in $\mathcal{N}$-flation.

I would also like to thank Anne Davis for support at Cambridge University, where the first two papers were written and Paul Steinhardt for hospitality at Princeton University where this thesis was written, the readers Martin Sloth and Iiro Vilja for reading this manuscript carefully and providing me with useful comments and suggestions, everyone at HIP, who have shown me nothing but kindness, Sami Nurmi and Niko Jokela for being so kind to share with me the template for this thesis, my office-mate Matti Kortelainen for having the patience to answer my questions regarding Finnish living, Shinsuke Kawai for his friendship, the secretaries, Paivi Lehto and Taina Harden for being ever so helpful.

And most importantly, I am especially grateful to Thorsten Battefeld, for invaluable feedback and relentless support.

This work was supported by the EU FP6 Marie Curie Research and Training Network "UniverseNet" (MRTN-CT-2006-035863).
Helsinki, August 2008

Diana Battefeld

D. Battefeld: Non-Gaussianities and Preheating from N-flation and magnetogenesis from rotating cosmic string loops, University of Helsinki, 2008, 125 p., Helsinki Institute of Physics Internal Report Series, HIP-2008-03, ISBN 987-952-10-3718-4 (printed version), ISSN 1455-0563, ISBN 987-952-10-3719-1 (pdf version).
INSPEC classification: A9880D, A9880B, A9870V
Keywords: cosmology, early universe, inflation, preheating, non-gaussianity, cosmic strings, magnetogenesis

Abstract

In this thesis we examine multi-field inflationary models of the early universe and compute deviations from a Gaussian spectrum of primordial perturbations by extending the δN-formalism. Non-Gaussianities (NG) offer a testbed to discriminate between models in upcoming observations. We focus on $\mathcal{N}$-flation, a specific type of assisted inflation motivated by string theory, and find that these models are generically indistinguishable with regards to non-Gaussianities as long as the slow roll approximation remains valid. In $\mathcal{N}$-flation NG are suppressed even after the slow roll conditions are violated.

Due to the challenges faced by existing single field models of inflation we are motivated to investigate further multi-field scenarios. Since the theory of preheating is not fully developed in the latter models, we examine quantitatively Cantor preheating, a generic multi-field preheating setup, again within the framework of $\mathcal{N}$-flation. By numerical and semi-analytic analysis we find that preheating via parametric resonance is suppressed, indicating that it is the old theory of preheating that is applicable.

We then shift gears and propose a mechanism to generate primordial magnetic fields via rotating cosmic strings loops. Magnetic fields in the μG range have been observed in galaxies and clusters. Yet, the evolution and especially the origin of primordial magnetic fields is an area of research that has baffled scientists for more than half a century. Though, as of today, cosmic strings have not been observed, they arise in many models of the early universe, for instance after brane inflation. Considering a network of strings, we find that rotating cosmic string loops, which are continuously produced in these networks, provide viable candidates to produce magnetic fields with relevant strength and lengths on galactic scales, as long as we assume reasonable high string tension (still within observational bounds) and also an efficient dynamo, as advocated by some authors.

Contents

List of publications

The articles included in this thesis are:

[1] D. Battefeld, T. Battefeld,
"Non-Gaussianities in N-flation," JCAP **0705**, 012 (2007) [arXiv:hep-th/0703012].

[2] D. Battefeld, T. Battefeld, D. H. Wesley and M. Wyman,
"Magnetogenesis from Cosmic String Loops," JCAP **0802**, 001 (2008) arXiv:0708.2901 [astro-ph].

[3] D. Battefeld, S. Kawai,
"Preheating after N-flation," Phys. Rev. D **77**, 123507, (2008) arXiv:0803.0321 [astro-ph].

Author's contribution

[1] This study is a direct application of [4], where the formalism for computing non-Gaussianities in multi-field models of inflation was developed. All analytic work was done in close collaboration with T.B. We made daily comparisons of results. T. B. wrote the first version of the draft, to which I contributed.

[2] Besides doing graduate work in physics at Brown University's Physics Department, I also carried out independent research on the origin of the Earth's magnetic field at Brown University's department of Geological Sciences. While working on this project I became intrigued by cosmological magnetic fields and their amplification through dynamos, which led me to investigate possible origins of primordial seed fields. This turned into a collaboration with Thorsten Battefeld who conversed with Stephon Alexander (University of Pennsylvania) about the possibility of sourcing vorticities and subsequently magnetic fields via cosmic strings. We quickly involved Mark Wyman due to his expertise in String Networks. T.B. and myself worked out the first analytic models and wrote the first draft, after which Daniel Wesley joined the collaboration at Cambridge. All further analytic work in the paper, except string network models, were done in close collaboration between myself and T.B. These include loop dynamics, gravitational dragging of a plasma by cosmic strings and loops, dynamo amplification, magnetogenesis via the Harrison-Reese mechanism, etc. All numerical work

(developing of novel code in C++), string network models, and plots are due to Mark Wyman and Daniel Wesley, who also contributed to the editing.

[3] This work was instigated initially by myself after repeated conversations with Richard Easther. All analytic and Maple computations were done by the author of this thesis. Numerical routines using Mathematica were developed by Shinsuke Kawai, who also provided the plots and contributed to the editing.

In all papers authors are listed alphabetically according to the particle physics convention.

Chapter 1

Introduction

Our current understanding of the early universe is primarily due to the study of the nearly scale invariant spectrum of primordial perturbations as observed in the temperature fluctuations of the cosmic background radiation (CMBR) or large scale structure (LSS). Since most simple models of inflation predict quasi scale invariant, nearly Gaussian perturbations, in the advent of improved observational constraints, any deviation from non-Gaussianity affords a test-bed to make a clear cut distinction between models. Hence non-Gaussianity is at present one of the most important tests to discriminate between models of inflation.

However, there may be other non-perturbative effects which differentiate between models, such as the presence of cosmic strings. If observed, cosmic strings may act as discriminators, since their properties depend on their origin. Further, the presence of string networks might help explain puzzles of the late universe, such as the presence of large scale magnetic fields in the micro-Gauss range.

The content of this thesis is entirely devoted to two distinct, major subject areas spanning three papers [1–3]: the first one comprises non-Gaussianities and reheating from $\mathcal{N}$-flation [1,3], a concrete model of multi-field inflation[1]. Our motivation is that in order to discriminate between models of the early universe, and ultimately confront them with high precision experiments, it is necessary to theoretically extract observable quantities such as the non linearity parameters characterizing non-Gaussianities. After estimating parameters characterizing the bi- and trispectrum in the horizon crossing approximation, we focus on the non-linearity parameter f_{NL}, a measure of the bispectrum; we compute its magnitude for narrow and broad spreads of masses, including the evolution of modes after horizon crossing. We identify addi-

[1]In this realization of assisted inflation, the masses of the many inflaton fields conform to a known distribution, meaning, the *mass spectrum* is known.

tional contributions due to this evolution and show that they are suppressed as long as the fields evolve slowly. This renders $\mathcal{N}$-flation indistinguishable from simple single-field models in this regime. Larger non-Gaussianities are expected to arise for fields that start to evolve faster. However, we show that such fast roll during inflation is not expected in $\mathcal{N}$-flation, leaving (p)reheating as the prevailing candidate for generating non-Gaussianities. Also within the framework of multi-field inflation, and again taking $\mathcal{N}$-flation as a case study, we investigate preheating. The goal here is to attain a thorough quantitative theory for multi-field preheating, a subject which has not been widely explored in the literature.

The second major topic concerns the generation of magnetic seed fields [2] needed in order to account for large-scale coherent magnetic fields that are observed in galaxies and clusters. We propose a mechanism whereby large vortices are created in cosmic string networks due to the presence of rotating string loops. These vortices cause magnetic fields through the Harrison-Rees mechanism. We present numerical results obtained by evolving semi-analytic models of string networks (including both the one-scale and the velocity-dependent one-scale model) in a ΛCDM cosmology, including the forces and torques on loops from Hubble redshifting, dynamical friction, and gravitational wave emission. Our predictions include the magnetic field strength as a function of correlation length, as well as the volume covered by magnetic fields. We conclude that string networks could account for magnetic fields on galactic scales, but only if coupled with an efficient dynamo amplification mechanism.

The concrete outline of this thesis is as follows: firstly, we give a detailed introduction to various aspects of cosmology that are needed to comprehend the articles [1–3]. We start by introducing the big bang cosmology and outlining its inherent problems (section 1.2). Some of these are alleviated by inflation (section 1.3), which we present in some detail. Within the framework of scalar field driven inflation we briefly outline the theory of cosmological perturbations and the δN formalism (section 1.4.1), followed by a list of problems encountered in single field inflation. We conclude our review of single field models by an account of preheating (section 1.4.3), a preamble for multi-field preheating discussed in section 1.5 and chapter 4; we continue with a discussion of multi-field inflation, including perturbations with a special focus on non-Gaussianities (section 1.5.1). As a concrete multi-field model we consider assisted inflation and its realization in $\mathcal{N}$-flation. We conclude our introduction to multi-field inflation with a summary of the qualitative aspects of preheating, a prelude for chapter 4. We then shift our attention to cosmic strings and loops (section 1.6), their origin, evolution, and effect on a primordial plasma. Finally, we discuss magnetic fields (chapter 1.7), possible

origins and subsequent evolution hitherto current observation, serving as an exposition needed in chapter 5. Closing the introduction, we enter the main part of the thesis which is comprised of original work that has been published in [1–3].

In chapter 2 we examine a certain class of multi-field inflationary models, focusing on N-flation, a model that employs the many axion fields of string theory as inflatons, providing an implementation of assisted inflation. Guided by the hope of distinguishing these models from simple single field ones, we compute non-Gaussian signatures. For later comparison, we first compute analytically the non-Gaussianities using slow roll and the horizon crossing approximation. We then move a step up and compute non-Gaussianities beyond the horizon crossing approximation by studying two cases: narrow mass spectra and general mass spectra, including broad ones. Observational limits on non-Gaussianities will improve considerably in imminent experiments. However, for the model studied here, our results show that the existence of a signal that is strong enough to be observed is not feasible is not feasible during slow roll.

In chapter 3, we comment on the feasibility of non-Gaussianities after the slow roll conditions are violated. However, within the framework of $\mathcal{N}$-flation, the fields evolve even slower than during slow roll, so that non-Gaussianities remain suppressed.

In chapter 4 we investigate preheating in multi-field inflationary models, with $\mathcal{N}$-flation as its focus. We use the slow roll approximation to set the initial state for preheating, and provide numerical results on Cantor Preheating [2]. Based upon these results, we comment on the efficiency of multi-field preheating as compared to non-perturbative preheating in single field models.

Finally in chapter 5 we provide a mechanism to generate primordial magnetic fields in galaxies via rotating cosmic string loops that stir up the plasma. We first develop an analytic model of loop dynamics, including translational and rotational movement as well as changes in loop size. We then give an analytic derivation of how the rotating cosmic string loops generate vortical flows in the primordial plasma as well as an analytic estimate of the expected magnetic field strength near decoupling. These analytical findings are accompanied by a numerical code which enables us to predict not only the magnetic field strength at a given length scale, but also what fraction of the horizon is imbued with such fields.

We conclude with a brief summary and outlook in chapter 6.

[2]Cantor Preheating is the generic type of preheating when more than one inflaton field contributes to the effective mass of a matter field.

1.1 Notation

The default units employed throughout this work are known as *fundamental* or *natural* units where $\hbar = c = 1$. In addition, we set the reduced Planck mass $m_{pl}^{-2} = 8\pi G \equiv 1$ in most of the text, with the exception of sections on string networks and magnetogenesis where we keep G explicit. Throughout we adopt the following notation: spacetime indices are denoted by Greek letters and run through the four values $0, 1, 2, 3$. Spatial indices are denoted by Latin letters and run through the three values $1, 2, 3$ (or x, y, z). Capital Latin indices $(I, J, K, \dots)$ indicate fields in multi-field inflation. Implicit summation over repeated indices is assumed, unless stated otherwise. A semicolon indicates the covariant derivative.

1.2 Big-Bang Cosmology

The standard model of the early universe can be traced back to two seminal observations: galaxies are receding faster the further away they are, indicating an expanding universe, and the cosmic microwave background radiation (CMBR) is highly homogeneous and isotropic.

The first observation of the velocity recession is due to Hubble (1929) [5], who found that redshifts of galaxies, and thus their velocity, are roughly proportional to their distance from us

$$v = Hr\,. \tag{1.1}$$

Here H is the Hubble parameter, usually written as

$$H = 100\,h\,\mathrm{km\,s^{-1}\,Mpc^{-1}}\,. \tag{1.2}$$

This observation put an end to static models of the Universe, replacing them by an expanding model starting from a "big bang" about 13.4×10^{12} years ago [6]. Naturally this observation has been improved over the years, leading to the current estimate of the Hubble parameter of [6]

$$h \simeq 0.732^{+0.031}_{-0.032}\,. \tag{1.3}$$

Furthermore, recent observations of type IA supernovae show that the universe is not only expanding, but the expansion is speeding up [7, 8]; this acceleration is attributed to dark energy, a form of energy with negative equation of state, or a cosmological constant.

The other unprecedented observation is the one of the CMBR, first performed by Penzias and Wilson in 1965 [9]; this radiation has a very accurate

blackbody spectrum with a temperature of $2.726K$ [10], indicating that the universe was very homogeneous and isotropic in its youth. To be precise, the CMBR is composed of the redshifted photons that were emitted when the universe was dense and hot and just became transparent to photons around 300 000 years after the big bang. This relic radiation was theoretically predicted by Alpher and Gamov in 1948 [11], but no one at the time envisioned that it could be detected. The observation of the CMBR is a strong indicator for the validity of the cosmological principle: the universe is homogeneous and isotropic on large scales, namely it looks the same in every direction from every point in space. Further evidence for the homogeneity and isotropy of the universe on largest scales originates from measurements of the large scale structure, such as by the Sloan Digital Sky Survey SDSS [12] or the 2dF survey [13] among others. Of course, the primary motivation for these experiments is the detection of deviations from homogeneity, which opens up a window into the very early universe.

Based on the cosmological principle, the line element in general relativity can then be written in the simple Friedmann-Robertson-Walker (FRW) form

$$ds^2 = dt^2 - a^2(t)dx^2\,, \tag{1.4}$$

where t is the physical time, $a(t)$ is the scale factor, and dx^2 is the line element on a three-dimensional space of constant curvature. In spherical coordinates, this metric can be written as

$$dx^2 = \frac{dr^2}{1-kr^2} + r^2(d\theta^2 + \sin^2\theta d\phi^2)\,, \tag{1.5}$$

where k is the curvature constant that determines the spatial topology of the universe, giving a universe that is closed, flat or open for $k > 0$, $k = 0$, and $k < 0$, respectively.

The scale factor in the metric (1.4) obeys Einstein's equations

$$R_{\mu\nu} - \frac{1}{2}g_{\mu\nu}R = 8\pi G T_{\mu\nu}\,, \tag{1.6}$$

which relates the Ricci tensor $R_{\mu\nu}$, and the Ricci scalar R to the matter content with energy momentum tensor $T_{\mu\nu}$. If the latter takes the form of a perfect fluid (without anisotropic stress) it has the same symmetries as the homogeneous FRW-metric (1.4) and can be written as

$$T_{\mu\nu} = (\rho + p)u_\mu u_\nu - p g_{\mu\nu}\,, \tag{1.7}$$

where the energy density ρ and the pressure p are functions of time t only, and u^μ is the four velocity of the comoving matter, namely, $u^0 = 1$ and

$u^i = 0$. Local energy conservation $T^{\mu\nu}_{;\nu} = 0$ implies,

$$\dot{\rho} + 3\frac{\dot{a}}{a}(\rho + p) = 0\,, \tag{1.8}$$

as the universe expands. The second term accounts for the dilution of the energy density, whereas the third represents the work done by the pressure of the fluid. In simple cases the energy density and pressure can be related by a constant $p = w\rho$ where w is the equation of state parameter ($w = 0$ for dust or non relativistic matter, $w = 1/3$ for radiation, or relativistic matter, and $w = -1$ for a cosmological constant). Then it follows from (1.8)

$$\rho \propto a^{-3(1+w)}\,. \tag{1.9}$$

Hence, it is evident that although in the past our universe was dominated by radiation, at some point dust appropriated because $\rho_m/\rho_r \propto a$, and even later dark energy ultimately took over, since $w_{de} \sim -1$ so that $\rho_{de} \sim$ const.

Given the FRW metric and an ideal fluid, the Einstein equations can be simplified to the Friedman equations

$$\left(\frac{\dot{a}}{a}\right)^2 = \frac{\rho}{3} - \frac{k}{a^2}\,, \tag{1.10}$$

$$3\frac{\ddot{a}}{a} = -\frac{1}{2}\left(\rho + 3p\right)\,, \tag{1.11}$$

where the Hubble parameter is identified as $H = \dot{a}/a$. It is customary to call H^{-1} the Hubble radius, Hubble horizon or just horizon [3]. From the second equation, which follows from the derivative of the first one in case $H \neq 0$, it is evident that $w < -1/3$ is needed in an accelerating universe such as ours. If the equation of state parameter is constant and $k = 0$, (1.10) is solved by

$$a = a_0 t^{2/(3+3w)}\,. \tag{1.12}$$

There is exactly one (time dependent) density for which the universe appears to be flat (see (1.10)), $\rho_{crit} \equiv 3H^2$. It is customary to define the dimensionless density parameter for each energy constituent

$$\Omega_i = \frac{\rho_i}{\rho_{crit}}\,, \tag{1.13}$$

so that a total density parameter is $\Omega_{total} = \sum_i \Omega_i$. For $\Omega_{total} < 1$, $\Omega_{total} = 1$, or $\Omega_{total} > 1$ we have an open, flat or closed universe respectively. Since $\Omega_{total} - 1 = k/(a^2H^2)$, any small deviation of Ω_{total} from one will increase in an expanding universe if $w > -1/3$. Current observations place Ω_{total} close to unity [6].

[3] The Hubble horizon should not be confused with the causal horizon.

1.2.1 Problems

The big-bang cosmology described above explains the Hubble expansion and the cosmic background radiation. In addition, the abundances of light elements can be computed [11] and they agree to high accuracy with observations. Thus, this model provides a successful description of the evolution of the universe back to a fraction of a second after its birth. However, if we extrapolate to the time $t = 0$ we encounter several inexplicable problems:

- *The horizon problem*: a main assumption above is the large scale homogeneity and isotropy of the universe. This is in agreement with the cosmic background radiation, whose temperature, if measured in two different patches of the sky, say opposite to each other, is the same to within at least one part in 10^4. The problem is that these patches have never been in causal contact in the standard big-bang model. Thus one has to assume that the universe was originally highly homogeneous and isotropic on scales larger than the causal horizon, indicating a high degree of fine-tuning.

- *The flatness problem*: the present density of the universe is close to the critical density, that is $\Omega_{total} \sim 1$. Nevertheless, deviations from $\Omega_{total} = 1$ grow in time. In order to have $\Omega_{total} \sim 1$ today, it must have been extremely close to one in the early universe, indicating another fine-tuning.

- *The density fluctuation problem*: today, we know that present day structure in the universe originated from small density fluctuations in the early universe. The statistical properties of these fluctuations cannot be accounted for by, for instance, thermal fluctuations in the big-bang model.

- *The exotic relics problem*: topological defects, exotic particles and black holes should be created during phase transitions in the early universe. One example is the overproduction of monopoles as predicted by grand unified theories. These remnants are not observed.

- *The initial singularity problem*: if we go back in time, we reach a singularity where density, curvature and temperature become infinite. General relativity is not reliable once Planckian densities are within reach, and a theory of quantum gravity, that is string theory, should be invoked.

Other problems include *the cosmological constant problem* (why is its value so small?), *the baryon asymmetry problem* (why do we have more matter than antimatter?) or the *the dark matter problem* (what is dark matter?). Some of these problems can be resolved by the inflationary paradigm according to which the universe goes through a period of rapid expansion during its early stages.

1.3 Inflation

In the previous section we outlined the successes and shortcomings of big-bang cosmology. Inflation was first conceived by Guth [14] to rid the hot big bang model from the monopole problem, but it was soon realized that the horizon and flatness problems could also be addressed. Furthermore, inflation makes concrete predictions for the statistical properties of perturbation, in agreement with recent observations.

The inflationary stage of the early universe begins about 10^{-35} seconds after its birth and lasts until about 10^{-32} seconds. During this time, the universe is in an unstable vacuum-like state at high energy density leading to an exponential[4] expansion of space

$$a \sim e^{H_{inf} t_{inf}} \,, \tag{1.14}$$

where t_{inf} is the duration of the inflationary phase and H_{inf} sets the energy scale of inflation. This implies that regions that were initially within the causal horizon blow up to sizes much larger than the present Hubble horizon. This solves the horizon problem if the expansion lasted for about 60 e-folds or more. Furthermore, the initial curvature radius of the universe increases by a large factor so the universe becomes locally indistinguishable from a flat one with $\rho = \rho_{crit}$.

During inflation any matter content is diluted, so the universe is empty and cold at the end of inflation. Thus, directly after inflation there needs to be a phase of reheating, whereby the energy driving inflation is to some extent converted into relativistic matter.

In the following sections, we give a brief account of inflation driven by a single scalar field, including reheating, which will serve as a basis for more complex multi-field models. See also [15–18] for reviews.

[4]Note the possibility of non-exponential inflation such as power law inflation.

1.4 Single-Field Inflation

Consider a scalar field with a canonical kinetic term so that the action takes the form

$$S = \frac{1}{2}\int d^4x\sqrt{-g}\left(\frac{1}{2}\partial^\mu\varphi\partial_\mu\varphi + V(\varphi)\right). \tag{1.15}$$

Variation with respect to the metric leads to the energy momentum tensor of an ideal fluid; assuming homogeneity we obtain

$$\rho_\varphi = \frac{1}{2}\dot{\varphi}^2 + V(\varphi) \tag{1.16}$$

$$p_\varphi = \frac{1}{2}\dot{\varphi}^2 - V(\varphi). \tag{1.17}$$

Variation of the action with respect to the homogeneous φ yields the Klein Gordon equation

$$\ddot{\varphi} + 3H\dot{\varphi} + V' = 0, \tag{1.18}$$

where a prime denotes a derivative with respect to the inflaton. This needs to be solved in conjunction with the Friedman equations (1.10) and (1.11) (for simplicity we consider a flat universe without any other energy sources, except the scalar field)

$$H^2 = \frac{1}{3}\left(V + \frac{1}{2}\dot{\varphi}^2\right), \tag{1.19}$$

$$\dot{H} = -\frac{1}{2}\dot{\varphi}^2. \tag{1.20}$$

Inflation occurs when the inflaton field evolves slowly $\dot{\varphi}^2 \ll V$. This is the case if the slow roll parameters

$$\varepsilon \equiv \frac{1}{2}\left(\frac{V'}{V}\right)^2, \tag{1.21}$$

$$\eta \equiv \frac{V''}{V}, \tag{1.22}$$

satisfy $\varepsilon \ll 1$, $|\eta| \ll 1$ [5]. Then the equations of motion become

$$H^2 \simeq \frac{V}{3}, \tag{1.23}$$

$$3H\dot{\varphi} \simeq -V'. \tag{1.24}$$

[5]The SR conditions are sufficient but not necessary for inflation to occur.

Thus the number of e-folds of inflation becomes

$$N \equiv \int_t^{t_{end}} H\, dt \tag{1.25}$$

$$\simeq \int_{\varphi_{end}}^{\varphi} \frac{V}{V'}\, d\varphi. \tag{1.26}$$

For instance, for a simple polynomial potential $V = \lambda\varphi^\alpha$ we get $N \simeq (\varphi^2 - \varphi_{end}^2)/2\alpha$. Inflation ends when the slow roll parameters become of order one, which occurs around $\varphi_{end} \sim \alpha$. Thus we see that we need super-Planckian initial field values to achieve the desired 60 e-folds of inflation. In this case we may then approximate $N \approx \varphi^2/2\alpha$.

The need for super-Planckian field values is a generic feature of single field inflationary models, and indeed problematic from a field theoretic point of view: if the inflaton is to be identified with some fundamental field in e.g. supergravity, we expect corrections to the Lagrangian whenever the field traverses a super-Planckian stretch in field space. This problem can be alleviated in multi-field models, as we shall see later.

Inflation with a simple quadratic potential ($\alpha = 2$ and $\lambda \equiv m^2/2$) is known as *chaotic inflation* (in [19] only $\lambda\varphi^4$ was considered, but potentials have been subsequently generalized; given that $\lambda\varphi^4$ potentials are excluded by current observations of the CMBR, it is customary to associate chaotic inflation via $m^2\varphi^2$ potentials): if the inflaton field is high up in its potential, quantum fluctuations can dominate over the classical force from the potential $\propto V'$. Due to the possibility of fluctuating up in the potential, most of the universe is eternally inflating [6] and only occasionally bubbles with a smaller value of the inflaton will form. Within those bubbles, the inflaton is then slowly rolling downhill. In this picture, our observable universe is enclosed in one single bubble. This differs from the erstwhile historical inflationary models, which were based on a first order phase transition; these models were hampered by the necessity of bubble nucleation which could not provide an observable universe resembling ours.

1.4.1 Perturbations and the δN-formalism

So far, we have been concerned with the homogeneous part of the inflaton. However, during inflation quantum fluctuations are constantly being seeded

[6] It is problematic to define a measure in eternal inflation, meaning, statements like "most of the universe" are ill-defined. More accurately, there are regions which continue to inflate, and since the inflaton is high up in its potential, these regions will inflate more than others.

at small scales. These fluctuations get stretched during inflation to super-horizon scales, at which point they freeze, up until they re-enter the Hubble horizon at later stages. As a result, the statistical properties of the fluctuations in the CMBR can be computed by means of cosmological perturbation theory from first principles, see [17, 20] for reviews.

The computation is complicated by the necessity of accounting not only for the perturbations in the inflaton $\delta\varphi(\mathbf{x}, t)$, but also in the gravitational sector, that is, perturbations in the metric [20]. The perturbation of the latter can be decomposed into scalar, vector and tensor degrees of freedom, which decouple at the linear level. Focussing on the scalar sector there are four degrees of freedom,

$$ds^2 = (1+2\phi)dt^2 + 2a\partial_i B dx^i dt - a^2\left((1-2\psi)\delta_{ij} + 2\partial_{ij}E\right)dx^i dx^j\,. \quad (1.27)$$

Two of these can be eliminated by a gauge transformation, for instance E and B if we choose the longitudinal gauge; the remaining two degrees of freedom are the two (gauge invariant) Bardeen potentials $\Phi = \phi$ and $\Psi = \psi$. In the absence of anisotropic stress, they are related via the i-j-Einstein equation resulting in $\Phi = \Psi$. Further, the 0-0 equation relates the perturbation in the metric to the perturbation in the inflaton field, so that only one degree of freedom remains, which can be straightforwardly quantized and evolved in time [20].

At the end of the day, we are interested in the curvature perturbation[7] on uniform density surfaces [21]

$$-\zeta \;\equiv\; \psi + \frac{H}{\dot\rho}\delta\rho\,. \quad (1.28)$$

The usage of this variable is advantageous, since it is constant on super horizon scales (at least in simple models); that is, after horizon crossing when $k = aH$, where k is the comoving wavenumber[8]. A further commonly used variable is the curvature perturbation on hypersurfaces orthogonal to comoving worldlines [20], or short comoving curvature perturbation

$$\mathcal{R} = \frac{2}{3}\frac{H^{-1}\dot\Phi + \Phi}{1+w} + \Phi\,, \quad (1.29)$$

which is identical to $-\zeta$ on large scales [17][9]. Since we are primarily interested

[7] Physically the curvature perturbation is responsible for temperature fluctuations that are observed in the CMBR.

[8] To be precise, ζ is constant in the absence of isocurvature perturbations, which will become important when we discuss multi-field inflationary models.

[9] On large scales and for single field inflation we may use $-\zeta \approx \mathcal{R} = \psi + \frac{H}{\dot\varphi}\delta\varphi$. Note that in [20], $\mathcal{R}$ is denoted by ζ.

in Fourier modes leaving the horizon early during inflation, we can readily switch between the two whenever needed.

Statistical information about primordial perturbations can be extracted from correlation functions of the temperature fluctuations in the CMBR. Thus, the correlation functions of ζ, or $\mathcal{R}$, are of prime interest. We can efficiently compute these correlation functions by means of the δN-formalism, which is based on the simple realization that ζ is identical to the perturbation in the local expansion rate, that is

$$\begin{aligned} \zeta(\mathbf{x}, t) &= \delta N & (1.30) \\ &= \frac{\partial N}{\partial \varphi} \delta\varphi & (1.31) \end{aligned}$$

where N is the number of e-folds from (2.39). To evaluate N one has to consider an initially flat hypersurface as well as a final uniform density hypersurface [22]. The linear formalism goes back to Starobinsky [23] and was extended by Sasaki and Stewart [22] among others [24–26]. It is then straightforward to compute the two point correlation function commonly denoted as the power-spectrum $\mathcal{P}_\zeta$, ($\langle \zeta_{\mathbf{k}_1}, \zeta_{\mathbf{k}_2} \rangle = (2\pi)^3 \delta(\mathbf{k}_1 + \mathbf{k}_2) \mathcal{P}_\zeta$), and extract observables such as the scalar spectral index $n_s \equiv \partial \ln \mathcal{P}_\zeta / d \ln k$. Higher order correlation functions, characterizing non-Gaussianities (NG), can be evaluated by the non linear δN-formalism put forward in [27, 28]. Here ζ is still conserved on large scales in simple models [29, 30][10]. We will discuss non-Gaussianities in more detail after introducing multi-field inflation, where the advantages of this technique will become apparent.

Back to single field slow roll inflation, the resulting spectral index reads [31]

$$n_s - 1 = -6\varepsilon + 2\eta \,. \tag{1.32}$$

Considering again the case of a polynomial potential $V \propto \varphi^\alpha$ we have $\varepsilon = \alpha^2/2\varphi^2$ and $\eta = \alpha(\alpha - 1)/\varphi^2$. Since $N \approx \varphi^2/2\alpha$ we can express the spectral index as

$$n_s - 1 = -\frac{\alpha + 2}{2N} \,, \tag{1.33}$$

that is we get a slightly red spectrum. Chaotic inflation with $\alpha = 2$ is thus still in agreement with recent observations of the CMBR $n_s^{obs} = 0.958 \pm 0.016$ [6].

[10] The separate Universe formalism developed by Rigopoulos and Shellard in e.g. [30] is equivalent to the δN-formalism.

The overall magnitude of the temperature fluctuation, commonly referred to as the COBE (Cosmic Background Explorer) normalization [10], sets the overall scale of single field inflation. To be precise, the density contrast $\delta_H^2 \equiv (4/25)\mathcal{P}_\zeta$ at the pivot scale $k_{pivot} \equiv 7.5 a_0 H_0$ is $\delta_H(k_{pivot}) = 1.91 \times 10^{-5}$ [31]. For single field inflation, this gives $(V^{3/2}/V') = 5.2 \times 10^{-4}$. Correspondingly, for chaotic inflation with $V = m^2\varphi^2/2$ we have $m = m_{pl}\, 5.2 \times 10^{-4}/(\sqrt{2}N_{pivot})$, where we reinstated the reduced Planck mass. Thus, the mass has to be quite small so that the potential is very shallow. This is a fine tuning problem shared by most models of inflation.

Higher order correlation functions are usually suppressed rendering non-Gaussianities unobservable. One can also compute the spectrum of gravitational waves, which is in agreement with current upper bounds.

1.4.2 Problems of Inflation

The simplest single field inflationary models, for instance slow roll models with a quadratic potential, are able to solve many cosmological puzzles and are still in agreement with the observed statistical properties of fluctuations in the CMBR. However, even though simple and compelling, these models are unsatisfactory from a theoretical point of view for several reasons, see e.g. [32]

- *Fine tuning of the potential [33]:* usually parameters in the inflaton's potential, such as the mass in $m^2\varphi^2$ potentials, have to be extremely small in order to provide the correct magnitude of fluctuations set by the COBE normalization (counter examples can be constructed).

- *Super Planckian field values [18]:* the inflaton has to traverse a distance in field space larger than the Planck mass in natural units. This is problematic from a field theoretic point of view, since non-renormalizable quantum corrections to the field's action are expected. Thus, the potential, which has to be severely fine tuned, would change drastically, potentially spoiling inflation. This is also known as the η-problem.

- *The trans-Planckian problem [34, 35]:* Fourier modes of the inflaton field have to be given initial values on length scales much smaller than the Planck length. At these length scales general relativity combined with ordinary quantum field theory is not applicable; a theory of quantum gravity, that is string or M-theory, should be used.

- *Fine tuning of initial conditions:* the inflaton has to start high up in its potential – why is it so far away from its true vacuum expectation value?

- *Initial Singularity [36]:* the initial singularity does not vanish but is merely pushed into the far past.

- *Identity of the inflaton:* scalar fields are not abundant in the standard model; furthermore, it has been challenging to identify an inflaton in e.g. extensions of the standard model (see however [37–39]) or in string theory. In recent years, several models arose within string theory, such as the KKLT construction (and followups) which stabilizes all but one degree of freedom during inflation [40, 41], or multi-field models such as $\mathcal{N}$-flation [42] or the proposal within M-theory by Becker/Becker/Krause considering multiple M5-branes [43]. Meanwhile, all reasonably successful models come with the price of high intricacy, a far cry from the simplicity of single field models previously discussed.

- *Entropy problem:* The low initial entropy of the initial state has to be assumed, just as in big-bang cosmology.

In the next chapters we will focus on multi-field models, which are able to address some of the above problems, such as the identity of the inflaton, super Planckian field values or tuning of the potential, while others remain. In addition, certain aspects of multi-field models, such as non-Gaussianities or reheating, are not worked out in great detail at present; hence, we will develop them further in the main part of this thesis (using $\mathcal{N}$-flation as an example).

1.4.3 Reheating

During inflation, the universe is homogenized leaving it devoid of particles and very cold. How then is the universe reheated after such an inflationary period?

Old Theory of Reheating

In the old theory of reheating [44,45], the inflaton field oscillates as a coherent wave of scalar particles, with a finite probability of decaying; such decays are determined by the the inflaton's (φ) coupling to other scalar χ or fermionic ψ fields in its Lagrangian, e.g. in the form of $g^2\sigma\phi\chi^2$ or $h\phi\psi\psi$; here σ has the dimensions of mass and g as well as h are dimensionless. When the mass of the inflaton is much larger than those of χ and ψ, that is, when $m \gg m_\chi, m_\psi$

the decay rates are

$$\Gamma_{\phi\to\chi\chi} = \frac{g^4\sigma^2}{8\pi m}\,, \tag{1.34}$$

$$\Gamma_{\phi\to\psi\psi} = \frac{h^2 m}{8\pi}\,. \tag{1.35}$$

To describe the damping of the scalar field φ during the rapid oscillation near the minimum of its potential, one adds an extra friction term to the equation of motion (1.18)

$$\ddot{\varphi} + 3H(t)\dot{\varphi} + \Gamma\dot{\varphi} + m^2\varphi = 0\,, \tag{1.36}$$

where $\Gamma = \Gamma_{\varphi\to\chi\chi} + \Gamma_{\varphi\to\psi\psi}$. Since the newly formed particles are ultra-relativistic, their energy density decreases faster than that of the oscillating inflaton. Thus, reheating ends only when $H \sim 2/(3t) < \Gamma$. The time when reheating ends is then given by

$$t_{reh} \sim \frac{2}{3\Gamma}\,. \tag{1.37}$$

At this point, most of the matter becomes ultra-relativistic and one can easily obtain an upper limit on the reheating temperature T_{reh}, since $\rho(t_{reh}) = 3H^2 = 3\Gamma^2$ and $\rho \propto T_{reh}^4$ so that [46]

$$T_{reh} = 0.2\left(\frac{100\cdot 8\pi m_{pl}^2}{g_*}\right)^{1/4}\sqrt{\Gamma}\,, \tag{1.38}$$

where g_* is the effective number of massless degrees of freedom which has the value of $g_* = 10^2 - 10^3$ in realistic models and we kept the reduced Planck mass explicit. To make sure that monopoles are not reintroduced into the theory [17], the reheat temperature should be below $T_{reh} < 10^6$GeV, a limit which is well below the GUT scale. This constraint is usually satisfied, since $m \sim 10^{-5} m_{pl}$ due to the COBE normalization.

Non-perturbative Effects and Parametric Resonance

Before addressing reheating in multi-field inflation, we review non-perturbative preheating via parametric resonance [47,48] (see also [46,49,50] and [17] for a review), whereby particles in a scalar matter field χ coupled to the inflaton field φ via the effective potential

$$V(\varphi,\chi) = \frac{1}{2}m^2\varphi^2 + \frac{1}{2}m_\chi^2\chi^2 + \frac{1}{2}g^2\varphi^2\chi^2\,, \tag{1.39}$$

are produced in short bursts while φ oscillates around the minimum of V. The produced particles interact with one another until a state of thermal equilibrium at the temperature T_{rh} is reached; the process of thermalization is non-trivial and may take much longer than the actual preheating process [51]. After preheating most of the energy initially stored in the inflaton field is transferred into the matter sector.

In the simple case of chaotic inflation, the exponential expansion of the universe ends when the slow roll conditions are violated at $\varphi \sim 1$. As an illustration, consider the case $m \gg m_\chi$ and ignore back-reaction[11] of χ particles so that (1.18) becomes

$$\ddot{\varphi} + 3H\dot{\varphi} = -m^2\varphi\,, \tag{1.40}$$

which has the solution

$$\varphi(t) = \Phi(t)\sin\omega t\,, \tag{1.41}$$

where

$$\Phi(t) = \frac{\sqrt{8}}{\sqrt{3}mt} \tag{1.42}$$

is the amplitude of oscillations, which decays due to Hubble friction as $1/a^{3/2} \propto 1/t$, and $\omega \equiv m$ is the frequency. After inflation, $H \ll m$, meaning, many oscillations take place in just one Hubble time. During preheating, the amplitude of oscillations of the inflaton would decrease faster than (1.42) if backreaction of the matter field were included.

Ignoring metric perturbations, the equation of motion for a fourier mode of the matter fields χ is

$$\ddot{\chi}_k + 3H\dot{\chi}_k + \left(\frac{k^2}{a^2} + m_\chi^2 + g^2\varphi^2\right)\chi_k = 0\,, \tag{1.43}$$

where $\mathbf{p} = \mathbf{k}/a$ is the physical momentum and the effective, time dependent mass of the matter field is

$$m_{\chi_{eff}}^2 \equiv \frac{\partial^2 V(\varphi,\chi)}{\partial\chi^2} = m_\chi^2 + g^2\varphi^2(t)\,. \tag{1.44}$$

Note that (1.43) is reminiscent of the harmonic oscillator with a time dependent mass.

[11] ignoring back-reaction is only justified in the early stages of reheating. Once sufficient χ particles are produced, its back-reactions may shut off reheating. Any complete theory of preheating covering also thermalization, necessarily needs to incorporate back-reaction.

In order to study preheating, ignore the expansion of the universe for the time being, consider $m_\chi = 0$ and introduce $q = g^2\Phi^2/4m^2$, $\tau = mt$ (dimensionless time, a prime denotes a derivative with respect to τ in this section), $A_k = 2q + k^2/m^2a^2$ as well as $X_k \equiv a^{3/2}\chi_k$ so that (1.43) becomes

$$X_k^{''} + (A_k - 2q\cos(2\tau))X_k = 0\,. \tag{1.45}$$

Here the term $-(3/4)(2a^{''}/a + a'^2/a^2)$ drops out since $a \propto \tau^{2/3}$. Treating Φ and A_k as constants, Eq. (1.43) is the Mathieu equation. It is well known that parametric resonance occurs for wavenumbers k within resonance bands [52]. The strength of the resonance within a given instability band is determined by the values of A_k and q. If k is within the $n'th$ resonance band, the corresponding mode increases as

$$X_k \propto e^{\mu_k^{(n)}\tau}\,, \tag{1.46}$$

where $\mu_k \gg 0$ is the Floquet index [52]. This corresponds to an exponential growth of the occupation number n_k (see Eq. 1.50) i.e., particle production. If we do not consider a quadratic potential for the inflaton but a $\lambda\phi^4/4$ type, the model becomes conformally invariant. In this specific case, expansion effects can be kept and the resulting equations for χ_k reduce to the Lame equation [50], which also exhibits well defined resonance bands.

The equations of motion for the Fourier modes of the matter field (1.43) becomes

$$X_k'' + \left(\frac{k^2}{a^2m^2} + \frac{g^2}{m^2}\varphi^2 + \Delta\right)X_k = 0\,, \tag{1.47}$$

where

$$\Delta(\tau) \equiv \frac{m_\chi^2}{m^2} - \frac{3}{2}\frac{a''}{a} - \frac{3}{4}\frac{a'^2}{a^2}\,. \tag{1.48}$$

As we saw, neglecting the expansion of the universe leaves us with the Mathieu equation, which, depending on the given value of g, can exhibit narrow ($g \ll m/\Phi$) and broad resonance ($g \gg m/\Phi$). If on the other hand, expansion effects are allowed, the behavior changes drastically, leading to stochastic resonance [46], which is a very efficient way of reheating and will be discussed in more detail below.

Notice that we have kept the mass term for the matter field in (1.48). A small non-zero mass doesn't change reheating qualitatively, but a large mass will immediately shut off parametric resonance. Thus we set $m_\chi \equiv 0$ from

now on, but keeping in mind that this constitutes fine tuning. As initial conditions for the matter field we take the usual Bunch-Davies vacuum state

$$X_k = \frac{e^{-i\omega_k t}}{\sqrt{2\omega_k}}\,. \tag{1.49}$$

In order to compute the generalized Floquet index, it is useful to examine the occupation number [46] of a given mode X_k

$$n_k = \frac{\omega_k}{2}\left(\frac{|X_k'|^2}{\omega_k^2}m^2 + |X_k|^2\right) - \frac{1}{2}\,, \tag{1.50}$$

where the energy per particle is defined as

$$\omega_k^2(\tau) \equiv \frac{k^2}{a^2} + g^2\varphi^2 + m^2\Delta\,. \tag{1.51}$$

We can interpret Eq. (1.50) as the ratio of the kinetic and potential energy to the energy per particle. Thus we can identify the maximal index as being twice the slope in an $\ln(n_k)$ over τ plot,

$$\mu_k \equiv \frac{1}{2(\tau_{max}-\tau_{min})}\ln(\sup(n_k(\tau)/n_k(\tau_{min}), \tau \in [\tau_{min}...\tau_{max}]|\varphi'(\tau)=0)) \tag{1.52}$$

Notice the factor of two due to n_k being quadratic in X_k. The supremum is introduced here since it is possible for the occupation number to decrease during stochastic resonance [46]. Another subtlety concerns the occupation number (1.50), which is ill defined whenever $\varphi \approx 0$, since during those instances particles are produced in bursts causing n_k to spike. Thus we evaluate μ_k only at the turning points of φ. Lastly, τ_{min} should be chosen such that $n_k(\tau_{min})$ is already reasonably large.

Before we elaborate on specific resonances, we would like to mention an elegant mathematical tool to compute the existence and position of instability bands, *spectral theory* [53–57]: here the equation of motion of χ_k is first rewritten in the form of a Schrödinger equation (or more general Hill equation). If one now computes the spectrum, one can show that the complement of the spectrum is a subset of modes with a positive generalized Floquet index. This tool is quite useful when confronted with more fields, as is the case in multi-field inflation, and we will come back to it later.

Narrow Resonance

In this simple case, we ignore all expansion effects so that $a = 1$ as well as $a' = a'' = 0$ and consider $g < m/\Phi$. The amplitude of oscillation of φ can be

estimated to $\Phi \approx \sqrt{8}/\sqrt{3}$ and we obtain narrow resonance for modes in well defined bands [52]. For instance, the first, and strongest resonance band is located between

$$1 - 3q \lesssim \frac{k^2}{m^2} \lesssim 1 - q \,, \tag{1.53}$$

with

$$q = \frac{g^2\Phi^2}{4m^2} \ll 1 \,. \tag{1.54}$$

and the resulting maximal Floquet index is $\mu_k \approx q/2$.

Broad Resonance

Neglecting expansion effects, we consider now the case $g > m/\Phi$ so that

$$q = g^2\Phi^2/4m^2 \gg 1 \,. \tag{1.55}$$

During broad resonance, a given Fourier mode scans many resonance bands during any given oscillation of the inflaton field. μ_k can be approximated analytically to [46]

$$e^{\pi\mu_k} = |\cos(\theta_k - \varphi_k)| \sqrt{1 + e^{-\pi\kappa^2}} + \sqrt{(1 - e^{-\pi\kappa^2})\cos^2(\theta_k - \varphi_k) - 1} \,, \tag{1.56}$$

where $\kappa^2 \equiv k^2/k_*^2$, $k_*^2 \equiv 2m^2q^{1/2}$, and $\theta_k - \varphi_k \approx 4\sqrt{q} + \frac{k^2}{8\sqrt{q}m^2}(\ln q + 9.474)$.

Stochastic Resonance

Due to expansion effects, a given Fourier mode of the matter field shifts to lower resonance bands over time until it passes the first resonance band and resides in a stable region. Due to the shifting, the occupation number appears to be changing erratically, hence the name stochastic resonance. However, it should be noted that the qualitative behavior can still be understood and even quantitatively estimated using the instability chart of the Mathieu equation [58]. Nevertheless, looking at the spectrum of μ_k, the latter appears to be a random variable which is more prone to be positive than negative, for example, if $\pi\kappa^2 \ll 1$ the ratio is $3:1$ [46]. The envelope within which μ_k resides can be derived analytically to [46]

$$\mu_k^{\pm} = \frac{1}{2\pi} \ln\left(1 + 2e^{-\pi\kappa^2} \pm 2e^{-\pi\kappa^2/2}\sqrt{1 + e^{-\pi\kappa^2}}\right) \,. \tag{1.57}$$

Other Approaches and Subtleties

We have only given the most basic description of (p)reheating, ignoring for instance *backreaction/rescattering* between the matter field and the inflaton field. If more and more χ particles are created, the term $\propto \chi^2\varphi^2$ acts as an effective mass, driving φ back to its origin, where production of χ-particles occurred. Further, once ρ_χ becomes comparable to ρ_φ, the expansion of the universe is affected. Backreaction can lead to interesting effects such as moduli trapping [59]. Naturally rescattering is especially important in the late stages of preheating too [46]. Other interesting models of (p)reheating, which we do not explain in detail, include:

Instant Preheating [60], where the scalar field is coupled to a Bosonic field χ which in turn is coupled to a Fermionic field ψ. When φ goes through zero, light χ particles are produced copiously. As the values of φ increase, the χ particles become more massive increasing the energy in the χ sector. However, before backreaction of χ particles onto φ becomes dominant, they decay into Fermions. Hence most of the energy of φ can be transferred to the matter sector in a few or even without oscillations [61]. The latter feature makes instant preheating attractive to frameworks which do not posses a confining potential.

Tachyonic Preheating is a form of fast preheating whereby the coupling term in the potential is replaced by $g\varphi^2\chi^2/2$ with $g < 0$, leading to an instability. This in turn causes an increased particle production, a process that can terminate fast within one oscillation [64], and implying larger μ_k as compared to the parametric resonant case ($g^2 > 0$). In order for the potential to be bounded from below, additional terms of the form $\alpha\chi^4$ or φ^4 have to be added to it. Cosmic strings are also produced during tachyonic preheating [63–65].

Cantor Preheating [66] can occur when more than one inflaton field is coupled to the same matter field. For two fields, a numerical study exists in the literature [57], Cantor preheating is expected to be an efficient means of preheating in multi-field models of inflation, since stability bands dissolve into a nowhere dense set (see section 1.5.4). We will discuss Cantor preheating in more detail in section 1.5.4 and in chapter 4.

Other approaches to preheating include *Geometric Preheating* [67] and *Fermionic Preheating* [68]. After preheating, the universe is in a highly non-thermal state. How thermalization occurs is in itself an interesting and challenging field of research, see e.g. [51] and references therein.

Efficiency and potential problems of non-perturbative effects

By efficiency we mean primarily how non-perturbative effects compare to the old methods of reheating, which are surely at work in the early universe. The efficiency of most of the aforementioned non-perturbative methods hinges crucially on well chosen values of the coupling constants as well as bare masses. For instance, a non zero bare mass of the matter field larger than the inflaton mass can shut off parametric resonance entirely [58]. Since the inflaton field is usually unnaturally light, this constitutes a serious fine-tuning. The same goes for the coupling constants, which need to be in a certain range for efficient reheating to occur. Thus it has been claimed [58], that parametric resonance effects are expected to be unimportant in generic, not fine-tuned, models of the early universe. In addition, too efficient preheating models might also be problematic, due to the possibility or producing unwanted relics, such as magnetic monopoles. This is corroborated by the fact that the state is highly non-thermal after preheating. As we will see later on, non-perturbative effects are not actually the norm for multi-field models of inflation, and the old theory of preheating is applicable.

1.5 Multi-Field Inflation

Multi-field models of inflation, see [69] for a review, have been considered ever since the introduction of hybrid inflation [70]. Here, only one field evolves during inflation and the role of the second field is to end inflation by creating an instability in a direction orthogonal to the classical inflationary trajectory. In contrast, true multi-field models employ at least two dynamical fields during inflation.

Consider $\mathcal{N}$ scalar fields φ_I, $I = 1 \ldots \mathcal{N}$, with canonical kinetic terms and for simplicity a flat metric in field space

$$S = \frac{1}{2}\int d^4x\sqrt{-g}\left(\frac{1}{2}\sum_{A=1}^{\mathcal{N}}\partial^\mu\varphi_A\partial_\mu\varphi_A + W(\varphi_1,\varphi_2,...)\right) \tag{1.58}$$

The generalized Klein Gordon equations read

$$\ddot{\varphi}_I + 3H\dot{\varphi}_I = -W_I \tag{1.59}$$

where we introduced $W_I \equiv \partial W/\partial\varphi_I$, and the Friedman equation becomes

$$3H^2 = W + \sum_I \frac{1}{2}\dot{\varphi}_I^2\,. \tag{1.60}$$

At the background level one can replace any multi-field model by an effective single field model, where the sole degree of freedom σ is identified with the distance traversed along the trajectory in field space [71–73]. Given a flat metric in field space, this yields

$$\sigma \equiv \int \sum_I \hat{\sigma}_I \dot{\varphi}_I \, dt \,, \tag{1.61}$$

where

$$\hat{\sigma}_I \equiv \frac{\dot{\varphi}_I}{\sqrt{\sum_J \dot{\varphi}_J}} \,. \tag{1.62}$$

This effective inflaton obeys

$$\ddot{\sigma} + 3H\dot{\sigma} = -\sum_I \hat{\sigma}_I W_I \,. \tag{1.63}$$

It should be noted that this effective model is not sufficient at the perturbed level since it only captures adiabatic fluctuations.

1.5.1 Perturbations and non-Gaussianities

A common approach to study perturbations with more than one field consists of employing the Sasaki-Mukhanov variables

$$Q_I \equiv \delta\varphi_I + \frac{\dot{\varphi}_I}{H}\psi \,. \tag{1.64}$$

which coincide with the corresponding field perturbation in the spatially flat gauge $Q_I = \delta\varphi_I|_{\psi=0}$. In terms of these variables, the comoving curvature perturbation is $\mathcal{R} = \sum_I \dot{\phi}_I Q_I / \sum_J \dot{\phi}_J^2$. The full equations of motion for these variables read [71]

$$0 \;=\; \ddot{Q}_I + 3H\dot{Q}_I + \frac{k^2}{a^2}Q_I + \sum_J \left(W_{IJ} - \frac{1}{a^3}\left(\frac{a^3}{H}\dot{\varphi}_I\dot{\varphi}_J\right)^{\cdot}\right) Q_J \,. \tag{1.65}$$

In this formalism, the distinction between adiabatic and isocurvature (or entropy) perturbations is not apparent. The easiest approach to visualize both is due to Gordon et. al [71]: the adiabatic perturbation is the perturbation along the field trajectory, that is $\delta\sigma$ where σ is defined in (1.61), and hence it corresponds to a local shift in time. Correspondingly, isocurvature modes are

perturbations perpendicular to the field trajectory (see [71] for a proper definition)[12]. The instantaneous adiabatic mode is seeded by isocurvature modes whenever the trajectory in field space makes a turn. This becomes apparent after a rotation in field space and rewriting (1.65) accordingly [69, 71]. Duly, $\mathcal{R}$ does not need to be frozen on large scales after horizon crossing.

To compute correlation functions, we employ again the δN-formalism, generalized to higher orders and more fields [27, 28]. The curvature perturbation ζ is then given by

$$\zeta \simeq \sum_I N_I \delta\varphi_{I\psi} + \frac{1}{2}\sum_{IJ} N_{IJ}\delta\varphi_{I\psi}\delta\varphi_{J\psi} + \frac{1}{3!}\sum_{IJK} N_{IJK}\delta\varphi_{I\psi}\delta\varphi_{J\psi}\delta\varphi_{K\psi} + \ldots \quad (1.66)$$

where $\delta\varphi_{I\psi} \equiv \delta\varphi_I|_{\psi=0}$ and we used the short hand notation $N_I = \partial N/\partial\varphi_I$, $N_{IJ} = \partial^2 N/\partial\varphi_I\partial\varphi_J$ etc. $N^I = \delta^{IJ}N_J$ using Einstein's summation convention. The power spectrum after Hubble exit is then given by

$$\mathcal{P}_\zeta = \sum_I N_I^2 \mathcal{P}_{\delta\varphi_{I\psi}}\,, \quad (1.67)$$

and higher order correlation functions, such as the bi- and tri-spectrum can also be computed. The ratio of the bispectrum to the power-spectrum squared is a measure of the non-Gaussianity, since the bispectrum vanishes identically for purely Gaussian perturbations. This ratio is measured by the non-linear parameter f_{NL} which was computed in [24–26] to

$$-\frac{6}{5}f_{NL} \;=\; \frac{r}{16}(1+f) + \frac{N_I N_J N^{IJ}}{(N_K N^K)^2}\,, \quad (1.68)$$

where repeated Latin indices are to be summed over. Here r is the usual scalar to tensor ratio ($r/16 < 0.1$ from [6]), and f characterizes the shape of the momentum triangle ($0 \le f \le 5/6$ [25, 74] and it is largest for an equilateral triangle). It follows then that the first term is small. However, the second contribution

$$-\frac{6}{5}f_{NL}^{(4)} \equiv \frac{N_I N_J N^{IJ}}{(N_K N^K)^2}\,. \quad (1.69)$$

may be larger[13]. To estimate the magnitude of the four point function, we

[12]For instance, in a two-field model where θ denotes the instantaneous angle between the trajectory and the φ_1-axis, the entropy perturbation is $\delta s = (\cos\theta)\delta\varphi_2 - (\sin\theta)\delta\varphi_1$.

[13]Note that $f_{NL}^{(4)}$ is denoted as f_{NL} in [69].

use the momentum independent parameters[14] [76, 77],

$$\tau_{NL} = \frac{N_{AB}N^{AC}N^{B}N_{C}}{(N_{D}N^{D})^{3}}, \tag{1.70}$$

$$g_{NL} = \frac{25}{54}\frac{N_{ABC}N^{A}N^{B}N^{C}}{(N_{D}N^{D})^{3}}. \tag{1.71}$$

Parameters characterizing higher order correlation functions can be defined systematically using the elegant diagrammatic approach found in [78]. It should be noted that the above expressions do not depend on the slow roll or the horizon crossing approximation.

Observationally, f_{NL} is constrained: $-54 < f_{NL} < 114$ by the WMAP3 data alone [6, 79, 80]. However, recent re-evaluations suggest a detection of a non-zero f_{NL} at 2σ [81]: $26.9 < f_{NL} < 146.7$, see also [82][15]. Future experiments [84–87] such as Planck will be able to unambiguously determine if f_{NL} is indeed so large or consistent with Gaussian perturbations (Planck alone will narrow down $|f_{NL}| \lesssim 5$ [84]).

The other parameters are constraint to $|\tau_{NL}| < 10^{8}$ [75] (to be improved down to $|\tau_{NL}| < 560$ by Planck [88])

1.5.2 Assisted Inflation

One well studied multi-field model is assisted inflation; originally proposed to relax fine tuning of potentials (see e.g. [89–92]), assisted inflation relies on $\mathcal{N}$ scalar fields, preferably uncoupled, assisting each other in driving an inflationary phase. Even though each individual field may not be able to generate an extended period of inflation on its own, they can do so cooperatively. The key feature is the increased Hubble friction, which slows down all fields. This phenomenological model is attractive, since super Planckian initial values of the fields can be avoided [89, 91, 92] if the number of fields is large. A string motivated implementation of assisted inflation is $\mathcal{N}$-flation [42, 93]: here the many fields are identified with axions arising from some KKLT compactification of type IIB string theory [93]. An additional implementation of assisted inflation within M-theory, making use of multiple M5-branes, is given in [43, 94, 95].

To see how assisted inflation works, lets us consider $\mathcal{N}$ uncoupled fields

[14] For gaussian fields the tri-spectrum can be written as $T_{\zeta}(\mathbf{k}_1, \mathbf{k}_2, \mathbf{k}_3, \mathbf{k}_4) = \tau_{NL}[\mathcal{P}_{\zeta}(|\mathbf{k}_1 + \mathbf{k}_3|)\mathcal{P}_{\zeta}(k_3)\mathcal{P}_{\zeta}(k_4) + (11\text{perms})] + \frac{54}{25}g_{NL}[\mathcal{P}_{\zeta}(k_2)\mathcal{P}_{\zeta}(k_3)\mathcal{P}_{\zeta}(k_4) + 3\text{perms.}]$

[15] This is in agreement with WMAP5 [83].

with potential

$$W \equiv \sum_{I=1}^{\mathcal{N}} V_I(\varphi_I) \tag{1.72}$$

and $V_I = m_I^2 \varphi_I^2/2$. This type of assisted inflation is realized in $\mathcal{N}$-flation. It does not possess a global attractor solution as opposed to models with exponential potentials [90]. Nevertheless, the solutions are stable with respect to classical perturbations [96] and one may even include some small coupling between the fields, which are expected in $\mathcal{N}$-flation, without spoiling stability [96].

To estimate the amount of inflation, let us work within the slow roll approximation, that is assume

$$\varepsilon_I \equiv \frac{1}{2}\frac{V_I'^2}{W^2} \quad , \quad \eta_I \equiv \frac{V_I''}{W}\,, \tag{1.73}$$

are small ($\varepsilon_I \ll 1$, $\eta_I \ll 1$) and

$$\varepsilon \equiv \sum_I \varepsilon_I \ll 1 \tag{1.74}$$

holds. The number of e-folds (1.26) becomes

$$N(t_{end}, t) \simeq -\sum_I \int_{\varphi_I}^{\varphi_I^{end}} \frac{V_I}{V_I'} d\varphi_I\,. \tag{1.75}$$

Thus, if all fields have the same initial value $\varphi_I \equiv \varphi$, we get $N \simeq (\varphi^2 - \varphi_{end}^2)\mathcal{N}/4 \approx \varphi^2\mathcal{N}/4$. Comparing this result to the single field model summarized in section 1.4, $N_{single} = \varphi^2/4$, we observe an additional factor of $\mathcal{N}$. On the other hand, for randomly chosen sub-Planckian initial field values, $\varphi_I \in [0 \ldots 1]$, the number of e-folds becomes $N \approx \mathcal{N}/12$ [97], independent of the mass spectrum. Thus if the number of fields is large enough, super-Planckian field values can be avoided while still supplying sufficient inflation. This is a generic feature of assisted inflation, making it rather appealing.

The fields evolve during slow roll according to

$$3H\dot{\varphi}_I \approx -\frac{\partial V_I}{\partial \varphi_I} \equiv -V_I'\,, \tag{1.76}$$

$$3H^2 \approx W\,, \tag{1.77}$$

leading to

$$\frac{\varphi_I^{end}}{\varphi_I} = \left(\frac{\varphi_J^{end}}{\varphi_J}\right)^{m_I^2/m_J^2}\,. \tag{1.78}$$

As previously mentioned, this is not a global attractor solution, and as a result, there is an unavoidable dependence on initial conditions if quadratic potentials are used.

Shifting our attention to perturbations, the scalar spectral index can be computed in the horizon crossing approximation (using the δN-formalism) [22, 98] to

$$n_s - 1 = -\sum_I \left(\frac{V_I'}{W}\right)^2 - \frac{2}{\sum_I (V_I/V_I')^2} + \frac{2}{W}\frac{\sum_I (V_I/V_I')^2 V_I''}{\sum_J (V_J/V_J')^2}\,. \qquad (1.79)$$

In the equal mass/initial condition case, this reduces to the single field slow roll result $n_s - 1 = -2/N$. In chapter 2 we investigate non-Gaussianities using $\mathcal{N}$-flation as a concrete example.

1.5.3 $\mathcal{N}$-flation

In $\mathcal{N}$-flation[16] the many inflatons needed for assisted inflation to work are conjectured to be axions in some KKLT compactification [42]. Closely related models were investigated in [91, 92, 99]. Even though a concrete construction has not yet been given, $\mathcal{N}$-flation provides a test-bed for multi-field inflation. In [93] it is argued, but not proven, that an effective quadratic potential for each field without cross couplings may be attainable. Based on results of random matrix theory, it is further argued in [93] that the masses for the $\mathcal{N}$ fields, originally considered identical in [42], would conform to the Marčenko-Pastur (MP) distribution [100]

$$p(m^2) \;=\; \frac{1}{2\pi\beta m^2\sigma^2}\sqrt{(m_1^2 - m^2)(m^2 - m_{\mathcal{N}}^2)}\,, \qquad (1.80)$$

where β and σ completely describe the distribution: σ is the average mass squared and β controls the width and shape of the spectrum, see Fig. 1.1. The latter parameter may be identified with the ratio of the number of axions to the total dimension of the moduli space (Kähler, complex structure and dilaton) in a given KKLT compactification of type IIB string theory; $\beta \sim 1/2$ is preferred due to constraints arising from the renormalization of Newton's

[16] Recently [83], it was argued that $\mathcal{N}$-flation is ruled out for $\beta = 1/2$ and $N = 50$, lying outside of the 95% CL. However, within $\mathcal{N}$-flation, the value of β is not tightly constrained; the preferred value of a 1/2 merely indicates that $0.1 < \beta < 0.9$ is a preferred range. In this study we consider this whole range. For $\beta = \mathcal{O}(0.1)$, $\mathcal{N}$-flation is still viable similar to $m^2\phi^2$ single field potentials. We tested all conclusions with different values of β and they remain qualitatively identical.

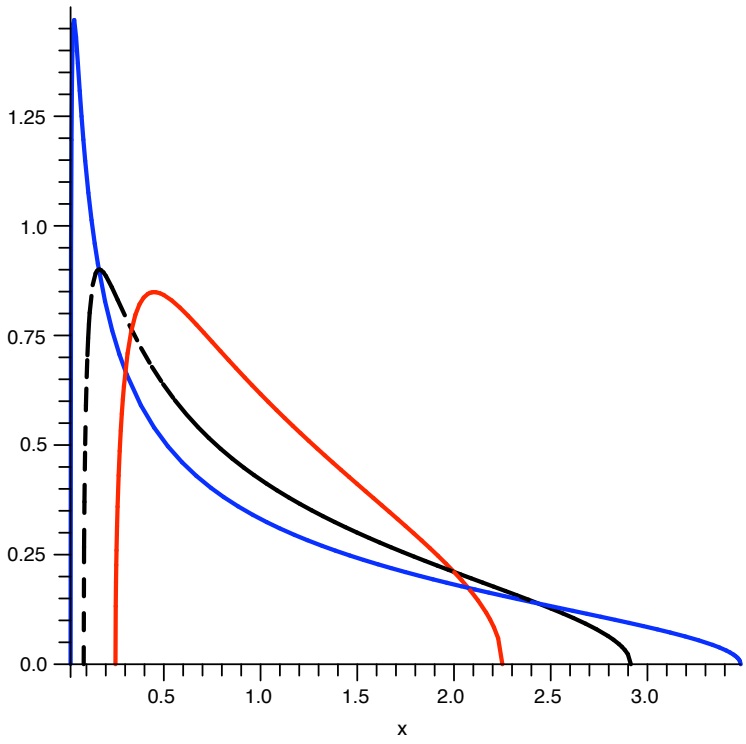

Figure 1.1: Probability of a given mass according to the Marčenko-Pastur distribution from (1.80), depending on β and the dimensionless square mass $x = m^2/m_1^2$, rescaled with the expectation value $\langle x \rangle$ (also dependent on β): $\beta_1 = 1/4$, $\beta_2 = 1/2$ and $\beta_3 = 3/4$; the closer β is to one, the broader the mass spectrum becomes.

constant [42]. In terms of β, the smallest and largest mass are given by

$$m_1^2 = a \equiv \sigma^2(1 - \sqrt{\beta})^2 \,, \tag{1.81}$$

$$m_{\mathcal{N}}^2 = b \equiv \sigma^2(1 + \sqrt{\beta})^2 \,. \tag{1.82}$$

The effect of this distribution on the power-spectrum has been computed in [93, 101], yielding a slightly redder spectral index. Further work on different aspects of $\mathcal{N}$-flation include [97, 102–111]. We will use this model as a concrete realization of multi-field inflation and investigate non-Gaussianities during slow roll in chapter 2 and beyond slow roll in chapter 3 as well as reheating in chapter 4.

1.5.4 Reheating

The old theory of reheating is still applicable in the presence of multiple inflatons, but little is understood whether or not non-perturbative effects play an important role. In the mathematical literature, an elegant method determining the presence of instabilities is known: spectral theory [53, 112]. The basic idea consists of recasting the equation of motion for the matter field χ into the form of the Schrödinger equation, and compute its spectrum. The complement of this spectrum will be a subset of modes with a positive Floquet index [66]. Expressly, renaming $x \equiv \tau$, $y \equiv X_k$ as well as $\lambda \equiv A_k$ (compare to section 1.4.3) we arrive at the one dimensional Schrödinger equation

$$-\frac{d^2y}{dx^2} + Q(x)y = \lambda y\,, \tag{1.83}$$

where the potential is determined by the time dependent mass of χ. In case of single field reheating, it is given by $Q(x) \equiv 2qP(2x)$ with $P(2x) \equiv \cos(2x)$ for the Mathieu equation and $P(\cdot) \equiv cn^2(\cdot)$ [50] for the Lame equation. Naturally, this transformation can also be performed for more intricate time dependent masses. If one solves (1.83) for the spectrum S in case of the Mathieu equation one recovers correctly the resonance bands by considering the complement $\bar{S}$ [57]. Further, as long as the potential Q is periodic, it is reasonable to expect well defined resonance bands.

Lets turn our attention to more than one inflaton field and assume that they are all coupled to the same matter field. Again neglecting the matter field's mass, we can write its equation of motion as follows,

$$\ddot{\chi}_k + 3H\dot{\chi}_k + \left(\frac{k^2}{a^2} + \sum_I g_I^2\varphi_I^2\right)\chi_k = 0\,. \tag{1.84}$$

Each inflaton will oscillate as $\varphi_I(t) = \Phi_I(t)\cos(\omega_I t + \alpha_I)$ with frequency $\omega_I = m_I$, some phase α_I and a decaying amplitude $\Phi_I(t)$ due to Hubble friction. If the masses are not related via rational numbers the resulting potential Q will only be quasi-periodic. In this case, analytic expressions for μ_k are not known even if one considers only two fields, in phase, without Hubble damping and with identical couplings. Nevertheless, spectral methods can still be applied to find instabilities. Roughly speaking, if Q is quasi-periodic the band structure of the spectrum of the Schrödinger equation will dissolve in most cases into a nowhere dense set on the real numbers, similar to a Cantor set [54, 66, 113]. Therefore the complement of the spectrum will be dense, and thus almost all modes will have $\mu_k > 0$[17]. This way of preheating

[17]Note that there are a few known cases of quasi-periodic potentials that still exhibit a band structure similar to the periodic case [56].

is sometimes referred to as *Cantor Preheating* [57].

Inflationary reheating for two inflaton fields and one matter field was studied numerically in [57, 66]; it was shown that the stability bands of the Mathieu equation indeed vanish for the quasi periodic potential under consideration [57]: in the strong coupling limit the stability bands of the Mathieu equation completely dissolve, resulting in $\mu_k > 0$ for almost all modes, accompanied by large peaks at certain wavenumbers. This is agreement with predictions of spectral theory [66]. To achieve a quasiperiodic potential in (1.84), the ratio of the inflaton field masses is chosen such that they are irrationally related; however, further investigations into more fields or a systematic variation of the masses and couplings is absent.

Before concluding this short review on multi-field reheating, we would like to point out another perspective onto the problem, indicating that non-perturbative effects could be important in multi-field reheating. Given a reasonably large number of fields, the potential Q will appear as if dominated by noise. Further, the effect of noise onto reheating has been studied in [114, 115], where it was found that even small amounts of noise on top of a periodic potential Q (which comes about in a $m^2\varphi^2$ theory), lead to an instability of almost all modes. This study relies on a different analytic technique by casting the equations of motion in terms of matrix equations and using the Fürstenberg theorem. The analytical findings are confirmed numerically; It is shown that a generic μ_k in the presence of noise is larger than the largest μ_k in the absence of noise. This indicates that multi-field reheating could be much more efficient than its single field counterpart. However, more recently the effect of white noise was re-examined in a model including a $\lambda\varphi^4$ term [116], with the result that amplification is almost always suppressed by the presence of noise.

Therefore, a careful numerical investigation of multi-field reheating is needed for a definite evaluation of its efficiency, which we provide in chapter 4.

1.6 Cosmic Strings and Loops

Cosmic strings are one dimensional topological defects with a mass per length μ. Through their movement they stir up the surrounding matter content, and as a result, if they are present in the early universe, they source perturbations in the CMBR [117]. Since the resulting CMBR spectrum does not exhibit acoustic peaks, strings are ruled out as the primary source of structure. Current observations of the CMBR indicate that they have to contribute less than about 10% of the primordial anisotropy, leading to an upper bound

on the mass density of $G\mu \leq 2 \times 10^{-7}$ [118, 119]. (Here and in the following we keep Newtons constant G explicit). Nevertheless, string networks remain attractive subjects of study because they persist throughout the history of the universe without over-closing it and they constantly source scalar, vector and tensor perturbations.

Recently, interest in cosmic strings has been revived, mainly because different kinds of such strings occur within many early universe models motivated by string theory. The primary difference lies in their intercommutation probability P, which is one for ordinary cosmic strings, but smaller for F and D strings [120]. Note that in any string network there will also be a population of loops which are being chopped off by intersecting strings.

String networks have been the subject of numerical studies for some time, and accurate semi-analytic network models have been developed. In the following we will summarize possible origins of string networks, how they evolve according to simple network models and what kind of loops are produced. We then proceed to discuss how individual strings interact with matter.

Further review material can be found in [117, 121].

1.6.1 Origins

String networks are a by-product of many models of the early universe. In this section we investigate a few examples. Perhaps the most commonly known strings are those originating after symmetry breaking phase transitions: a network of topological defects will generically arise due to the Kibble mechanism [122]. For instance, a solitonic string solution arises in any gauge theory with a broken $U(1)$ symmetry. At the phase transition, when the universe cools below a critical temperature T_c, the Higgs field rolls from the origin to one of the supersymmetry breaking vacua. A string network is generated because strings do not return to their original starting point, instead, as shown by numerical simulations, they are in an infinite random walk. The underlining reason is due to causality, meaning that over large distances, the phase is not correlated.

Such phase transitions occur in breaking down of GUTs but also at the end of hybrid inflation models within supersymmetry and supergravity theories. As the universe expands and cools, it undergoes a number of phase transitions, breaking symmetry along the way.

The resulting cosmic strings form a network composed of infinitely long strings and a distribution of closed loops, which are constantly produced in the network: whenever two strings intersect (or one string self intersects), there is a chance of reconnection so that a loop gets chopped off [123]. In turn, a newly formed loop, one without cusps and intersections, may rapidly

intercommute with itself and fragment into smaller loops through excision of the cusp regions. The work of [124] suggests that as much as 80% of the total string length goes into small loops while 20% remains in large loops.

Braneworld models can also generate cosmic strings [125]: the low energy dynamics of D-brane annihilation at the end of many brane inflation models produce D-strings [125] [18].

Heterotic cosmic strings can arise from M5-branes wrapped around 4-cycles of a Calabi-Yau in heterotic M-theory compactifications [126], avoiding the known problems [127].

1.6.2 String Network Models

In the many numerical studies performed on string networks, it is shown that such networks evolve towards a scaling solution; meaning that the ratio of the characteristic length-scale of the network, the correlation length, to the Hubble radius is a constant, see [117] for a review. Two such semi-analytic loop network models are the one-scale model (OSM) and its extension, the velocity-dependent one-scale model (VOS). The acquisition of the equations determining the evolution of the long string energy density is provided by both models. Then, energy conservation is employed to determine the energy supplied to the loop population, in the form of newly formed loops. Our primary interest is the length spectrum

$$N(\ell, t) = \frac{\mathrm{d}N_{loops}}{\mathrm{d}\ln \ell} \tag{1.85}$$

where ℓ is the loop length and N_{loops} the number of loops per comoving Hubble volume. This spectrum can be extracted in both models and exhibits a distinctive loop size. The existence of a peak can be understood heuristically: at large loop size the spectrum decreases since these loops are created later, during a time of slower loop production. Additionally, the spectrum has to fall off for very small loops, since these loops are rapidly disappearing due to the emission of gravitational waves. Thus, there must be some intermediate scale where the spectrum peaks. Knowledge of this spectrum will be a crucial ingredient to make quantitative predictions of magnetic fields caused by rotating loops in chapter 5.

[18] Braneworld models of inflation, in geometries such as the Klebanov-Strassler (KS) throat, allows the formation of fundamental cosmic strings or F-strings and Dirichlet brane cosmic strings, or D-strings.

The one scale model (OSM)

According to the OSM [117, 128, 129] we can write the absolute number of loops N_{loops} as

$$\frac{\mathrm{d}N_{loops}}{\mathrm{d}L_H(t)} = \frac{V(t)}{L_H(t)^4}\frac{C}{\alpha} \tag{1.86}$$

where $V(t)$ is the physical volume, C is constant (different in matter- or radiation-dominated epochs), α is the size of newly created loops as a fraction of $L_H(t)$, the particle horizon measured in physical units defined as

$$L_H(t) = a(t)\int_0^t \frac{\mathrm{d}t'}{a(t')}\,. \tag{1.87}$$

Consider next a loop formed at some time t_F with initial length $\ell(t_F) = \alpha L_H(t_F)$. Due to the emission of gravitational waves the loop loses energy and shrinks. This emission of gravitational waves also influences the loop's movement, which will be discussed in more detail in chapter 5. Nevertheless, in this section we are interested on the length at time t of a loop formed at $t_F < t$; this is given by

$$\ell(t, t_F) = f_r \alpha L_H(t_F) - \Gamma_\ell G\mu(t - t_F) \tag{1.88}$$

where f_r accounts for the energy loss from the redshifting of the loop's peculiar velocity immediately after formation, and Γ_ℓ is a dimensionless parameter controlling the efficiency with which the loop emits gravitational radiation.

We would like to compute the length-spectrum $N(\ell, t)$ based on the fundamental OSM equations (1.86) and (1.88). First, assume that the volume simply follows the Hubble expansion $V(t) = (a(t)R)^3$. With this in mind, we can simply integrate (1.86) so that (1.85) yields the absolute number of loops per (cubical) comoving volume R^3. Further, we take $L_H(t) = 2t = 1/H(t)$ in the radiation dominated epoch. To calculate the length-spectrum we rewrite (1.85) as

$$N(\ell, t) = \frac{\mathrm{d}N_{loops}}{\mathrm{d}L_H(t_F)}\frac{\mathrm{d}L_H(t_F)}{\mathrm{d}\ln\ell}. \tag{1.89}$$

To continue, we need $L_H(t)$: a loop that has a length ℓ at time t must have formed at a time t_F when, using (1.88), the particle horizon $L_H(t_F)$ had a size of

$$L_H(t_F) = 2\left(\frac{\ell + \Gamma_\ell G\mu\, ct}{2\alpha f_r + \Gamma_\ell G\mu}\right). \tag{1.90}$$

Taking the derivative provides the second factor in (1.89). To obtain the first one, we pick a fiducial time t_0 during radiation domination, set $a(t_0) = 1$,

and fix $R = L_H(t_0)$. This yields the number of loops per logarithmic interval in ℓ, at time t, in a comoving volume equal to one Hubble volume at a time t_0, as

$$N(\ell, t) = \frac{30}{\alpha}\left(\alpha f_r + \frac{\Gamma_\ell G\mu}{2}\right)^{3/2} \frac{L_H(t_0)^{3/2}\ell}{\left(\ell + \frac{\Gamma_\ell G\mu}{2} L_H(t)\right)^{5/2}}\,, \tag{1.91}$$

where we have taken the value $C \sim 30$ during radiation domination, as in [128]. The spectrum possesses a peak at the characteristic length

$$\ell_{peak}(t) = \frac{\Gamma_\ell G\mu}{2} L_H(t) \sim 50 \cdot G\mu \cdot ct \tag{1.92}$$

taking $\Gamma_\ell \sim 50$ [128,130,131]. As expected, the spectrum falls off for $\ell > \ell_{peak}$ (slower loop production), and also for $\ell < \ell_{peak}$ (loop vanishing). Similar expressions can be derived in the matter era.

The velocity-dependent one-scale model (VOS)

The VOS model of refs. [132, 133] is a more realistic extension of the OSM. Here the string population is characterized by a length scale L, a velocity v, and a string number density n. Like the OSM model, it has several dimensionless parameters, which are commonly called c_1, c_2, and c_3. These are fixed by matching to numerical simulations [132], but differ in the radiation and matter era. Comparing with [132] the scaling values of H, L and v, we find $c_1 = 0.21$ $(0.2475), c_2 = 0.18$ (0.3675) in the radiation (matter) eras. The third parameter, $c_3 = 0.28$, fixes the scaling string number density. The physical origin of the VOS equations and their parameter inputs is discussed extensively in ref. [132]; matching between the equations used below and those of ref. [132] is explained in ref. [133]. In the VOS model the length scale evolves according to

$$\frac{\mathrm{d}L}{\mathrm{d}t} = HL + c_1 v \tag{1.93}$$

where the loop parameter $c_1 \leq 1$ is dimensionless. The velocity v obeys

$$\frac{\mathrm{d}v}{\mathrm{d}t} = \frac{-2Hv + c_2/L}{1 - v^2}, \tag{1.94}$$

and the comoving number density of long strings $N = a^2 n$ is governed by

$$\frac{\mathrm{d}N}{\mathrm{d}t} = -\frac{c_2 N v}{L} - \frac{c_3 N^2 L v}{a^2}\,. \tag{1.95}$$

To derive the loop creation rates from the above equation, we plug the rate of change of cosmic string energy density into the loop creation rate formula from ref. [128] and taking $\rho_\infty = n\mu$ we arrive at

$$\frac{\mathrm{d}N_{loops}}{\mathrm{d}t} = -\frac{V(t)}{\mu\alpha L_H(t)}\left[\dot{\rho}_\infty + 2\frac{\dot{a}}{a}\rho_\infty\left(1+\langle v^2\rangle\right)\right] . \tag{1.96}$$

Here L_H is again the Hubble radius, V the horizon volume and α is the ratio of the loop size to the Hubble radius.

1.6.3 Effect on Plasma

Whenever massive objects, such as cosmic strings or loops, move through a plasma, they will interact with it gravitationally. As a result, the plasma might drift or even get stirred up. Below we review the dragging effects due to a straight string, first via a the full GR treatment, followed by an approximate Newtonian derivation. The latter can easily be generalized to rotating cosmic string loops and will be used in chapter 5.

Gravitational Dragging: GR computation

Let us investigate gravitational effects onto a plasma through which long, straight strings move following [134,135]: consider a stationary straight string stretching in the z-direction

$$T^\nu_\mu = \delta(x)\delta(y)\mathrm{diag}(\mu, 0, 0, T) , \tag{1.97}$$

where μ is the energy per unit length and T is the tension. Working in the weak field limit such that

$$h_{\mu\nu} = g_{\mu\nu} - \eta_{\mu\nu} \tag{1.98}$$

is small, one can integrate the linearized Einstein equations to

$$h_{00} = h_{33} = 4G(\mu - T)\ln(r/r_0) , \tag{1.99}$$
$$h_{11} = h_{22} = 4G(\mu + T)\ln(r/r_0) , \tag{1.100}$$

where r_0 is a constant of integration and r the distance from the z-axis. For a straight string without any small scale wiggles on it we have $\mu = T \equiv \mu_0$, so that the only non-zero components of $h_{\mu\nu}$ are $h_{11} = h_{22} = 8G\mu_0\ln(r/r_0)$. After a coordinate transformation, the metric becomes identical to the one of an Euclidian space where a wedge of deficit-angle $\Delta_0 = 8\pi G\mu_0$ is removed.

Let the string move in the $-\hat{\mathbf{x}}$-direction with velocity $\mathbf{v}_s$ such that it sweeps over the x-z-plane in time. Further, consider a test particle of mass m a distance R away from the x-z-plane, e.g. at $\mathbf{r} = R\hat{\mathbf{y}}$. One can now integrate the geodesic equation in the weak field limit for the test particle's trajectory due to the gravitational interaction [134–137]. The resulting velocity after the encounter becomes [134]

$$v_y = -4\pi\mu_0 G v_s \gamma_s \tag{1.101}$$

where $\gamma_s = (1 - v_s^2)^{-1/2}$.

So far we ignored any small scale structure on the string. The origin of the string wiggles is due to string crossings and the fact that the expansion does not smooth out modes falling well within the horizon. If we do not probe in close proximity of the string, that is if R is much larger than the amplitude of the wiggles, we arrive again at an (effective) straight string. However, its mass density does not match up with its tension any more. To be precise, if one averages over the wiggles the effective tension and mass density satisfy [134, 138]

$$\mu T = \mu_0^2 \,, \tag{1.102}$$

where $\mu \approx 1.9\mu_0$ in the radiation era and $\mu \approx 1.5\mu_0$ in the matter era [117]. Using again the metric from (1.99) and (1.100) in the linearized geodesic equation for the test particle one gets [134]

$$v_y = -\frac{2\pi G(\mu - T)}{v_s \gamma_s} - 4\pi G \mu v_s \gamma_s \,. \tag{1.103}$$

The new first term, which can be recognized as the classical gravitational attraction of an infinite rod with mass density $\lambda = \mu - T = \mu(1 - \mu_0^2/\mu^2)$ (see Sec. 1.6.3), will dominate for a small drift velocity v_s. If we confine ourselves to the matter era, that is $t \geq t_{eq}$, a small drift velocity is expected for a wiggly string: even if the wiggles move very fast, e.g. with an RMS velocity of $v_{RMS} \approx 0.6$, the velocity of the string averaged over a correlation length is very small $v_s \equiv \bar{v}_{RMS} \approx 0.15$ [134]. Therefore, we may focus on the first term only with $\lambda \approx 0.56\mu_0$, but keep in mind that we should not probe the space in close proximity to the string. In addition, we are justified to use the non-relativistic limit, since $\gamma_s \approx 1$.

Newtonian limit and plasma dragging

We now derive the infall velocity v_y before estimating the dragging velocity v_x, both in the Newtonian limit. Again, assume an infinite straight string

stretching in the $\hat{z}$-direction and moving in the $-\hat{x}$-direction with velocity v_s (which we assume to be small right from the start $\mathbf{v}_s \ll 1$), along with a test particle located a distance R away from the x-z-plane, e.g. at $\mathbf{r} = R\hat{\mathbf{y}}$. The Newtonian gravitational force becomes

$$d\,\mathbf{F} = -Gm\lambda d\,z\frac{\mathbf{r}}{r^3}\,, \tag{1.104}$$

where r measures the distance between the test mass and the line element dz of the string with mass per unit length $\lambda = \mu - T$. Thus, the total attractive force towards the string becomes $F = 2mG\lambda/R$. If we now let the string move from $-\infty$ to ∞, we see that to first order the particle acquires a net velocity towards the x-z-plane of

$$v_y = -2G\lambda R\int_{-\infty}^{\infty}\frac{1}{R^2 + x_s(t)^2}d\,t\,, \tag{1.105}$$

where $x_s(t)$ is the x-coordinate of the string. Noting that $dt = d\,x_s/v_s$ we arrive at

$$v_y = -\frac{2\pi G(\mu - T)}{v_s}\,, \tag{1.106}$$

where we plugged in $\lambda = \mu - T$. This is of course nothing else than the non-relativistic limit of the first term in (1.103) derived in [135, 137]. To first order, the force in the x-direction averaged over the encounter cancels out. However, the velocity in the y-direction towards the x-z-plane in (1.106) induces a net drag behind the string. This is easily understood as follows: the test particle is closer to the plane during the departure of the string, resulting in a net force in the direction of the string movement. To derive the drag velocity, we first compute $v_y(x_s)$ in order to arrive at the particle's trajectory $y_m(x_s)$ to first order, which can then be used to evaluate v_x. Leaving the upper bound in (1.105) finite, we get

$$v_y(x_s) = v_0\left(1 + \frac{2}{\pi}\arctan(x_s/R)\right)\,, \tag{1.107}$$

where $v_0 = -\pi G\lambda/v_s$, so that

$$\begin{aligned} y_m(x_s) &= R + \frac{v_0}{v_s}\Bigg(x_s\left(1 + \frac{2}{\pi}\arctan(x_s/R)\right) \\ &\quad -\frac{R}{\pi}\ln(1 + x_s^2/R^2)\Bigg) \qquad (1.108) \\ &\approx R + \frac{v_0}{v_s}x_s\,, \qquad (1.109) \end{aligned}$$

where we set $y_m(0) = R$ and we expanded around $x_s/R = 0$ in the last step. Consider next the x-velocity

$$v_x = \frac{G\lambda 2}{v_s} \int_{-\infty}^{\infty} \frac{x_s}{y_m^2(x_s) + x_s^2} d\, x_s \,. \tag{1.110}$$

If we Taylor expand the integrand for $x_s \ll R$ we see that the term proportional to x in $y_m(x_s)$ causes a net drag velocity of $v_x \sim v_y^2/v_s$.

Based on the above, we see first of all that a straight string attracts matter towards its trajectory with a net velocity of $v_y \sim G(\mu - T)/v_s$ after the encounter. This velocity increases with a decrease of the string velocity v_s, since the plasma particle spends more time in closer proximity to the string so that the overall gravitational attraction is larger. This flow is obviously not rotational. Furthermore, due to the symmetry of the flow with respect to the x-z plane, there is no net momentum of the plasma after the encounter. We also computed the drag velocity $v_x \sim v_y^2/v_s$. This flow has a net momentum in the direction of the string movement and slows the string down. This flow is not rotational either.

1.7 Magnetic Fields

The existence of large-scale magnetic fields in galaxies and galactic clusters today is an observational signature of magnetism in the primordial universe (see [138–141] for reviews).

Faraday rotation measurements in galaxies and galactic clusters have confirmed the existence of fields in the μG range [139, 140, 142]. If magnetic fields of this strength were present in the very early universe, they would have drastically altered the history of structure formation [143–145]. This constraint suggests that magnetic fields formed at much weaker fluxes, then grew through some kind of dynamical amplification. While magnetohydrodynamic processes in such collapsed structures can magnify pre-existing magnetic fields in a process known as a dynamo, all presently known dynamo mechanisms require the existence of a magnetic seed field prior to the operation of an amplification mechanism.

Primordial magnetic seed fields cannot arise from first order scalar density perturbations present after simple models of inflation. Many out-of-equilibrium early universe processes can produce reasonably strong magnetic fields, but the fact that the observed cosmological magnetic fields are on scales of kiloparsecs means that any field formed in the very early universe would have to be expanded, after formation, to length-scales far larger than those on which it was formed. This expansion would have to be much faster

than the simple stretching due to the Hubble expansion. There are some proposals, such as inverse cascades, but whether they truly work or not is still under debate. In addition, the field strength suffers dramatically under this stretching, making it challenging to achieve the desired μG strength.

On the other hand, the non-perturbative remnants of early universe phase transitions can naturally exist on cosmological length scales and can survive far beyond the very early – and very tiny – epoch in which they were formed. In particular, cosmic strings, which are formed generically in braneworld models of inflation and which are present in many unified field theory models, are just such a non-perturbative artifact. We are going to examine the possibility to seed magnetic fields in string networks in chapter 5, but first we review the evolution of magnetic fields and alternative proposals of their origin.

For background material on the observations that have identified these fields, the operation of the dynamo mechanism, and other review material, see Refs. [139–141].

1.7.1 Possible Origins and Problems

When one thinks for a plausible explanation of large scale magnetic fields, inflationary perturbations come immediately to mind: such perturbations are naturally stretched to super-Hubble scales during inflation, so coherence length is not a problem. However, to first order in perturbation theory, the vector perturbations required to create magnetic fields decay with cosmic expansion. Thus any field generation caused by inflationary perturbations must be a second order effect [146]. A different approach asserts that fields initially formed at very small scales (through, for example, phase transitions), and were subsequently amplified by an "inverse cascade" arising from turbulent MHD processes [140, 147, 148].

Ultimately all of these mechanisms come up against the correlation length problem, which itself arises since causal mechanisms can only operate on sub-horizon scales: except for redshifts close to decoupling, such mechanisms produce fields on comoving lengths that are too small to explain the correlation length of fields observed in galaxies and clusters. For most mechanisms, this problem can only be solved by invoking large scale field averaging, inverse cascades, or the super-horizon correlations produced by cosmic inflation [147]. The speculative nature of these proposals is an indication of how challenging it is to generate fields with the proper length scales.

Another proposal, which we build upon in chapter 5, breaks up the problem into two separate challenges: first, a coherent, reasonably strong magnetic seed field is created before galaxy collapse, but not necessarily in the

very early universe. Thus, it is possible to achieve the needed correlation length by causal physics within the horizon. Thereafter, one needs an efficient amplification by means of a dynamo. Whether the latter is efficient enough or not is still uncertain. We will elaborate on this proposal below.

1.7.2 Harrison-Rees Mechanism

Harrison [149] considered a model in the radiation era, inside the Hubble radius, whereby a magnetic seed field is generated by vortical perturbations of the ionized plasma. He noted that a circular current develops when there is a differential rotational flow between ions and the electron-photon gas. Due to Thompson scattering non relativistic electrons are tightly coupled to the radiation bath; the result of this coupling is that the angular momentum of ions is damped more efficiently due to the expansion of the universe, than that of electrons. Hence, a net current carried by the electron fluid develops, which in turn generates the magnetic field. In analogy to Harrison's scheme, Rees [150] suggested a method by which the angular velocity of the electron fluid is hindered through Compton drag on the microwave background, while the ions remain unchanged.

If the vorticity is assumed to be present prior to decoupling, the magnetic field can be related to the vorticity by [151]

$$B = \frac{2m}{e}\omega_{plasma} \approx 10^{-4}\omega_{plasma}\,, \tag{1.111}$$

where ω_{plasma} has to be specified in 1/seconds to get B in Gauss. The problem with this mechanism, however, is that it can only produce magnetic fields when Compton scattering is efficient, which means that it ceases to work after decoupling.

1.7.3 Evolution since Matter-Radiation Equality and Constraints on Magnetic Seed Fields

Once magnetic fields are produced at a redshift z_F, their (proper) correlation length ξ grows with the expansion of the universe as

$$\xi(z) = \frac{1+z_F}{1+z}\xi(z_F), \tag{1.112}$$

and their field strength evolves according to

$$B(z) = \left(\frac{1+z}{1+z_F}\right)^2 B(z_F), \tag{1.113}$$

as a result of flux conservation. Once galaxy formation begins, the evolution of magnetic fields becomes far more complicated. As a protogalactic cloud becomes non-linear and begins to collapse, the correlation length decreases but the field strength is amplified. While there may be some amplification of the field during collapse [152,153], we assume that no dynamo is active at this stage and the field strength is primarily governed by flux conservation [154,155]. The net pre-dynamo amplification factor in a spiral galaxy can be estimated to [141][19].

$$\frac{B_i}{B_{gf}} \approx 8 \times 10^3 \,, \tag{1.114}$$

where $B_{gf} = B(z_{gf})$. Once the protogalactic cloud collapsed, the field can be amplified exponentially by a dynamo mechanism [141], such as the $\alpha\omega$-dynamo [20]. This dynamo begins operation when stellar winds and explosions generate interstellar turbulence, which transforms into cyclonic motions through the Coriolis forces associated with the galactic rotation [156, 157]. The magnetic field surrounding the galaxy has two modes, a toroidal and a poloidal component. The dynamo converts the poloidal to toroidal flux by differential rotation of the galactic disk (the ω-effect) and the toroidal to poloidal through cyclonic motions (the α-effect) [158]. The combined effects can amplify the magnetic field strength by many orders of magnitude [141, 158–160].

We parameterise the dynamo by an efficiency factor Γ_{dy}, such that Γ_{dy}^{-1} is the field strength e-folding time, and the field B_0 measured today is related to the initial field B_i by

$$\ln \frac{B_0}{B_i} = \Gamma_{dy} \left(t_f - t_i\right) \,, \tag{1.115}$$

where $t_i \gtrsim t_{gf}$ indicates the onset of dynamo amplification, $t_f \lesssim t_0$ is the time at which the fields reach the observed value and t_{gf} is the time at which the protogalactic cloud collapses. We take $t_i = t_{gf}$ and $t_f = t_0$ to arrive at the most optimistic lower bound of the seed field. The resulting amplification is weakly sensitive to the choice of t_{gf}, and here we take $t_{gf} = 475$ Myr, which corresponds to $z_{gf} = 10$. Although the value of Γ_{dy} is crucial to estimate the necessary seed field, its value is a matter of considerable debate.

In the literature, one finds many values for Γ_{dy} scattered in the range $0.2\,\mathrm{Gyr} < \Gamma_{dy}^{-1} < 0.8\,\mathrm{Gyr}$ [159, 161, 162]. Recently, some have contended

[19] This expression includes: formation of a halo, gain of angular momentum through tidal interactions with neighboring galaxies, and disc formation, see [141] for a review.

[20] The $\alpha\omega$-dynamo assumed here applies to galactic magnetic fields growing in discs only.

galaxy formation		Γ_{dy}^{-1}			
z_{gf}	t_{gf}	0.2 Gyr	0.3 Gyr	0.5 Gyr	1.0 Gyr
6	1 Gyr	3.8×10^{27}	2.4×10^{18}	1.1×10^{11}	3.3×10^{5}
10	475 Myr	($\star$) 5.2×10^{28}	1.4×10^{19}	3.1×10^{11}	5.5×10^{5}

Table 1.1: The amplification factor B_0/B_i, tabulated with a variety of assumptions regarding the time t_{gf} and redshift z_{gf} of galaxy formation and the efficiency Γ_{dy} of the galactic dynamo. The value we take to get the most optimistic lower bound on B_{seed} in (1.116) is marked with a "$\star$."

that even larger values, $\Gamma_{dy}^{-1} \gtrsim 1.1 - 1.4\,\mathrm{Gyr}$, are more likely [141]. The amplification factors for various choices of Γ_{dy} and t_{gf} are given in Table 1.1. To obtain the present field of $B_0 = 10^{-6}\,\mathrm{Gauss}$ under these assumptions, the field B_{seed} that must be present at decoupling with $z_{dec} = 1089$ is

$$B_{seed} \approx 2 \times 10^{-35}\,\mathrm{G}\,. \tag{1.116}$$

This is a very optimistic lower bound for the seed field at t_{dec}. For seed fields between this limit and $10^{-20}\,\mathrm{G}$, only the most efficient dynamos might work, though the existence of such dynamos in nature remains controversial [141].

In addition to constraints on its strength, the seed field must possess a sufficiently large correlation length. The correlation length after protogalactic collapse ξ_{gf} must satisfy $\xi_{gf} \geq 100\,\mathrm{pc}$ for the dynamo to commence [155]. Estimating the comoving correlation length x_{corr} before galaxy collapse (using a simple spherical collapse model for galaxy formation) leads to [155]

$$x_{corr} > \eta\, x_{gal} = 0.95\,\eta\,(\Omega_m h^2)^{-1/3} M_{12}^{1/3}\,[\mathrm{Mpc}]\,, \tag{1.117}$$

where $M_{12} = M/10^{12} M_{\odot}$, M is the mass of the galaxy, x_{gal} is the comoving length of the galaxy at formation, and η is the fraction of a galaxy over which the magnetic field has to be correlated. Taking $M_{12} \approx 0.1$ and $\eta \approx 1/150$ (corresponding to $\xi_{gf} \approx 100\,\mathrm{pc}$) yields

$$x_{corr} \approx 5.8\,\mathrm{kpc}\,, \tag{1.118}$$

Consequently, the seed fields must have a physical correlation length ξ_{seed} at decoupling of

$$\xi_{seed} = \frac{x_{corr}}{1 + z_{dec}} > \quad 5.4\,\mathrm{pc}\,. \tag{1.119}$$

which compares favorably with the particle horizon of about 200 kpc at $z \approx 1000$. Larger seed field correlation lengths are even better: the 5.4

pc minimum quoted here should cover only about 10% of the protogalactic cloud, which is only marginally adequate. A seed field with a longer length scale – say 50 pc – would comfortably imbue the whole protogalactic cloud with a single coherent field.

Chapter 2

Non-Gaussianity in N-flation

2.1 Introduction

Observations of the CMBR show a nearly scale-invariant spectrum of primordial perturbations. These perturbations are observable to us today because prior to re-entering the late universe, inflation stretches them out beyond the Hubble radius. Single field inflationary models exhibit nearly scale-invariant, almost Gaussian, adiabatic perturbations. Thus, deviations from purely Gaussian statistics allows, in principle, to discriminate between different incarnations of inflation, namely, single-field or multi-field inflationary models or scenarios involving the curvaton mechanism. Due to the fact that fluctuations freeze when their wavelength crosses the Hubble radius, non-Gaussianity in single field models are rather small, of order of slow roll parameters. For multi-field models, on the other hand, a deviation from a purely Guassian spectrum is expected; the reason being that the presence of multiple degrees of freedom perpendicular to the adiabatic direction allows for isocurvature perturbations; as a consequence the comoving curvature perturbation ζ can evolve after horizon crossing, leading to potentially larger non-Gaussianity. This is the case in curvaton models, where the sudden turn of trajectory in field space leads to a conversion of isocurvature perturbations into adiabatic ones while simultaneously causing reasonably large non-Gaussianities.

To quantify non-Gaussianities one needs to study higher order correlation functions, such as the bi- and tri-spectrum. As a case in point, the non-linearity parameter $f_{NL}^{(4)}$ introduced in (1.69) estimates non-Gaussianities measured by the bi-spectrum, otherwise known as the three-point correlation function. The WMAP3 data alone leads to $-54 < f_{NL} < 114$ by [6, 79, 80], but recent re-evaluations suggest $26.9 < f_{NL} < 146.7$ at 2σ [81] (see also [82]).

Future experiments such as Planck will improve upon these [84–87].

In this chapter we compute non-Gaussianities in $\mathcal{N}$-flation, a concrete realization of assisted inflation with an arbitrary, but large number of fields ($\mathcal{N} \gg 1$), quadratic, uncoupled potentials V_I and a known mass spectrum – see section 1.5.2 and 1.5.3. We use this model primarily because the known mass spectra makes an analytic approach possible. We focus on the non-linearity parameter f_{NL} and compute its magnitude for narrow and broad mass spectrum. We incorporate the evolution of modes after horizon crossing (HC), but stay within the slow roll regime in order to use analytic techniques. The formalism employed in this study was developed in [4], its application, however, was limited to simple toy models. A comparison with simple estimates as well as the HC-limit, which is re-derived for completeness, reveals that additional contributions due to the evolution of modes after horizon crossing are present, but their magnitude is limited to a few percent of the HC result.

This chapter is an abbreviated version of [1] and aimed to be easily accessible based on the foundation laid out in the introduction.

2.2 Obtaining Non-Gaussianities

In $\mathcal{N}$-flation the masses conform to the Marčenko-Pastur distribution (1.80). Inflation is achieved by the collective input of many scalar fields; it is thus appropriately called *assisted inflation*. The winning feature of these models lies in the fact that no field must traverse a super-Planckian stretch in field space. Further, the many existing axion fields in string theory provide suitable candidates for the many inflaton fields. We work specifically with the three-point correlation function and the associated non-linear parameter $f_{NL}^{(4)}$ from (1.69), within slow roll, to describe non-Gaussianities. In the horizon crossing approximation, assisted inflation is indistinguishable from its single field counterpart, where the evolution of modes is absent after horizon crossing, leading to indistinguishable spectra of scalar and tensor perturbations [18]. We compute $f_{NL}^{(4)}$ by the non-linear δN-formalism [27, 28], see section 1.4.1 and 1.5.1.

We begin by writing the unperturbed volume expansion rate from a flat hypersurface at t_* to a final hypersurface at t_c

$$N(t_c, t_*) \equiv \int_{t_*}^{t_c} H dt \,. \tag{2.1}$$

Consider $\mathcal{N} \sim 1000$ scalar fields responsible for driving inflation. Each of these fields is identified with axion fields; all cross-couplings vanish when

expanding the periodic axion potentials in the vicinity of their minima. Thus we can write this potential as

$$W(\varphi_1, \varphi_2, ...\varphi_{\mathcal{N}}) \;=\; \sum_{I=1}^{\mathcal{N}} V_I(\varphi_I)\,, \tag{2.2}$$

with $V_I = m_I^2\varphi_I^2/2$ and arrange the fields according to the magnitude of their masses, that is $m_I > m_J$ if $I > J$. The mass spectrum is evaluated by means of random matrix theory and conforms to the Marčenko-Pastur law [93], see section 1.5.3,

$$p(m^2) = \frac{1}{2\pi\beta m^2\sigma^2}\sqrt{(b-m^2)(m^2-a)}\,, \tag{2.3}$$

where σ is the average mass, set by the COBE normalization (see the end of section 1.4.1). $\beta \sim 1/2$ is identified as the ratio of the number of axions contributing to inflation to the total dimension of moduli space [93] and controls the width and shape of the spectrum. We treat β as a free parameter but note that due to constraints from the renormalization of Newton's constant, a value of $\beta = 1/2$ is preferred.

Let's define

$$x_A \;\equiv\; \frac{m_A^2}{m_1^2}\,, \tag{2.4}$$

$$z \;\equiv\; \sqrt{\beta}\,, \tag{2.5}$$

$$\xi \;\equiv\; \frac{m_{\mathcal{N}}^2}{m_1^2} = \frac{(1+z)^2}{(1-z)^2}\,., \tag{2.6}$$

so that expectation values with respect to the Marčenko-Pastur-distribution can be written as

$$\langle f(x)\rangle \;\equiv\; \frac{1}{\mathcal{N}}\sum_{A=1}^{\mathcal{N}} f(x_i)\,, \tag{2.7}$$

$$\;=\; \frac{(1-z)^2}{2\pi z^2}\int_1^{\xi}\sqrt{(\zeta-x)(x-1)}\frac{f(x)}{x}dx\,. \tag{2.8}$$

Since $f(x) = x^{\alpha+1}y^{\lambda x}$ will appear frequently in our analysis, we introduce a more convenient notation and define functions $\mathcal{F}_\alpha^\lambda$ by

$$\mathcal{F}_\alpha^\lambda(y) \equiv \mathcal{F}_\alpha(y^{\lambda\xi})\,, \tag{2.9}$$

where

$$\mathcal{F}_\alpha(\omega) \equiv \int_{1/\xi}^1 \sqrt{(1-s)(s-\xi^{-1})}s^\alpha\omega^s\,ds\,, \tag{2.10}$$

so that the expectation values become

$$\left\langle x^{\alpha+1} y^{\lambda x} \right\rangle = \frac{(1-z)^2}{2\pi z^2} \xi^{\alpha+2} \mathcal{F}_\alpha^\lambda(y)\,. \tag{2.11}$$

2.2.1 The $\mathcal{F}_\alpha$ Functions

Let us digress for a moment and gather some properties of the $\mathcal{F}_\alpha$ functions. First note that analytic expressions are known if $\omega = 1$: for $\alpha \geq -1$ the functions become [93, 100]

$$\mathcal{F}_\alpha(1) = 2\pi z^2 \frac{(1-z)^2}{(1+z)^{2(\alpha+1)}} \sum_{i=1}^{\alpha+1} \frac{1}{\alpha+1} \left(\begin{array}{c} \alpha+1 \\ i \end{array} \right) \left(\begin{array}{c} \alpha+1 \\ i-1 \end{array} \right) z^{2(i-1)}\,, \tag{2.12}$$

by relating $\mathcal{F}$ to the moments of the Marčenko-Pastur mass distribution, as analyzed in [100]. Furthermore, the expectation values $\langle x^{-1} \rangle$ and $\langle x^{-2} \rangle$ were computed in [93], yielding

$$\mathcal{F}_{-2}(1) = \frac{(1-z)^2}{1-z^2} \frac{\xi}{a}\,, \tag{2.13}$$

$$\mathcal{F}_{-3}(1) = \frac{(1-z)^4}{(1-z^2)^3} \frac{\xi^2}{a}\,, \tag{2.14}$$

with $a = (1-z)^2/2\pi z^2$.

We can also write down analytic expressions for general ω in the limit $\xi \to \infty$, which corresponds to the limit $z \to 1$: first note that

$$\bar{\mathcal{F}}_0(\omega) \equiv \lim_{z \to 1} \mathcal{F}_0(\omega) \tag{2.15}$$

$$= \frac{\pi \sqrt{y}}{2 \ln(y)} \mathcal{I}_1(\ln(y)/2)\,, \tag{2.16}$$

where $\mathcal{I}$ is a Bessel function of the first kind. All other $\bar{\mathcal{F}}_\alpha$ can be computed via recursion since

$$\mathcal{F}_{\alpha+1}(\omega) = \omega \frac{\partial \mathcal{F}_\alpha(\omega)}{\partial \omega}\,, \tag{2.17}$$

$$\mathcal{F}_{\alpha-1}(\omega) = \int_0^\omega \frac{1}{\tilde{\omega}} \mathcal{F}_\alpha(\tilde{\omega}) d\tilde{\omega}\,, \tag{2.18}$$

follows directly from the definition (2.10).

2.3 Slow Roll and Horizon Crossing Approximation

Since we restrict our analysis to the slow roll approximation, we can use the solution to the field equations in (1.78), that is

$$\frac{\varphi_I^c}{\varphi_I^*} = \left(\frac{\varphi_J^c}{\varphi_J^*}\right)^{m_I^2/m_J^2} . \tag{2.19}$$

Note that a unattractive feature of $\mathcal{N}$-flation is its dependence on initial conditions. This fact is crystallized by the fact that (2.19) is not an attractor solution. For the case of interest, a broad spectrum of masses with $\beta \sim 1/2$ leading to $\xi \sim 34$, the heavier fields drop out of slow roll before the lighter fields, even as inflation proceeds.

We want to estimate the magnitude of the three and four-point correlation function using the δN-formalism, as described in section 1.5.1. Thus, we would like to compute

$$-\frac{6}{5} f_{NL}^{(4)} = \frac{N_I N_J N^{IJ}}{(N_K N^K)^2} , \tag{2.20}$$

$$\tau_{NL} = \frac{N_{IJ} N^{IK} N^J N_K}{(N_L N^L)^3} , \tag{2.21}$$

$$g_{NL} = \frac{25}{54} \frac{N_{IJK} N^I N^J N^K}{(N_L N^L)^3} . \tag{2.22}$$

Since we assume that modes do not evolve once they cross the Hubble radius at t^*, we set

$$\varphi_I^c = 0 , \tag{2.23}$$

and because we make use of the slow roll approximation we have

$$N(t_c, t_*) = -\sum_{I=1}^{\mathcal{N}} \int_{\varphi_I^*}^{\varphi_I^c} \frac{V_I}{V_I'} d\varphi_I . \tag{2.24}$$

Using for simplicity equal energy initial conditions

$$m_I^2 \varphi_I^{*2} = m_J^2 \varphi_J^{*2} , \tag{2.25}$$

we obtain

$$N_I = \frac{V_I}{\sqrt{2\epsilon_I} W} , \tag{2.26}$$

$$N_{IJ} = \delta_{IJ} \left(1 - \frac{\eta_I V_I}{2\epsilon_I W}\right) , \tag{2.27}$$

$$N_{IJK} = 0 . \tag{2.28}$$

Here we replaced first derivatives with respect to φ_A^* by

$$V_I' = \sqrt{2\epsilon_I} W \,, \tag{2.29}$$

and all potentials and slow roll parameters, defined in section 1.5.2, are evaluated at t^*. The non-Gaussianity parameters evaluated to leading order in slow roll approximation become

$$-\frac{6}{5} f_{NL}^{(4)} = \frac{1}{2N} \,, \tag{2.30}$$

$$\tau_{NL} = \frac{1}{(2N)^2} \,, \tag{2.31}$$

$$g_{NL} = 0 \,. \tag{2.32}$$

Note that this result is independent of the mass spectrum of N-flation, and it is indistinguishable from that of single field inflationary models with a quadratic potential [76]. The value of g_{NL} is zero because the third derivative of a quadratic potential vanish. This result is expected since the evolution of perturbations after HC is neglected.

2.4 Beyond the Horizon Crossing Approximation

As we saw in the previous section, neglecting the evolution of perturbations leads to results that are indistinguishable from single field models. Here we would like to include the evolution of modes after horizon crossing, still within slow roll approximation. Under these conditions, the general expression of $f_{NL}^{(4)}$ was derived in [4]

$$-\frac{6}{5} f_{NL}^{(4)} = 2 \frac{\sum_{I=1}^{\mathcal{N}} \frac{u_I^2}{\epsilon_I^*} \left(1 - \eta_I^* \frac{u_I}{2\epsilon_I^*}\right) + \sum_{J,K=1}^{\mathcal{N}} \frac{u_J u_K}{\epsilon_J^* \epsilon_K^*} \mathcal{A}_{JK}}{\left(\sum_{L=1}^{\mathcal{N}} \frac{u_L^2}{\epsilon_L^*}\right)^2} \,, \tag{2.33}$$

where

$$u_I \equiv \frac{\Delta V_I}{W^*} + \frac{W^c}{W^*} \frac{\epsilon_I^c}{\epsilon^c} \,, \tag{2.34}$$

with

$$\Delta V_I \equiv V_I^* - V_I^c > 0 \,, \tag{2.35}$$

and the symmetric $\mathcal{A}$-matrix

$$\mathcal{A}_{JK} = -\frac{W_c^2}{W_*^2}\left[\sum_{I=1}^{\mathcal{N}} \epsilon_I \left(\frac{\epsilon_K}{\epsilon} - \delta_{KI}\right)\left(\frac{\epsilon_J}{\epsilon} - \delta_{JI}\right)\left(1 - \frac{\eta_I}{\epsilon}\right)\right]_c . \tag{2.36}$$

We evaluate this expression by first computing the field values at t_* and t_c. The needed $2\mathcal{N}$ conditions are given by: the $\mathcal{N}-1$ dynamical relations between fields from (2.19)

$$\frac{\varphi_1^c}{\varphi_1^*} = \left(\frac{\varphi_I^c}{\varphi_I^*}\right)^{m_1^2/m_A^2} , \tag{2.37}$$

the $\mathcal{N}-1$ initial values, chosen to satisfy equal energy initial conditions,

$$\varphi_I^* = \frac{m_1}{m_I}\varphi_1^* , \tag{2.38}$$

the requirement that t_* be N e-folds before t_c

$$4N = \sum_{I=1}^{\mathcal{N}} \left[(\varphi_I^*)^2 - (\varphi_I^c)^2\right] , \tag{2.39}$$

and lastly, demanding that a slow roll condition gets violated at least for one field at t_c, which in our case occurs when

$$\eta_{\mathcal{N}}^c = 1 . \tag{2.40}$$

Once we specify the masses, finding a solution for these conditions is possible. To this aim, we concentrate on two distinct cases: first, we consider narrow mass spectra with $\beta \ll 1$, which result in a simple analytic expression. Second, we study more realistic broad mass spectra for which $\beta \sim 1/2$.

2.5 Narrow Mass Spectra

For simplicity we consider narrow mass spectra ($\beta \to 0$), an unrealistic, yet easier case and we define

$$\delta_A \equiv 1 - \frac{m_1^2}{m_A^2} \ll 1 , \tag{2.41}$$

$$\delta \equiv \frac{1}{\mathcal{N}}\sum_{A=1}^{\mathcal{N}} \delta_A \ll 1 . \tag{2.42}$$

Using the Marčenko-Pastur distribution, we obtain a relation between δ and $z = \sqrt{\beta}$

$$\delta \;=\; 1 - \left\langle x^{-1} \right\rangle = 1 - \frac{(1-z)^2}{1-z^2}\,. \tag{2.43}$$

Using eqns (2.40)-(2.43) we can evaluate the field values φ_I^* and φ_I^c and the corresponding slow roll parameters. In [4] it was found that the second term in (2.33) becomes second order in the slow roll parameters and δ, that is

$$\frac{\sum_{J,K=1}^{\mathcal{N}} \frac{u_J u_K}{\varepsilon_J^* \varepsilon_K^*} \mathcal{A}_{JK}}{\left(\sum_{L=1}^{\mathcal{N}} \frac{u_L^2}{\varepsilon_L^*}\right)^2} \;=\; \mathcal{O}(\delta^2/N^2)\,. \tag{2.44}$$

By the same method, the first term in (2.33) becomes

$$\frac{\sum_{I=1}^{\mathcal{N}} \frac{u_I^2}{\varepsilon_I^*}\left(1 - \eta_I^* \frac{u_I}{2\epsilon_I^*}\right)}{\left(\sum_{L=1}^{\mathcal{N}} \frac{u_L^2}{\varepsilon_L^*}\right)^2} = \frac{1}{2(2N+1)}\left(1 - \frac{\delta_{\mathcal{N}} - \delta}{2N+1}\right) + \mathcal{O}(\delta^2)\,, \tag{2.45}$$

which includes a contribution proportional to $1/N$ as exhibited in the expression for the horizon crossing approximation. Therefore we obtain all in all

$$-\frac{6}{5} f_{NL}^{(4)} = \frac{1}{(2N+1)}\left(1 - \frac{\delta_{\mathcal{N}} - \delta}{2N+1}\right) + \mathcal{O}(\delta^2)\,, \tag{2.46}$$

where we only kept the leading order contribution in δ. If we now use (2.43) and

$$\delta_{\mathcal{N}} = 1 - \frac{(1-z)^2}{(1+z)^2}\,, \tag{2.47}$$

we attain after expanding in $z = \sqrt{\beta}$ our first major analytic result:

$$-\frac{6}{5} f_{NL}^{(4)} = \frac{1}{(2N+1)}\left(1 - \frac{2\sqrt{\beta}}{2N+1}\right) + \mathcal{O}(\beta)\,. \tag{2.48}$$

Comparing this expression with (2.30) we see an extra term proportional to $\sqrt{\beta}$. This term vanishes if all the masses are the same, as expected in this case since modes would not evolve after horizon crossing. On the other hand, for a mass distribution of non-zero width, isocurvature modes are sourced, leaving an imprint onto $f_{NL}^{(4)}$. From this result we conclude that if the mass spectrum is narrow, single field models of inflation and multi-field models, such as N-flation, are indistinguishable during slow roll with respect to the bi-spectrum.

2.6 Broad Mass Spectra

The preferred mass spectrum for $\mathcal{N}$-flation is the broad mass spectrum with $\beta \sim 1/2$. Here we compute the exact value of $f_{NL}^{(4)}$ for this case and compare it to the small β expansion obtained in (2.48).

2.6.1 Computation and Results

As we saw in section 1.5.3, the mass spectrum in $\mathcal{N}$-flation conforms to the Marčenko-Pastur distribution (1.80). To compute $f_{NL}^{(4)}$ we proceed as follows: first, we calculate the field values at t^c and t^* using (2.37)-(2.40), where we take t^* to be the time when the heaviest mass violate the slow roll condition (2.40); since there is no cross coupling between fields, the remaining fields can proceed to drive inflation. That is, t^* does not correspond to the end of inflation if the mass spectrum is stretched out. After t^c several e-folds of inflation are expected, which means that the volume expansion rate may be smaller than the usual $N \sim 60$. Second, we compute the potential and slow roll parameters in (2.33)-(2.36). Finally, given the expectation values (2.8) and (2.11) we evaluate all sums in (2.33).

Firstly, we compute the field values φ_1^* and $\varphi_1^c \equiv \varphi_1$ (we drop the superscript "c" from here on): inserting (2.19) into (2.38) we obtain

$$\varphi_1^{*2} = \frac{4N}{\mathcal{N}} \frac{1}{\langle x^{-1} \rangle - \langle x^{-1} y^x \rangle} \tag{2.49}$$

where all sums are replaced by the expectation values introduced in (2.8), and we defined

$$y \equiv \frac{\varphi_1^2}{\varphi_1^{*2}} . \tag{2.50}$$

Furthermore, after using (2.19), (2.38) and (2.49) in (2.40) we obtain the uncoupled equation

$$\frac{\xi}{2N} = \frac{\langle y^x \rangle}{\langle x^{-1} \rangle - \langle x^{-1} y^x \rangle} . \tag{2.51}$$

This equation needs to be solved for y. Using the definition (2.11), (2.51) can be equivalently written as

$$0 = 1 - 2N \frac{\mathcal{F}_{-1}^1(y)}{\mathcal{F}_{-2}^0 - \mathcal{F}_{-2}^1(y)} . \tag{2.52}$$

To solve this equation, we employ a standard numerical routine as implemented in MAPLE, and we denote the solution to (2.52) with $\bar{y}(\beta)$ (see

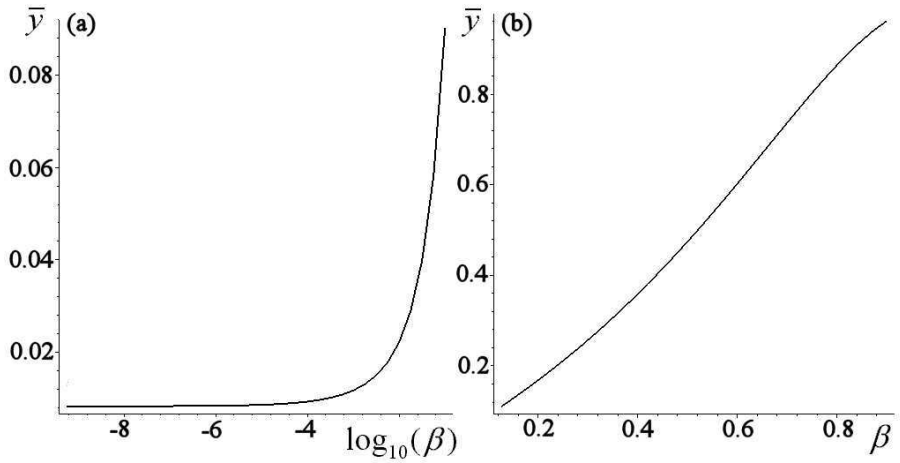

Figure 2.1: Solving (2.52) numerically leads to $\varphi_1^2/\varphi_2^{*2} \equiv \bar{y}(\beta)$ for (a) $-9 \leq \log_{10}(\beta) \leq -1$, (b) $0.1 \leq \beta \leq 0.9$. We took $N = 60$ in all plots.

Fig. 2.1 for a plot of $\bar{y}$ over β for $N = 60$). From here on all $\mathcal{F}$-functions are to be evaluated at $\bar{y}$.

The field values φ_I^{*2} and φ_I^2 and slow roll parameters can be computed in a straightforward, but tedious way (see [1] for details).

The value of u_I in (2.34) appearing in (2.33) becomes

$$u_I = \frac{1}{\mathcal{N}} \left(1 - \bar{y}^{x_I} + \bar{c} x_I \bar{y}^{x_I}\right) , \tag{2.53}$$

where we defined

$$\bar{c} \equiv \frac{\mathcal{F}^0_{-2} - \mathcal{F}^1_{-2}}{2N\xi\mathcal{F}^1_0} . \tag{2.54}$$

After some more algebra, we can evaluate the two components of $f_{NL}^{(4)}$ in (2.33)

$$-\frac{6}{5} f_{NL}^{(4)}(\beta) \;=\; 2\left(f(\beta) + F(\beta)\right) . \tag{2.55}$$

to

$$f(\beta) \;\equiv\; \frac{\sum_{I=1}^{\mathcal{N}} \frac{u_I^2}{\varepsilon_I^*}\left(1 - \eta_I^* \frac{u_I}{2\epsilon_I^*}\right)}{\left(\sum_{L=1}^{\mathcal{N}} \frac{u_L^2}{\varepsilon_L^*}\right)^2} \tag{2.56}$$

$$\begin{aligned} &= \frac{\mathcal{G}}{4N\alpha} \times \left(\mathcal{F}^0_{-2} - \mathcal{F}^1_{-2} - \mathcal{F}^2_{-2} + \mathcal{F}^3_{-2} + \bar{c}\xi\left[\mathcal{F}^1_{-1} + 2\mathcal{F}^2_{-1} - 3\mathcal{F}^3_{-1}\right]\right. \\ &\quad \left. + \bar{c}^2\xi^2\left[-\mathcal{F}^2_0 + 3\mathcal{F}^3_0\right] - \bar{c}^3\xi^3\mathcal{F}^3_1\right) \\ &\quad \times\Big(\left(\mathcal{F}^0_{-2} - 2\mathcal{F}^1_{-2} + \mathcal{F}^2_{-2} - 2\bar{c}\xi\left[\mathcal{F}^2_{-1} - \mathcal{F}^1_{-1}\right] + \bar{c}^2\xi^2\mathcal{F}^2_0\right)^2\Big)^{-1} \end{aligned} \tag{2.57}$$

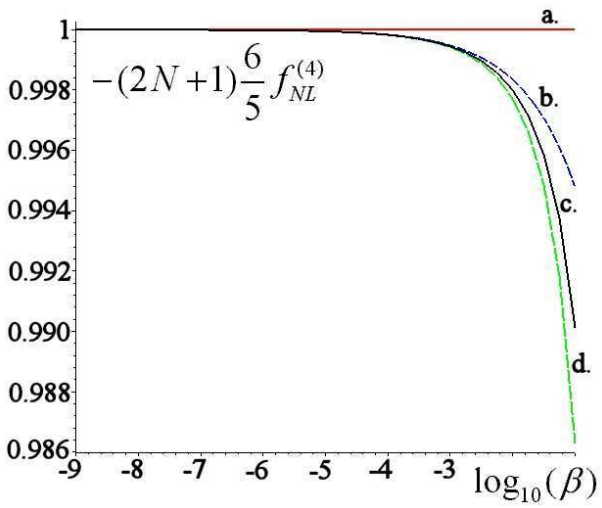

Figure 2.2: $-f_{NL}^{(4)}(2N+1)6/5$ over $\log_{(10)}(\beta)$ computed using: a. the horizon crossing approximation $-f_{NL}^{(4)}(2N+1)6/5 = 1$, b. the δ-expansion from (2.48), c. the "exact" expression from (2.55) and d. the approximation from (2.62). We took $N = 60$ in all plots. Note that b. and d. are both good approximations up until $\beta \sim 0.1$.

and

$$F(\beta) \equiv \frac{\sum_{J,K=1}^{\mathcal{N}} \frac{u_J u_K}{\varepsilon_J^* \varepsilon_K^*} \mathcal{A}_{JK}}{\left(\sum_{L=1}^{\mathcal{N}} \frac{u_L^2}{\varepsilon_L^*}\right)^2} \tag{2.58}$$

with

$$\alpha \equiv \frac{(1-z)^2}{2\pi z^2}\,, \tag{2.59}$$

$$\mathcal{G} \equiv \alpha\left(\mathcal{F}_{-2}^0 - \mathcal{F}_{-2}^1\right)\,. \tag{2.60}$$

The analytic, yet cumbersome, expression for F can be found in [1]. This is our second major result.

2.6.2 Discussion

A plot of $f_{NL}^{(4)}$ versus β can be found in Figures 2.2 and 2.3. In these figures we compare the analytic approximation (2.48), the horizon crossing approximation $-f_{NL}^{(4)}6/5 = 1/(2N+1)$ and the approximation in (2.62) with the full analytic result (2.55). The approximation in (2.48) is good in the range $\beta \leq \bar{\beta} \sim 1/10$. In this region, the leading order contribution to the exact

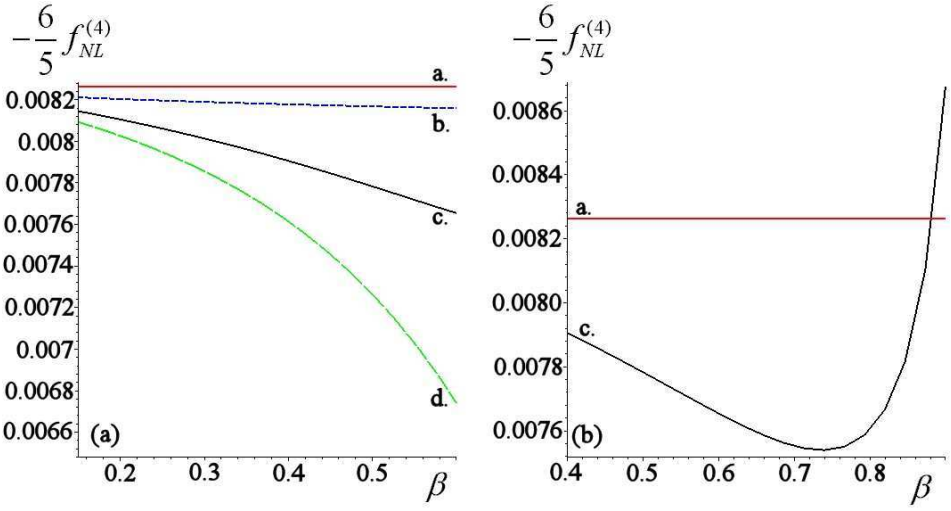

Figure 2.3: $-f_{NL}^{(4)}6/5$ over β computed using: a. the horizon crossing approximation $-f_{NL}^{(4)}(2N+1)6/5 = 1$, b. the δ-expansion from (2.48), c. the exact expression from (2.55) and d. the approximation from (2.62). We took $N = 60$ in all plots. Note that both approximations fail to recover the turn of $f_{NL}^{(4)}$ observable in Figure (b).

expression in (2.55) originates from the prefactor in (2.57), which includes a dependence on β via $\mathcal{G}$ defined in (2.60), and the first summands. Hence we may also use

$$-\frac{6}{5} f_{NL}^{(4)}(\beta) \approx \frac{\mathcal{G}}{2N\alpha} \frac{1}{\mathcal{F}_{-2}^{0}} \tag{2.61}$$

$$= \frac{1}{2N} \frac{\mathcal{F}_{-2}^{0} - \mathcal{F}_{-2}^{1}}{\mathcal{F}_{-2}^{0}} \tag{2.62}$$

as an approximation for small β. Here $\mathcal{F}_{-2}^{0} = (1-z)^2/(1-z^2)$ from (2.13) and $\mathcal{F}_{-2}^{1}(\bar{y})$ is defined in (2.9) where $\bar{y}(\beta)$ is the solution to (2.52). Naturally, we recover the horizon crossing result in the limit $\beta \to 0$.

Both, the δ-expansion and the above approximation in (2.62), fail for $\beta \sim 1/2$, see Fig. 2.3. However, the contribution due to F defined in (2.58) is negligible even for very broad spectra (e.g. up to $\beta = 9/10$ in Fig. 2.3 b), in agreement with the conclusions of [4], where two-field models with a large ratio of the two masses are solved analytically and an additional slow roll suppression is found for F. Hence we may use

$$f_{NL}^{(4)} \approx -\frac{5}{3} f(\beta) \tag{2.63}$$

as an approximation in the preferred region of $\mathcal{N}$-flation, $\beta \sim 1/2$. In this region, the magnitude of $-f_{NL}^{(4)}$ is a few percent smaller than the horizon crossing result (see Fig. 2.3). Such a deviation will never be observable. The minimum is reached for $\beta \approx 0.74$ and $-f_{NL}^{(4)}$ increases for larger values of β so that it intersects the horizon crossing result around $\beta \approx 0.88$. For even larger values of β the magnitude of the non-linearity parameter increases to a point where it becomes significantly large. However, in the limit $\beta \to 1$ this result should be taken with caution since it corresponds to an infinitely broad mass spectrum. In the above result, we took the final time t_c to be the time at which the heaviest field leaves slow roll and we assumed that sixty e-folds of inflation occurred between t_* and t_c. However, if the spectrum of masses is indeed very broad, there will be a considerable amount of inflation even after the heaviest fields leave/left slow roll; hence, the potentially large value for $-f_{NL}^{(4)}$ at t_c might very well be a transient phenomenon, due to a few heavy fields. Note that according to the Marčenko-Pastur distribution the majority of fields will have relatively light masses in the broad spectrum case, see Figure 2.1 and that the majority of the masses are smaller than the average one for β close to one. As a result, one might actually neglect the few heavy fields altogether, meaning, one might want to truncate the mass spectrum, since heavy fields will rapidly settle in their minimum. Naturally, once a field leaves slow roll, our formalism is not applicable any more up until the field settled in its minimum.

It is beneficial at this point to stress the limitations of our approach: first, we focused on potentials without cross-couplings between fields. In the case of $\mathcal{N}$-flation it is arguable that vanishing or very small couplings are the norm if the fields remain close to the minima of their potential [93]. Nevertheless, such an assumption is rather artificial, especially if we assume that the initial field values are randomly chosen in the interval $[0 \dots m_{pl}]$ [1]. The presence of such couplings could lead to an enhanced production of non-Gaussianities. Second, we considered only quadratic potentials with mass spectra conforming to the Marčenko-Pastur distribution $\beta \sim 1/2$. This class is desirable since the MP-distribution properly describes the spread of masses in the large $\mathcal{N}$ limit, though we do not expect qualitative differences for other spectra. If on the other hand the potentials are not quadratic, but say quartic, or even exponential, we expect additional suppression since an attractor solution is present for potentials of this type (see e.g. [90]); then, isocurvature perturbations will be suppressed and in turn any evolution of modes after horizon crossing will also be suppressed, resulting in an addi-

[1] We thank F. Quevedo for useful comments regarding this point. Naturally, this means that the conditions for successful assisted inflation are hard to satisfy.

tional reduction of non-Gaussianities. Finally, we considered equal energy initial conditions, mainly for simplicity. Since there is no attractor solution for quadratic potentials, there is a dependence on the chosen initial state. This unavoidable sensitivity to the initial configuration of fields is a serious flaw of $\mathcal{N}$-flation, since the model becomes less predictive. However, the evident slow roll suppression of non-Gaussianities is insensitive to the chosen initial state, see e.g. the two-field cases studied in [4].

2.7 Conclusion

First, we evaluated the non-linearity parameters characterizing the bi and tri-spectrum in the horizon crossing approximation. In this limit $\mathcal{N}$-flation and single field inflationary models are indistinguishable. To lift this degeneracy, we incorporated the evolution of perturbations after horizon crossing, which is merited to the presence of isocurvature modes. Taking into account this evolution allows the possibility to differentiate between models, at least in principle. Since f_{NL} is a measure of the strength of the bi-spectrum and since it is expected to be constraint by near-future observations, we focused on this non-linearity parameter. We computed analytically the magnitude of f_{NL} for narrow and generic mass distributions, including broad ones that are favored in $\mathcal{N}$-flation. Additional contributions were found, but they constitute only a few percent of the horizon crossing result at most, leading to the conclusion that they will never be observable. The insignificance of these additional terms is primarily owed to the slow roll approximation employed in this study. However, larger, but perhaps transient contributions to f_{NL} should be expected from fast rolling fields, which might be present in multi-field inflationary models other than $\mathcal{N}$-flation.

Chapter 3

Non-Gaussianity Beyond Slow Roll?

3.1 Introduction

In chapter 2 we found that multi-field models of inflation such as $\mathcal{N}$-flation do not generate large non-Gassianities during slow roll. Here we consider non-Gaussianity beyond slow roll. In other words, we want to investigate analytically the evolution in $\mathcal{N}$-flation after the slow roll condition is violated for one or more of the axion fields and to establish whether non-Gaussianities are generated. The general setup, notation and conventions are identical to the previous chapter, with one notable exception: the field index will be denoted with small latin indices $i, j, k, \ldots$ instead of $I, J, K, \ldots$, since we would like to use I and II to indicate two different effective single field models.

3.2 Effective Single Field Models during Inflation

Given equal energy initial conditions for the $\mathcal{N}$ axion fields, the slow roll parameter $\eta_{\mathcal{N}}$ of the heaviest field will be the first one to become of order unity [4]. During the preceding slow roll stage, non-Gaussianities are heavily suppressed, see chapter 2. During slow roll, we can safely implement an effective model composed of a single field σ which evolves according to an effective potential $W_{eff}(\sigma)$, as introduced in section 1.5, equation (1.61). However, after $\eta_{\mathcal{N}}$ became of order one, the corresponding field $\varphi_{\mathcal{N}}$ does not speed up but slows down, since $\eta_{\mathcal{N}} > 0$. Furthermore, the corresponding

potential energy $V_{\mathcal{N}}$ is very small compared to that of the lighter fields; this is due to the fact that $\varphi_{\mathcal{N}}$ was the fastest rolling field up until this stage. This particular behavior has two important consequences: first, if we were to continue using the effective description with σ and $W_{eff}(\sigma)$, we arrive at a lower bound to the true evolution of the total potential energy. Second, if we were to hold $\varphi_{\mathcal{N}}$ fixed after $\eta_{\mathcal{N}}$ became of order one, we arrive at an upper bound to the true evolution. Additionally, owing to the comparatively small energy stored in the heavy field, the difference between the lower and the upper bound will be equally small. Naturally, it is possible to continue in a similar manner when the next heaviest field violates slow roll and so on and so forth, up until either the total energy in the heavy fields becomes comparable to the one in the remaining light fields, or slow roll fails for σ, after which light fields will actually start to evolve faster and pre-heating starts, a subject which we will delve into in chapter 4.

On account of both approximations corresponding to slowly evolving fields, non-Gaussianities will not be generated during that regime. The reason for this is that additional non-Gaussianities are attributed to the evolution of the adiabatic mode ζ after horizon crossing. In order for this to occur, isocurvature modes, which are present in $\mathcal{N}-$flation, have to source the adiabatic one. However, the source-term in the equation of motion for ζ is proportional to the curvature of the trajectory in field space, which is small when fields evolve slowly. Only a sharp turn will lead to an enhancement of the non-Gaussianity; for instance, if the evolution of a field becomes indeed faster.

In the following subsections, we derive the two approximations mentioned above. It is important to note that we can trust our approximations up until preheating starts, where there might be a possibility for the appearance of non-Gaussianity.

We will see that the actual difference between the two approximations, that is the difference between the two potential energies, is quite small. This is the reason why we can use the slow roll approximation to set the initial stage for preheating, even if the slow roll conditions are violated for the majority of fields.

3.2.1 A Lower Bound on W

Here we derive an effective single-field model based on the slow roll approximation, which supplies a lower bound to the evolution of the total potential energy. As introduced in section 1.5, we identify the effective inflaton field σ as the path-length of the trajectory in the $\mathcal{N}$ dimensional field space. For instance, for $\mathcal{N}$ scalar fields φ_i we defined (1.61) with (1.62) [69]. To reit-

erate, the φ_i can be computed given the dynamical relations (2.37), which are valid during slow roll, as well as the initial conditions (2.38). Note that $\sigma = 0$ at the initial time t_*. We introduce a variable to parametrize how far the lightest field rolled down its potential

$$y \equiv \frac{\varphi_1^2}{\varphi_i^{*2}} \,. \tag{3.1}$$

Since y is smoothly decreasing in time up until reheating commences, we may also use y as a time variable. Further, we use again the dimensionless mass variable $x_i \equiv m_i^2/m_1^2 \geq 1$ so that we can rewrite the dynamical relations in (1.78) as

$$\varphi_i^2 = \varphi_1^{*2} \frac{y^{x_i}}{x_i} \,. \tag{3.2}$$

Since we would like to avoid super-Planckian initial conditions we set

$$\varphi_1^* \equiv 1 \,, \tag{3.3}$$

so that

$$\varphi_i^2 = \frac{y^{x_i}}{x_i} \,. \tag{3.4}$$

Moreover the Klein Gordon equations during slow roll along with the Friedman equation yield

$$\dot{\varphi}_i^2 = m_1^4 \frac{x_i y^{x_i}}{3W} \,, \tag{3.5}$$

so that the differential of y becomes

$$dy = -\frac{2m_1^2 y}{\sqrt{3W}} dt \,, \tag{3.6}$$

with

$$W = \frac{1}{2} m_1^2 \sum_{i=1} y^{x_i} \,. \tag{3.7}$$

Using the above, the effective single field (1.61) becomes

$$\sigma_I(y) = \int_y^1 \left(\sum_{i=1}^{\mathcal{N}} x_i s^{x_i} \right)^{1/2} \frac{ds}{2s} \tag{3.8}$$

$$= \frac{\sqrt{\mathcal{N}}}{2} \int_y^1 \sqrt{\langle x s^x \rangle} \frac{ds}{s} \,, \tag{3.9}$$

where we used the definition of the expectation values from (2.8) in the last step. Similarly, the corresponding potential in (3.7) can be computed to

$$W_I(y) = \mathcal{N}\frac{m_1^2}{2}\langle y^x\rangle \,, \tag{3.10}$$

where m_1 is related to the average mass m_{avg}, which is set by the COBE normalization (see the end of section 1.4.1) by

$$m_1^2 = m_{avg}^2(1-z)^2 \,. \tag{3.11}$$

Equations (3.9) and (3.10) provide an implicit means of computing $W_I(\sigma_I)$, see Figure 3.2. Using the definition of the expectation values (2.8), the number of e-folds from (1.75) becomes

$$\begin{aligned} N(y) &= \frac{1}{4}\sum_{i=1}^{\mathcal{N}}\frac{1}{x_i} - \sum_{i=1}^{\mathcal{N}}\frac{y^{x_i}}{x_i} && (3.12)\\ &= \frac{1}{4}\mathcal{N}\left[\left\langle x^{-1}\right\rangle - \left\langle x^{-1}y^x\right\rangle\right] \,. && (3.13) \end{aligned}$$

If we take $\mathcal{N} = 1500$ we get $N_{max} \equiv N(0) \approx 64.3$, which is large enough to solve the standard cosmological problems. Here and in the following we use the preferred $\beta = 1/2$ so that the ratio of the heaviest to the lightest mass squared in (1.82) is about $\xi \approx 34$. It is important to realize at this point that one cannot use (3.9) and (3.10) up until $y = 0$, since slow roll ends earlier. Strictly speaking, our first solution is only valid as long as the slow roll conditions are satisfied, that is until $\eta_{\mathcal{N}} = 1$. This condition determines $\bar{y}$ along with the definition of ξ (2.6) as the solution of

$$\langle \bar{y}^x\rangle \frac{\mathcal{N}}{2\xi} = 1 \,, \tag{3.14}$$

resulting in $\bar{y} \approx 0.487$. The number of e-folds at this instant is $N(\bar{y}) \approx 55.6$ and we see that there is still a breadth of inflation to come. If we ignore this fact, we could use σ_I up until this effective degree of freedom leaves its own slow rolling regime when

$$\epsilon_\sigma \equiv \frac{1}{2}\left(\frac{W_I'}{W_I}\right)^2 = 1 \,. \tag{3.15}$$

This equation can be rewritten as

$$2\langle xy^x\rangle = \mathcal{N}\langle y^x\rangle^2 \,, \tag{3.16}$$

where we used

$$W_I' \equiv \frac{\partial W_I}{\partial \sigma_I} = \sum_{i=1}^{\mathcal{N}} \hat{\sigma}_i \frac{\partial V_i}{\partial \varphi_i} \tag{3.17}$$

$$= \sum_{i=1}^{\mathcal{N}} \hat{\sigma}_i m_i^2 \phi_i \tag{3.18}$$

$$= -m_1^2 \sqrt{\mathcal{N} \langle x y^x \rangle}\,. \tag{3.19}$$

Equation (3.16) can be solved to obtain $y_{end} \approx 0.084$ so that $\sigma_I(y_{end}) \approx 17.6$ and $N(y_{end}) \approx 63.8$, indicating that inflation comes to an end and pre-heating is about to commence. The potential at this instant is about $W_I(y_{end}) \approx 0.13 m_{avg}^2$. The solution provides a lower bound for the potential energy at the end of inflation, $W_{end} > W_I(y_{end})$, because the heavy fields evolve slower than it was previously assumed. In the next section we derive an upper bound on the potential energy and discuss its implications.

3.2.2 An Upper Bound on W

As mentioned in the previous section, σ_I and W_I from (3.9) and (3.10) can only be used as long as the slow roll conditions for all fields are satisfied, that is up until $\bar{y}$ from (3.14). Heavy fields will violate $\eta_i < 1$ first and thereafter they will evolve slower than anticipated due to the positive η. Thus, in order to derive an upper bound on the potential energy, we could hold fields fixed as soon as their slow roll parameter becomes equal to one. Naturally, dealing with $\mathcal{N} = 1500$[1] fields complicates the picture substantially. On that account, in order to simplify matters we can proceed by first taking the continuum limit so that we can make use of the Marčenko-Pastur law for the continuous mass variable $1 \leq x \leq \xi$. Second, we partition this interval into $\mathcal{M}$ bins according to a simple rule and denote the upper boundaries of each bin with X_A, $A = 1, \ldots, \mathcal{M}$, so that $X_{\mathcal{M}} = \xi$. Third, whenever η_A (corresponding to some X_A) becomes of order one, we hold fixed all fields with masses in the $(A+1)$'th bin. Naturally, one recovers the full microscopic model if one takes $\mathcal{M} = \mathcal{N} - 1$ and uses the Marčenko-Pastur law as a rule for choosing the bins so that $X_A = x_{A-1}$. If $\mathcal{M} < \mathcal{N} - 1$, one gets a more tractable model but with a larger estimate for W. In practice $\mathcal{M} \sim 50$ is fully satisfactory for our purposes. The validity of this approximation is justified as long as the energy left in the heavy fields is small compared to the energy in the light fields; this will suffice for the range of y-values that we are interested in.

[1] We choose $\mathcal{N} = 1500$ fields in order to achieve $N > 60$ with sub-Planckian initial field values, see Table 3.1. Note that this number of axions is attainable within string theory.

Naming the above described solution as W_{II} (and σ_{II}), we arrive at $W_I < W < W_{II}$, where W is the true value of the potential energy. At this point, we would like to bring out a subtlety in our model, $\sigma_I(y)$ does not need to coincide with $\sigma_{II}(y)$ for two reasons. Firstly, a number of fields are artificially held fixed and no longer contribute to the path length σ. Secondly, since the total potential energy is bigger, the light fields evolve slightly slower in the second approximation. These two points yield only small corrections since the fields which we held fixed are already near the minimum of their potential. At that stage, they would not, anyhow, contribute much to σ. Moreover, we only use the second approximation if the energy in the fixed fields is small as compared to that of the dynamical ones. Consequently, we have $y_{II} \sim y_I$ and $\sigma_{II} \sim \sigma_I$.

We now proceed to compute W_{II} and σ_{II} as outlined above. We assume first a partition $\{X_1, \ldots, X_{\mathcal{M}}\}$ of the interval $1 \leq x \leq \xi$ and denote with Y_A the values of y where $\eta_{(\mathcal{M}-A+1)} = 1$ (note that $Y_A < Y_B$ if $A > B$). If we further denote the energy W_{II} that is valid in the range $Y_A < y < Y_{A-1}$ with W_A, we can calculate the corresponding Y_A as the solution to

$$W_A(Y_A) = m_1^2 X_{\mathcal{M}-A+1}\,, \tag{3.20}$$

starting with $W_1 \equiv W_I$ from the previous section. Note that $Y_1 = \bar{y}$ from (3.14), as it should. We can then compute W_A for $A \geq 2$ to

$$W_A(y) = \frac{m_1^2 \mathcal{N}}{2} \left(\langle y^x \rangle \Big|_1^{X_{\mathcal{M}-A+1}} + \sum_{n=1}^{A-1} \langle Y_n^x \rangle \Big|_{X_{M-n}}^{X_{M-n+1}} \right) . \tag{3.21}$$

Similarly, if we denote with σ_A the effective field which is valid in the range $Y_A < y < Y_{A-1}$ (so that $\sigma_1 = \sigma_I$), we arrive at

$$\sigma_A(y) = \sigma_{A-1}(Y_{A-1}) + \frac{\sqrt{\mathcal{N}}}{2} \int_y^{Y_{A-1}} \frac{1}{s} \sqrt{\langle x s^x \rangle \Big|_1^{X_{M-A+1}}}\, ds\,, \tag{3.22}$$

and finally the number of e-folds becomes

$$N_A(y) = N_{A-1}(Y_{A-1}) + \int_{Y_A}^{Y_{A-1}} \frac{W_A(y)}{2 m_1^2 y} dy\,, \tag{3.23}$$

with $Y_0 = 1$.

In the large $\mathcal{M}$-limit the above approximation becomes independent of the partition, which is of course our aim. We would like to use W_{II} up to when W_I is no longer a viable lower bound for the true energy W, that is, until $\sigma \approx \sigma_I(y_{end})$. This is possible if we limit the first bin by $X_1 = 1.75$

while partitioning the remaining interval $X_1 < x < \xi$ into $\mathcal{M} - 1 = 49$ bins, according to Figure 3.1. That way, we achieve $\sigma_{II}(Y_\mathcal{M}) = \sigma_I(y_{end})$ with an energy ratio of

$$R \equiv \frac{W_{heavy}}{W_{light}} \tag{3.24}$$

$$= \frac{\frac{2}{\mathcal{N}m_1^2} W_{II}(Y_\mathcal{M}) - \langle Y^x_\mathcal{M} \rangle \Big|_1^{X_1}}{\langle Y^x_\mathcal{M} \rangle \Big|_1^{X_1}} \tag{3.25}$$

$$\approx 0.53\,, \tag{3.26}$$

which is still smaller than one, so that we can trust our approximation [2]. The number of light fields, that is fields in the first bin which are still dynamical at $Y_\mathcal{M}$, is about 70.

In addition, the ratio of the potential energies is

$$\frac{W_{II}(Y_\mathcal{M})}{W_I(y_{end})} \approx 1.17\,, \tag{3.27}$$

with the real total potential energy sitting snugly between $W_I(y_{end}) < W_{end} < W_{II}(Y_\mathcal{M})$. In other words the difference between the two approximations is 17% whereby roughly twice as much energy is in the light fields as compared to the heavy ones. Duly, we are justified in using our first approximation, which corresponds to using slow roll for all fields, to set the initial conditions for preheating, even though the slow roll condition $\eta < 1$ is violated for the majority of fields; see also Figure 3.3, where it is evident that the heavy fields do not contribute much to the total potential energy and correspondingly, inflation.

3.3 Discussion

The approximations of the previous two sections can be visualized in Figure 3.2, which shows an exaggerated schematic for the potential W versus the path length of the trajectory in field space, σ. In region A all fields roll slowly, corresponding to the first approximation derived in section 3.2.1; region B shows an additional upper bound to the true evolution, for which fields with heavy masses are successively held fixed. This second approximation is described in section 3.2.2. Finally, region C starts at the breakdown

[2] Remember, if $R > 1$ one can not trust the approximation, since the heavy fields, which we held fixed by hand, would dominate the dynamics of the Hubble factor.

of slow roll for the effective degree of freedom σ_I when $\epsilon_{\sigma_I} \sim 1$, indicating the end of inflation and the onset of preheating. Figure 3.3 provides the actual plot of W_I and W_{II} vs the path length σ_I and σ_{II}. Note that the two curves are nearly indistinguishable up until slow roll breaks down for σ_I; furthermore, it is apparent from Figure 3.3 that the number of e-folds is insensitive to the approximation used. We compare the upper and lower bound solution in table 3.2, where we also vary the number of fields. It is evident that the solutions approach each other in the large $\mathcal{N}$ limit[3]. Henceforth, the numerical solution is well approximated by either one in the case of $\mathcal{N}$-flation, where we deal with thousands of fields, and consequently, we are justified to use the slow roll approximation to set the initial stage for preheating.

$\mathcal{N}$	$y_{\mathcal{N}}$ / y_{end}	$\sigma_I(y_{\mathcal{N}})$ / $\sigma_I(y_{end})$	Solution I		Numerical	
			$W_I(y_{\mathcal{N}})$ / $W_I(y_{end})$	$N_I(y_{\mathcal{N}})$ / $N_I(y_{end})$	$W(y_{\mathcal{N}})$ / $W(y_{end})$	$N(y_{\mathcal{N}})$ / $N(y_{end})$
100	0.964	0.541	34.0	0.758	34.0	1.10
	0.502	3.27	2.43	3.67	2.83	4.34
200	0.879	2.00	34.0	3.72	34.3	4.14
	0.331	5.40	1.97	8.00	2.27	8.83
400	0.762	4.37	34.0	10.9	34.4	11.4
	0.211	8.33	1.73	16.6	1.95	17.6
1500	0.488	12.87	34.0	55.61	34.4	56.3
	0.084	17.60	1.49	63.80	1.62	65.1

Table 3.1: Comparison of analytic and numerical solutions for the effective single-field values W and N at $\sigma(y_{\mathcal{N}})$ and $\sigma(y_{end})$, for the number of inflatons $\mathcal{N} = 100, 200,$ 400 and 1500. The values of σ_I are found by (3.9) and corresponding analytic and numerical values for W/m^2_{min} and N are shown. Apart from the conspicuous disagreement in the e-folding number N for small $\mathcal{N}$, the extrapolated slow-roll solutions (I) are relatively in good agreement with the numerical solutions, roughly within 15% difference. Typically, the results of solution (I) slightly underestimate the potential W.

In addition, we know that the real evolution of the heavy fields after $\eta < 1$ was violated is very slow. Accordingly, non-Gaussianities are not produced up until slow roll fails for the effective degree of freedom σ_I, which corresponds to

[3]As we decrease the number of fields, for instance, $\mathcal{N} = 200$ fields, R increases, meaning that the second approximation ceases to be valid. This is so because the fields were artificially held fixed and as a result, the energy density does not decrease any more, thus acting as a cosmological constant, which is unphysical.

$\mathcal{N}$	X_1	$\sigma_{II}(Y_M)$	$W_{II}(Y_M)$	$\frac{W_{II}(Y_M)}{W_I(y_{end})}$	$\frac{N_{II}(Y_M)}{N_I(y_{end})}$	R
200	2.90	5.40	2.91	1.47	1.07	0.97
400	2.15	8.32	2.15	1.24	1.01	0.74
1500	1.75	17.57	1.75	1.17	1.00	0.53

Table 3.2: Comparison of the approximation II with the slow roll result I from table 3.1. X_1 is chosen such that $\sigma_{II}(Y_{\mathcal{M}}) \approx \sigma_I(y_{end})$. Note that the second approximation approaches the slow roll result for increasing $\mathcal{N}$. The numerical results in table 3.1 lie snugly between the two approximations.

individual fields starting to evolve faster. The reason why non-Gaussianities do not arise is the rather smooth trajectory in field space; as a result, there is no sourcing of the adiabatic mode via isocurvature modes after horizon crossing and since it is this evolution which causes non-Gaussianities [1], it follows that they will not be produced.

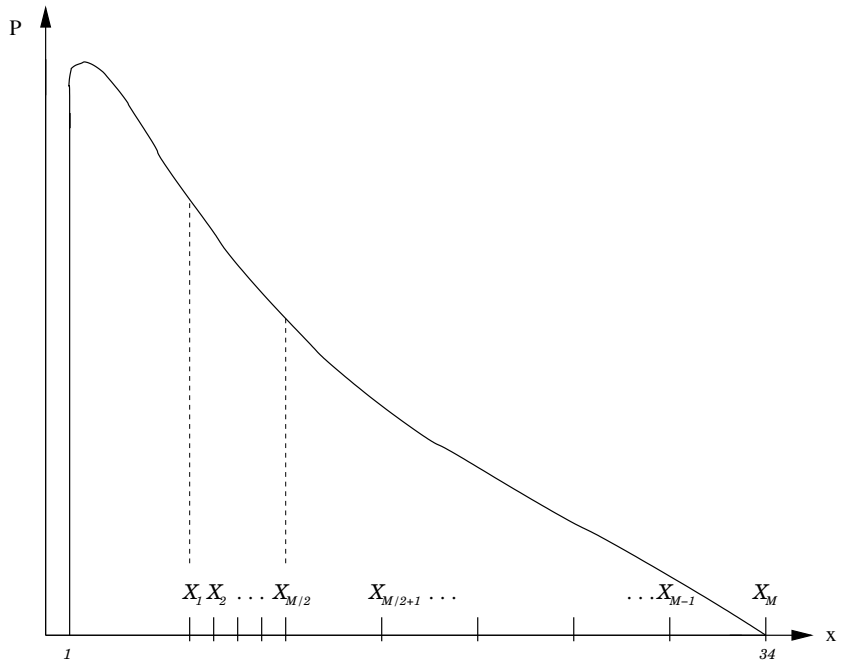

Figure 3.1: Schematic of the probability over the dimensionless mass variable $x = m^2/m_1^2$, showing how the mass-bins were chosen. We use a partition of $\mathcal{M} = 50$ bins and distributed them by first choosing X_1 as large as possible in order for the ratio in (3.24) to be small, while keeping X_1 small enough to ensure that the second approximation remains applicable up until σ_I leaves slow roll (e.g. $X_1 = 1.75$ in our case). To distribute the remaining bins, we choose to have $(\mathcal{M}-2)/2$ narrow bins from X_1 up until $X_{\mathcal{M}/2} \approx 11$ (the MP distribution peaks in that region so that the majority of fields resides here), followed by the remaining bins up until $X_{\mathcal{M}} = \xi \approx 34$. One could of course arrange a more refined spreading of bins, for instance with bin sizes according to the MP-distribution, but this simple method is sufficient for our purposes. Note that $\mathcal{M}$ should be large enough so that there is no huge impact onto e.g. the ratio in (3.27) if it were to be increased further. This is the case for $\mathcal{M} \geq 50$.

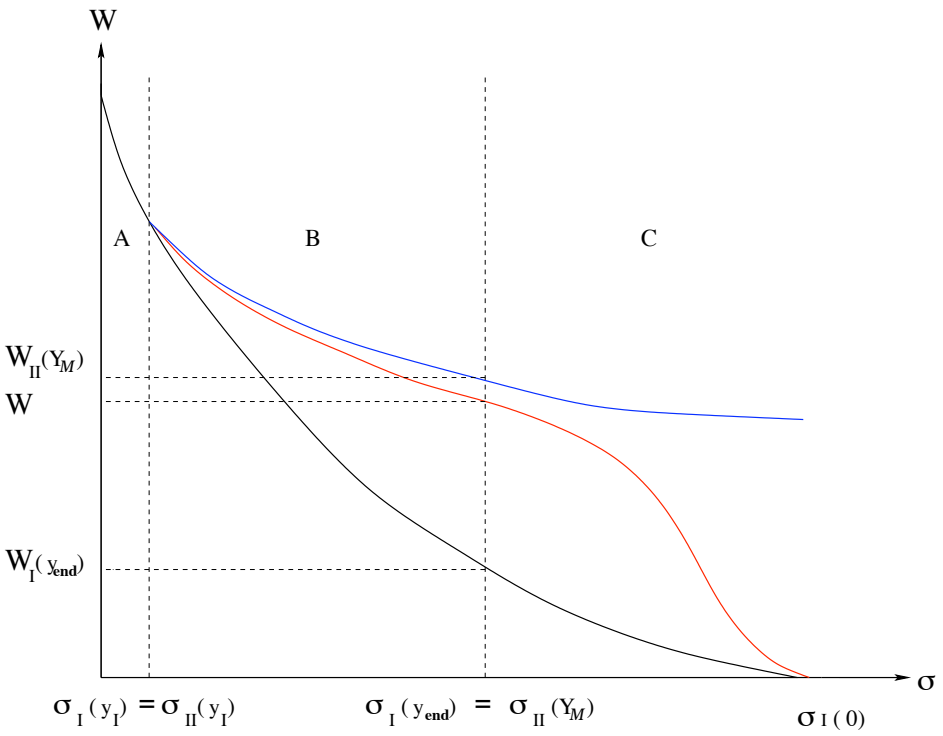

Figure 3.2: Schematic of the effective potential W vs. the path length of the trajectory in field space, σ. In our model, region A corresponds to the first approximation (during slow roll (blue)), section 3.2.1. In region B we have the additional upper bound from section 3.2.2, which is due to the second approximation. Region C begins where (p)reheating commences once $\epsilon_\sigma \sim 1$. Note that the scale in this picture is exaggerated and the true W (red) is well approximated either by W_I or W_{II}, see Figure 3.3.

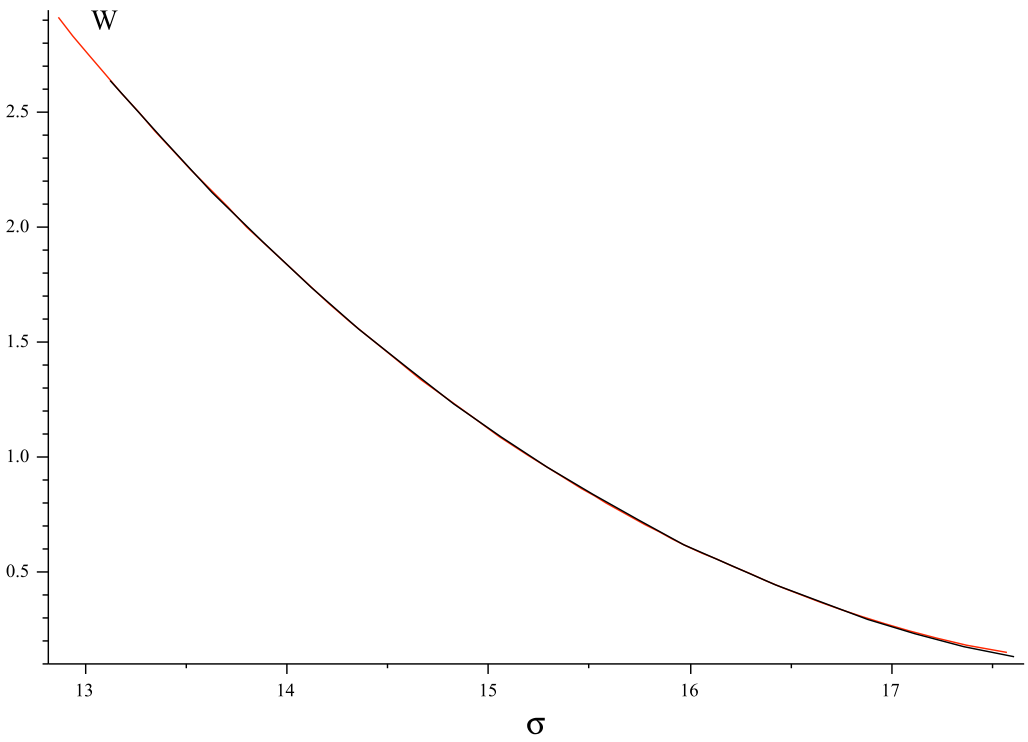

Figure 3.3: A plot of the effective potential W/m_{avg}^2 vs. the path length of the trajectory in field space σ corresponding to region B as illustrated in Figure 3.2, using $\mathcal{N} = 1500$, $\beta = 1/2$ and a distribution of bins as explained in the caption of Figure 3.1. In this region, the first and second approximation (derived in sections 3.2.1 and 3.2.2 respectively) are nearly indistinguishable from one another. Hence, the true potential energy is well approximated by either W_I or W_{II}.

Chapter 4

Preheating in Multi-field Inflation

4.1 Introduction

In this chapter we investigate preheating in multi-field inflationary models. Even though single field models of inflation are considered the most economic explanation of a Gaussian, nearly scale invariant spectrum of primordial fluctuations, they are not easy to construct in string theory. Further, upcoming observations of the CMBR such as by the Planck satellite [163] could reveal non-Gaussianity and put single field models to the test (see [82, 164]). It is for these reasons that multi-field inflationary models have sprang up in the last few years. Among the setups are $\mathcal{N}$-flation [42], inflation from multiple M5-branes [43] or inflation from tachyons [165]. For concretness, in this chapter, we take $\mathcal{N}$-flation as a case study.

Recently, aspects of preheating in the context of $\mathcal{N}$-flation have been considered in [106], pointing out the danger of transferring energy preferably to hidden sectors instead of standard model particles. This reveals an additional need for fine-tuning, a possible problem for many string-motivated models of inflation. The study in [106] is based entirely on an effective single field description of $\mathcal{N}$-flation. Hence, the common lore of single field preheating seems to be applicable. Here we take the optimistic view that preheating does indeed occur in the visible sector. However, we go beyond the single field model.

4.2 Preheating

In chapter 3 we found that at the end of inflation the majority of the energy is confined to only a few $\tilde{\mathcal{N}}$ light fields in a very narrow mass range. The remaining heavier fields have already evolved to the bottom of their potentials. It is thus these light inflaton fields which are relevant to preheating. To arrive at this conclusion we considered two approximate analytic solutions during inflation as well as a direct numerical integration. These indicate that slow roll is a good approximation although the heavier fields violate the slow roll condition $\eta_i < 1$ long before preheating starts.

As a consequence, we take as initial values for preheating the slow roll values of the $\tilde{\mathcal{N}}$ light fields. Owing to the fact that these lightest fields are highest up in their potentials, fields will join preheating in a staggered manner, adding to the difficulty of the problem. This and the large number of fields calls for a numerical treatment, which we provide.

4.2.1 Initial State of Preheating

We take as the initial state of preheating the one corresponding to the end of slow roll for σ_I see chapter 3. The potential energy left over at this stage is concentrated predominantly in a few light fields. To compute its magnitude, we first calculate the overall mass scale given by the average mass m_{avg} defined in (3.11), which is set by the COBE normalization $\delta_H \approx 1.91 \times 10^{-5}$. The power spectrum for a multi-field model [101]

$$\mathcal{P}_{\mathcal{R}} = \sum_i \frac{m_i^2 \varphi_i^2}{96\pi^2 m_{pl}^6}\,, \tag{4.1}$$

is related to δ_H by

$$\delta_H = \frac{2\sqrt{\mathcal{P}_{\mathcal{R}}}}{5}\,. \tag{4.2}$$

(Note that we restore the reduced planck mass m_{pl} in this subsection to avoid confusion). If we evaluate $\mathcal{P}_{\mathcal{R}}$ at $t = t_*$, meaning $y = 1$ in (3.1), and use the equal energy initial conditions defined in (2.38) along with $\varphi_1^* = m_{pl}$ we get

$$\mathcal{P}_{\mathcal{R}} = m_1^2 \frac{\mathcal{N}^2 \langle x^{-1} \rangle}{96\pi^2 m_{pl}^2}\,, \tag{4.3}$$

so that the mass of the lightest field is

$$m_1 = \frac{10\sqrt{6}\pi\delta_H}{\mathcal{N}\sqrt{\langle x^{-1}\rangle}} m_{pl} \tag{4.4}$$

$$\approx 2.37 \times 10^{-6} m_{pl}\,, \tag{4.5}$$

where we used

$$\left\langle x^{-1}\right\rangle = \frac{(1-z)^2}{(1-z^2)}\,, \tag{4.6}$$

with $z = \sqrt{\beta} = \sqrt{1/2}$ and $\mathcal{N} = 1500$. Hence, the average mass defined in (3.11) is

$$m_{avg} = \frac{m_1}{1-z} \approx 8.07 \times 10^{-6} m_{pl}\,. \tag{4.7}$$

The number of light fields carrying 96.5% percent of the total energy $W_I(y_{end})$ is $\tilde{\mathcal{N}} = 150$, corresponding to the mass range

$$1 < \frac{m^2}{m_1^2} < \tilde{x}\,, \tag{4.8}$$

where $\tilde{x} \approx 2.435$ is obtained by solving

$$\tilde{\mathcal{N}} = \mathcal{N} \int_1^{\tilde{x}} p(x) dx \tag{4.9}$$

numerically for $\tilde{x}$. At this point, let us note that the relevant mass scale for preheating is set by the mass of the light fields and not the average mass m_{avg}. Employing a very naive picture of perturbative preheating by a single field, which could be identified as a combined single degree of freedom, we obtain the temperature of preheating according to (1.38) [46] (see section 1.4.3)[1]. However this simplistic view would be insufficient if non-perturbative effects are important. From here on we set the reduced Planck mass $m_{pl}^{-2} = 8\pi G \equiv 1$ again.

4.2.2 Coupling to Bosonic Matter

Given the just computed overall mass scale m_{avg}, the individual axion masses follow from the MP-distribution; we further know that $\tilde{\mathcal{N}} = 150$ light axions carry 96.5 % of the total potential energy at $y = y_{end}$. For the matter into which the axions decays we assume a massless bosonic field χ coupled to the φ_i via $\frac{1}{2}g^2\varphi_i^2\chi^2$; for simplicity, we take the coupling strength to each axion to be the same. The model we consider is then described by the following Lagrangian,

$$\mathcal{L} = -\sum_{i=1}^{\tilde{\mathcal{N}}} \left\{ \frac{1}{2} g^{\mu\nu} \nabla_\mu \varphi_i \nabla_\nu \varphi_i + \frac{1}{2} m_i^2 \varphi_i^2 + \frac{1}{2} g^2 \varphi_i^2 \chi^2 \right\} \tag{4.10}$$

$$-\frac{1}{2} g^{\mu\nu} \nabla_\mu \chi \nabla_\nu \chi. \tag{4.11}$$

[1] On the other hand, if we set $\rho_{rh} \equiv V_I(y_{end})$ we get an upper bound $T_{rh} < 8.46 \times 10^{-13} m_{pl} \approx 1.20 \times 10^{20} K$.

The equations of motion are

$$\ddot{\varphi}_i + 3H\dot{\varphi}_i + \left(m_i^2 + g^2\left\langle\chi^2\right\rangle\right)\varphi_i = 0, \tag{4.12}$$

$$\ddot{\chi}_k + 3H\dot{\chi}_k + \left(\frac{k^2}{a^2} + g^2\sum_i \varphi_i^2\right)\chi_k = 0, \tag{4.13}$$

$$3H^2 = \frac{1}{2}\sum_i \dot{\varphi}_i^2 + \frac{1}{2}\sum_i m_i^2\varphi_i^2 \tag{4.14}$$

$$+ \frac{1}{2}\left\langle\dot{\chi}^2\right\rangle + \frac{1}{2}g^2\left\langle\chi^2\right\rangle\sum_i \varphi_i^2, \tag{4.15}$$

where χ_k is the mode operator of the matter field and $\langle\cdot\rangle$ is the mode sum over k. We consider the axions and gravity as the background and ignore backreaction from χ_k, since we are interested in the early stages of preheating; hence, $\langle\chi^2\rangle$ and $\langle\dot{\chi}^2\rangle$ can be ignored.

4.2.3 Parametric Resonance in the Equal-Mass Case

Before addressing the more involved preheating scenario of $\mathcal{N}$-flation, we discuss a toy model with $\tilde{\mathcal{N}} = 150$ inflatons, all having the same mass $m_i \equiv m$. In this case, the equal energy initial conditions yield the same initial field value for all $\tilde{\mathcal{N}}$ axions, resulting in the identical (in phase) evolution of the axions. Neglecting backreaction of the matter field we can write the equations of motion as,

$$\ddot{\varphi}_i + 3H\dot{\varphi}_i + m^2\varphi_i = 0, \tag{4.16}$$

$$\ddot{\chi}_k + 3H\dot{\chi}_k + \left(\frac{k^2}{a^2} + \tilde{\mathcal{N}}g^2\varphi_i^2\right)\chi_k = 0\,, \tag{4.17}$$

$$3H^2 = \frac{\tilde{\mathcal{N}}}{2}\left(\dot{\varphi_i}^2 + m^2\varphi_i^2\right). \tag{4.18}$$

Defining $\varphi \equiv \sqrt{\tilde{\mathcal{N}}}\varphi_i$, the equations of motion reduce to those of the well-understood single field model of non-perturbative preheating [17, 46–48, 50] (see chapter 1.4.3 for a short review). The Klein-Gordon equation for φ reads

$$\ddot{\varphi} + 3H\dot{\varphi} = -m^2\varphi\,, \tag{4.19}$$

whose solution is approximated by

$$\varphi(t) = \Phi(t)\sin(mt)\,, \tag{4.20}$$

where $\Phi(t) = \sqrt{8}/(\sqrt{3}mt)$ [46] is a slowly decaying amplitude (due to Hubble friction). The corresponding equation for a Fourier mode of the matter field reads

$$\ddot{\chi}_k + 3H\dot{\chi}_k + \left(\frac{k^2}{a^2} + g^2\varphi^2\right)\chi_k = 0\,, \tag{4.21}$$

where $\mathbf{p} = \mathbf{k}/a$ is the physical momentum. Due to the inflaton field's oscillations, the mass of the matter field becomes time dependent and resonances can occur. To see this, introduce $q = g^2\Phi^2/4m^2$, $\tau = mt$, $A_k = 2q + k^2/m^2a^2$ and $X_k \equiv a^{3/2}\chi_k$ so that (4.21) becomes

$$\frac{d^2X_k}{d\tau^2} + (A_k - 2q\cos(2\tau))\,X_k = 0\,, \tag{4.22}$$

where we also neglected the term proportional to the pressure [2], $-(3/4)(H^2 + 2\ddot{a}/a)$. If we ignore the time dependence of the amplitude Φ in q and of A_k, Eq. (4.22) is the Mathieu equation. It is known that parametric resonance occurs for wavenumbers k within resonance bands (see [46, 52] for the stability/instability chart). This means if k is within the n'th resonance band the corresponding mode increases exponentially

$$X_k \propto e^{\mu_k^{(n)}\tau}\,, \tag{4.23}$$

where $\mu_k^{(n)} > 0$ is the Floquet index [52] defined in Eq. (1.52). Physical parameters evolve along the $A_k = 2q$ line from large q to $q \sim 0$, as the inflaton amplitude Φ decays slowly. As it evolves, the system crosses resonance bands where exponential particle production takes place. Particle production is efficient in the large q ($q \gg 1$) region, *broad resonance* (or *stochastic resonance* when expansion effects are included). For small q the resonance effect is limited as it is not strong enough to hold against redshifting $\chi_k \propto a^{-3/2}$. Then the main concern is whether it is possible to have large q in a given model. A stringent constraint comes from radiative corrections, restricting the value of the coupling to $g \lesssim 10^{-3}$ [46, 58].

From the above discussion we infer that having many inflatons does not give larger q so that resonance effects are not enhanced. Given that the equations of motion lead to the one of the single field model, $\varphi(= \sqrt{\tilde{\mathcal{N}}}\varphi_i)$ starts oscillating with initial amplitude $\sim 0.1m_p$. Each inflaton φ_i oscillates with smaller amplitude $\Phi/\sqrt{\tilde{\mathcal{N}}}$, while q is unaltered. Figure 4.1 illustrates the evolution of the oscillating term φ^2 in the equal mass case. Here we used $\tilde{\mathcal{N}} = 150$ and $m = m_0 = 2.4 \times 10^{-6}$. The initial values of φ_i are taken

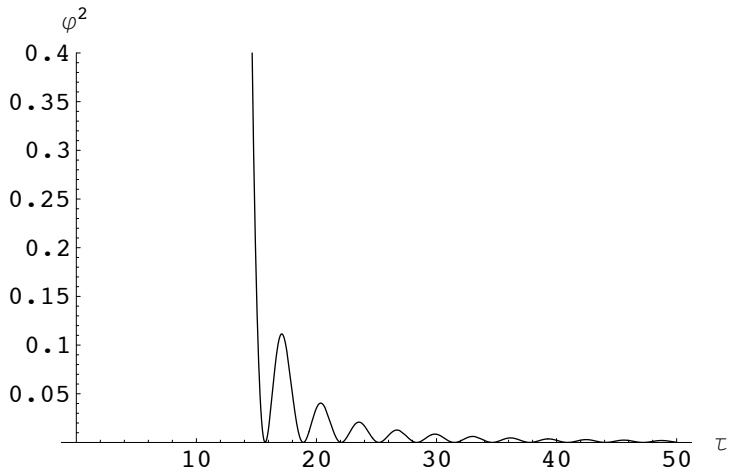

Figure 4.1: The evolution of the oscillating term φ^2 that drives the parametric resonance. The horizontal axis τ is the dimensionless time using the mass $m = m_0$. Since $\varphi = \sqrt{\tilde{\mathcal{N}}}\varphi_i$ and φ_i are chosen to start from $m_p = 1$, φ^2 start from $\tilde{\mathcal{N}} = 150$ at $\tau = 0$.

to be $\varphi_i = m_p = 1$ and the initial velocities $\dot{\varphi} = 0$. Ignoring backreaction and rescattering effects, Figure 4.2 shows the evolution of the matter field mode function χ_k and the comoving occupation number of particles (defined in equation (1.50) with (1.51)) for $g = 10^{-3}$ and $k/a_{initial} = 6.0 \times m$, corresponding to a fast growing mode. Equation (1.51) reduces to

$$\omega_k = \sqrt{\frac{k^2}{a^2} + g^2\varphi^2}\,. \tag{4.24}$$

The condition on the resonance parameter $q = g^2\Phi^2/4m^2 \gtrsim \mathcal{O}(1)$ corresponds to $|\varphi|^2 \gtrsim 10^{-5}$ for $g = 10^{-3}$, resulting in $\tau \lesssim 4000$.

In the following section we investigate the effect of different masses, which are present in $\mathcal{N}$-flation. We show that contrary to the generic expectation, preheating is less efficient for a large number of fields; this is still in agreement with spectral theory (see section 1.5.4), since the latter makes no predictions regarding the efficiency of preheating, specifically, about the magnitude of the generalized Floquet index.

[2]The energy density of the axions scales as a^{-3} during the oscillations in a quadratic potential, so that $H^2 + 2\ddot{a}/a = 0$.

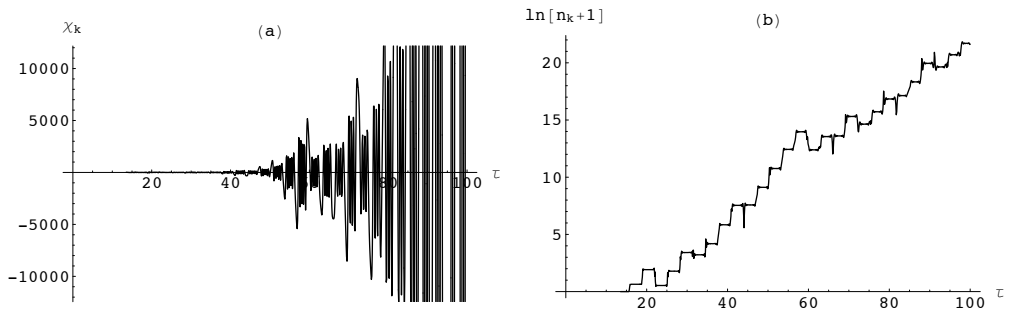

Figure 4.2: The evolution of (the real part of) the mode χ_k (a) and the occupation number n_k (b). The initial conditions for χ_k are set by the positive-frequency solution at $\tau = 13.5$, when the slow-roll conditions break down. The coupling constant is $g = 10^{-3}$ and the wavenumber is chosen as $k/am = 6.0$ at $\tau = 13.5$. One can see amplification due to typical stochastic resonance, i.e. the overall amplitude grows exponentially while there are occasional decreases of the amplitude. We are ignoring backreaction so that resonances are present until $q \approx \mathcal{O}(1)$, corresponding to $\tau \approx 4000$ for $g = 10^{-3}$. Backreaction from the matter field shuts off resonances earlier.

4.2.4 Parametric Resonance for spread out masses?

Still ignoring backreaction and rescattering[3] ($\langle\chi^2\rangle = \langle\dot{\chi}^2\rangle = 0$), consider now multiple fields whose masses obey the MP law, still coupled to the same matter field. Recall that we focus on $\tilde{\mathcal{N}} = 150$ axion fields only, since the heavier 90% of the fields do not contribute much to the late time dynamics of $\mathcal{N}$-flation.

As in the previous sections on $\mathcal{N}$-flation, the $\tilde{\mathcal{N}}$ fields φ_i have potentials

$$V_i = \frac{m_i^2}{2}\varphi_i^2 + \frac{g_i^2}{2}\varphi_i^2\chi^2 \tag{4.25}$$

and masses according to

$$m_i^2 = x_i m_1^2\,, \tag{4.26}$$

where the x_i are determined by solving

$$i - 1 = \mathcal{N}\frac{(1-z)^2}{2\pi z^2}\int_1^{x_i}\sqrt{(\xi - x)(x-1)}\frac{1}{x}\,dx \tag{4.27}$$

numerically. For simplicity, we still take all coupling constants to the matter field χ to be the same, that is $g_i \equiv g$ for $i = 1\ldots\tilde{\mathcal{N}}$. Using again the

[3]This is justified, since in the end we find that the amplification of the matter field is found to be suppressed.

dimensionless time $\tau \equiv mt$, where $m^2 = \bar{x} m_1^2$ from

$$
\begin{aligned}
m^2 &\equiv \frac{m_1^2 \int_1^{\tilde{x}} p(x) x \, dx}{\int_1^{\tilde{x}} p(x) \, dx} && (4.28)\\
&= m_1^2 \frac{\mathcal{N}(1-z)^2}{\tilde{\mathcal{N}} 2\pi z^2} \int_1^{\tilde{x}} \sqrt{(\xi - x)(x-1)} \, dx && (4.29)\\
&\equiv \bar{x} \, m_1^2 && (4.30)
\end{aligned}
$$

where we have truncated the MP-distribution to $\tilde{x} = 2.435$ from (4.9), $z = \sqrt{\beta}$, $\xi = (1+z)^2/(1-z)^2$, $m_1 = 2.37 \times 10^{-6}$ from (4.5) and we used (4.9), we find $\bar{x} \approx 1.77$.

The equations of motion for the axions read

$$
\varphi_i'' + 3\frac{a'}{a}\varphi_i' = -\frac{x_i}{\bar{x}}\varphi_i \, , \tag{4.31}
$$

which need to be solved in conjunction with the Friedmann equations

$$
\begin{aligned}
3\frac{a'^2}{a^2} &= \frac{1}{2}\sum_{i=1}^{\tilde{\mathcal{N}}} \left(\frac{x_i}{\bar{x}} \varphi_i^2 + \varphi_i'^2 \right) , && (4.32)\\
\frac{a''}{a} - \frac{a'^2}{a^2} &= -\frac{1}{2}\sum_{i=1}^{\tilde{\mathcal{N}}} \varphi_i'^2 \, . && (4.33)
\end{aligned}
$$

According to section 3.2.1, for each individual field we take as initial conditions[4]

$$
\begin{aligned}
\varphi_i(\tau_{in}) &= \sqrt{\frac{y_{end}^{x_i}}{x_i}} \, , && (4.34)\\
\varphi_i'(\tau_{in}) &= -\sqrt{\frac{2 x_i y_{end}^{x_i}}{3\bar{x}}} \left(\sum_{j=1}^{\tilde{N}} y_{end}^{x_j} \right)^{-1/2} , && (4.35)
\end{aligned}
$$

where $y_{end} = 0.084$.

Short Time Scales

Figure 4.4(a) shows the evolution of $\sum_i \varphi_i^2$ up to $\tau = 50$. In the MP distribution, all the masses are different, resulting in a different evolution of

[4]The initial condition for the matter field is set by the positive frequency mode function, $\chi_k(t) = a^{3/2}\chi_k(t) \simeq e^{-im\omega_k(t-\tau_{end}/m_0)/\sqrt{2\omega_k}}$, at $\tau = \tau_{end} = 11.6$, which corresponds to the onset of preheating at $y = y_{end}$.

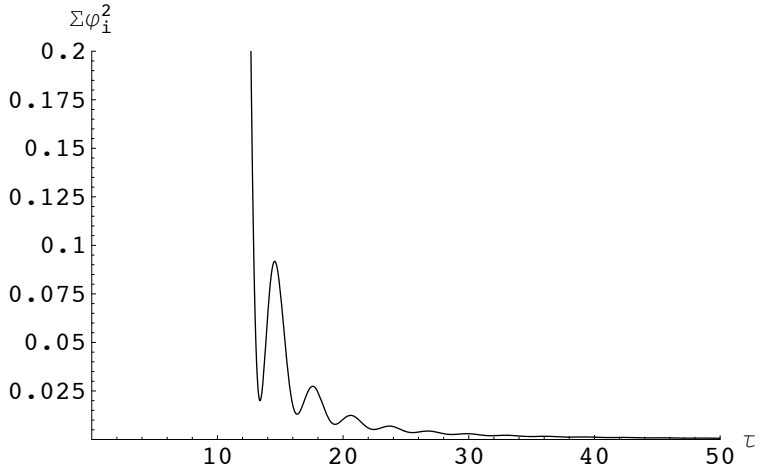

Figure 4.3: The evolution of the term $\sum_i \varphi_i^2$ that couples to the matter field. The oscillation is less sharp, never reaching zero, and the damping is faster than in the equal-mass case.

$\sum_i \varphi_i^2$ from the equal mass case we discussed before. It is evident that the oscillations are more obtuse and the damping is faster than in Fig.4.1. This can be attributed to the dephasing of the axion oscillations owed to relative mass differences and the redshift due to the cosmic expansion. During the oscillations, we may expect some resonance effects in the dynamics of χ_k, analogous to the equal-mass example explained in the previous section. Figure 4.4 shows the time evolution of the matter field (neglecting backreaction and rescattering), for $g = 10^{-3}$ and $k/am_0 = 6.0$ at $\tau = \tau_{end}$ as in the equal mass case. The temporal enhancements of the amplitude (which are clearly seen for small τ) is caused by parametric resonance with (the collective behavior of) the axions. In contrast to the equal-mass case, the overall amplitude of χ_k decrease in time, indicating that resonances are not strong enough to hold against damping caused by the cosmic expansion, even when the coupling constant is as large as $g \sim 10^{-3}$.

Using again $X_k = a^{3/2}\chi_k$, we may separate out the effect of cosmic expansion. The equation of motion for X_k is

$$\ddot{X}_k + \left[\frac{k^2}{a^2} + g^2 \sum_i \varphi_i^2 - \frac{3}{4}(2\dot{H} + 3H^2)\right] X_k = 0. \tag{4.36}$$

Since the last term, proportional to the pressure $p = -(2\dot{H} + 3H^2)$, is negligible during preheating, X_k satisfies the equation of motion for χ_k with the friction term $3H\chi_k$ set to zero by hand. Figure 4.4(b) shows numerical

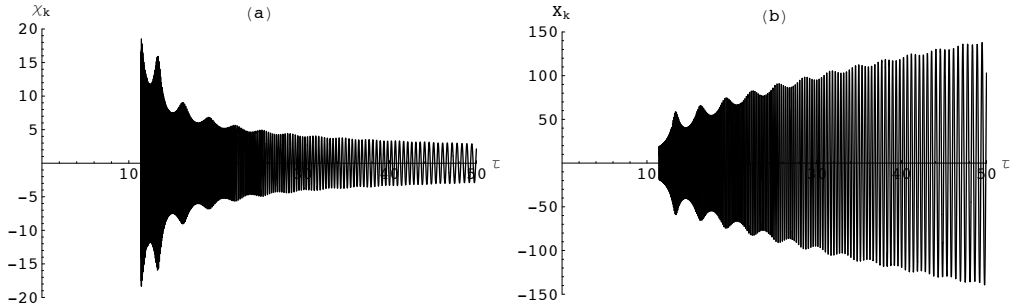

Figure 4.4: (a) The evolution of the mode function of the matter field χ_k, in $\mathcal{N}$-flation using the MP mass distribution. The coupling is $g = 10^{-3}$ and the wavenumber is chosen as $k/am_0 = 6.0$ at $\tau = \tau_{end} = 11.6$. (b) The evolution of $X_k = a^{3/2}\chi_k$ for the same parameters. There are wiggles in the oscillation amplitude (these are evident for small τ and become smaller for larger times) indicating some effect of parametric resonance. This resonance is, however, weak and the amplitude of χ_k decays on average.

results for the evolution of X_k. First, note that there is small wiggling of the amplitude[5], a resonance effect since the peaks occur at the minima of the mass term (see Fig.4.3). The minima of the mass term do not go to zero, due to dephasing by the relative mass difference of the axion fields, yielding a small value of $\dot{\omega}_k/\omega_k^2$ and inefficient preheating; second, the envelope of the amplitude exhibits power-law like growth[6], which is slower than $a^{3/2}$ so χ_k as a whole still decays. In Table 4.1 we show the power $\chi_k \approx a^{-\gamma}$ that approximates the numerical behavior of χ_k in larger time scales. The power γ is within $3/4 \leq \gamma \leq 1$. In the mass term of (4.36), k^2/a^2 remains dominant since $a^{-2} \sim t^{-4/3}$, $\varphi_i^2 \sim t^{-2}$, $\dot{H} \sim t^{-2}$ and $H^2 \sim t^{-2}$ as $a \sim t^{2/3}$ during preheating. Hence (4.36) becomes $\ddot{X}_k + Ct^{-4/3}X_k = 0$ for some constant C. This can be solved exactly in the form $X_k \sim t^{\alpha}F(t)$, where $F(t)$ is a fast oscillating function. Discarding the decaying solution, we find $\gamma = 3\alpha/2 = 0.5$. For smaller k, X_k grows faster than $\sim a^{0.5}$, but the enhancement is minimal.

Long Time Scales

In the equal-mass case (section 4.2.3), with a large enough value of g, the resonance parameter is $q \gg 1$ and resonances arise for reasonably long time scales, specifically, up until $\tau \approx 4000$ for $g = 10^{-3}$ (ignoring backreaction).

[5]The peaks occur when $\sum_i \varphi_i^2$ in Figure 4.3 reach the local minima and $\dot{\omega}_k/\omega_k^2$ becomes large (see Figure 4.5); whenever the system becomes less adiabatic, parametric resonance can occur.

[6]This does not necessarily mean particle production because it is mainly due to redshifiting

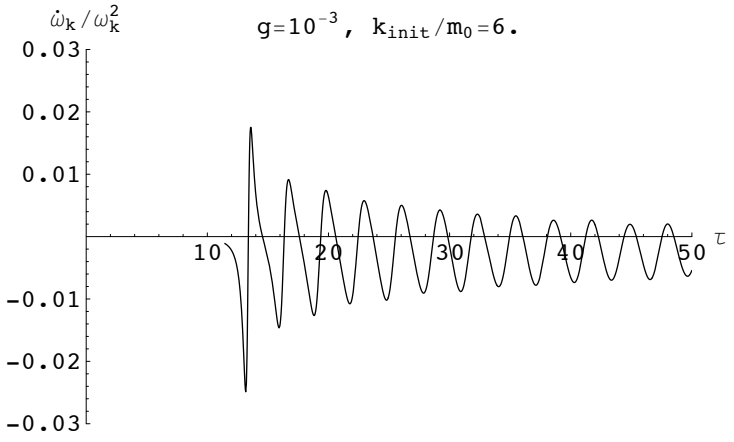

Figure 4.5: The adiabaticity parameter $\dot{\omega}_k/\omega_k^2$, for $\tau \lesssim 50$. The slight negative shift is due to the cosmic expansion.

$k^2/a_{init}^2 m_0^2$	0	10	10^2	10^3	10^4	10^5
$g = 10^{-5}$	0.75	0.95	0.99	1.00	1.00	1.00
$g = 10^{-4}$	0.75	0.76	0.87	0.96	0.99	1.00
$g = 10^{-3}$	0.75	0.75	0.75	0.76	0.85	0.97

Table 4.1: Numerical results of the decaying power γ, where $\chi_k \approx a^{-\gamma}$, for various coupling g's and the wave number k's.

Similarly, in the MP case, even though there is no well-defined q-parameter, resonances can ensue during short time intervals for large τ, again assuming a similar large coupling g. In this case, the collective behavior of the axions is crucial and the adiabaticity parameter develops a complicated behavior (see Figure 4.6(a)). Since the mass differences between the neighboring axions[7]

[7]Adding two oscillations leads to beats: since $\sin(\omega_1 t)+\sin(\omega_2 t) = 2\cos((\omega_1-\omega_2)/2)-t)(\sin((w_1+\omega_2)/2)-t$, the beat frequency is $\omega_{beat} = \Delta\omega/2 = |\omega_1-\omega_2|/2$. Our fields oscillate as $\varphi_i \sim \sin(\omega_i\tau)$, where $\omega_i = m_i/m_0 = \sqrt{x}_i$; in the mass term for X, they appear as $\sum\varphi_i^2$, so lets lets look at nearest neighbors, for instance at $\varphi_1^2+\varphi_2^2$. To get a rough estimate we assume that initially all fields are in phase. Further, $\Delta x = x_i - x_{i-1} \sim \mathcal{O}(0.01)$ (it is between 0.01 and 0.02 for most light masses) where $x_i = m_i^2/m_0^2$; Thus $\varphi_1^2+\varphi_2^2 \sim \sin^2\sqrt{x}_1\tau + \sin^2\sqrt{x}_2\tau$ and since $\sin^2(\omega t) = 1/2(1-\cos(2\omega t))$, we obtain $\varphi_1^2+\varphi_2^2 \sim 1-1/2(\cos 2\sqrt{x}_1\tau + \cos 2\sqrt{x}_2\tau)$. Then $\omega_1 = 2\sqrt{x}_1$, $\omega_2 = 2\sqrt{x}_2$, and the beat frequency is $\omega_{beat} = |\omega_1-\omega_2|/2 = |\sqrt{x}_1 - \sqrt{x}_2|$. Let $x_2 = x_1 - \alpha$ with $\alpha \sim 0.01 \ll x_1, x_2$. Then $\sqrt{x}_2 = \sqrt{x_1+\alpha} = \sqrt{x}_1\sqrt{1+\alpha/x_1}$. Expanding the latter, we can write $\omega_{beat} \sim \alpha/2$. As a result, we expect nearest neighbors to be roughly in phase again after $\tau \sim \pi/\omega_{beat} \sim \pi 2/\alpha$. For $0.01 \lesssim \alpha \lesssim 0.02$ (roughly the range of α) we get $314 \lesssim \tau \lesssim 628$ so that $\bar{\tau} \sim 471$

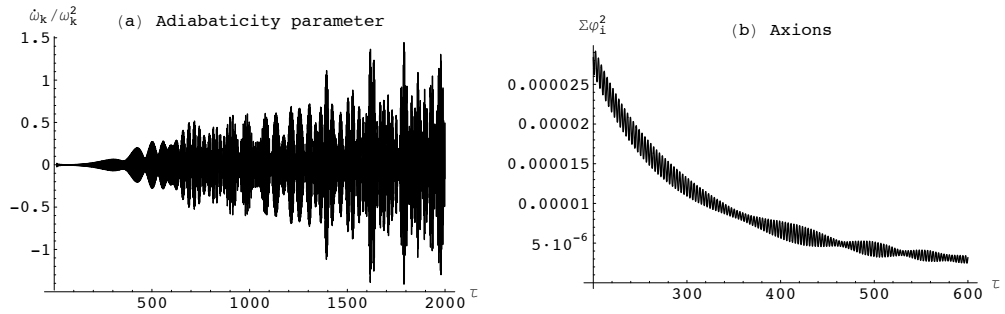

Figure 4.6: (a) The long time scale behavior of the adiabaticity parameter $\dot{\omega}_k/\omega_k^2$. (b) The sum of axions' squared amplitudes $\sum_i \varphi_i^2$, for the time scale $\tau = 200$ to 600. The coupling g and the wavenumber k are the same as in Fig.4.4.

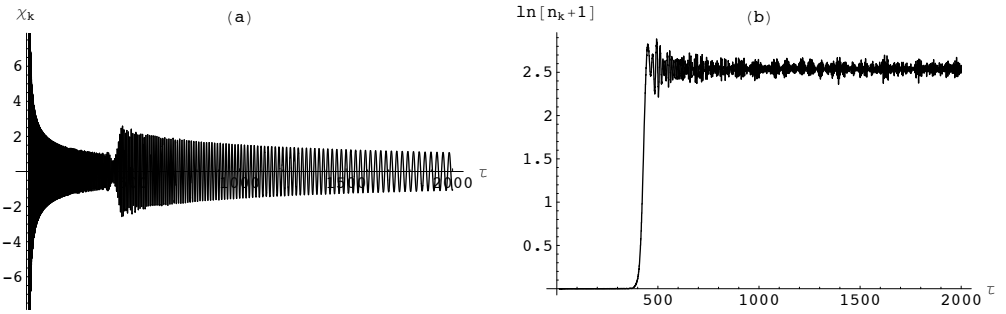

Figure 4.7: (a) Long time behavior of χ_k, exhibiting short lived, weak resonances around $\tau \approx 450$. The choice of parameters is the same as in Fig.4.4. (b) The comoving occupation number n_k calculated for X_k.

with $\mathcal{N} = 1500$ is typically of order of $\Delta m^2 \approx \mathcal{O}(10^{-2}) \times m_0^2$, once dephased, the axions' collective oscillations return to near-coherence in time scales of order $\Delta\tau \approx \mathcal{O}(10^2) \sim \mathcal{O}(10^3)$, causing beats in the effective mass for χ_k (see Figure 4.6(b)). To be concrete, considering nearest neighbor fields with $0.01 \lesssim x_i - x_{i-1} \lesssim 0.02$ (relevant for the light fields under consideration) we expect a beating frequency $\omega_{beat} \sim (x_i - x_{i-1})/2$ in the effective mass for χ_k. Hence, the time at which some fields are in phase again is between $314 \lesssim \tau \lesssim 628$, consistent with Figure 4.6(b).

Indeed, on these time scales, for $g \gtrsim 10^{-3}$, we find the occasional amplitude enhancement of a few orders of magnitude (see Figure 4.7): Figure 4.7(a) illustrates the evolution of χ_k up to $\tau = 2000$; the evolution of the

is the expected time at which the nearest neighbors are in phase again, since all all fields were more or less in phase initially (this is not exactly true, but sufficient for the present argument). Henceforth, we expected most fields to be more or less in phase after $\bar{\tau} \sim 471$.

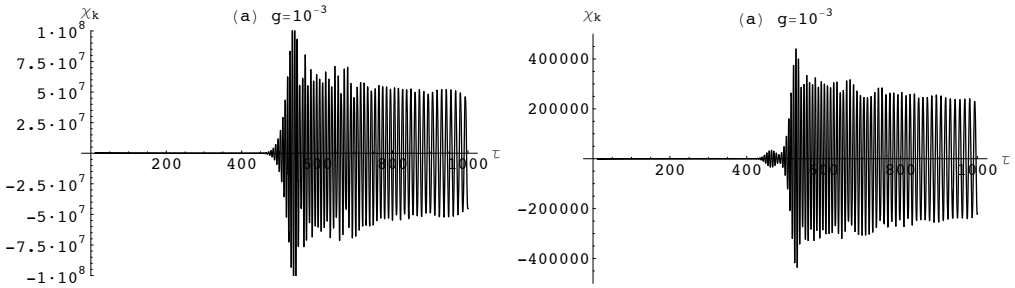

Figure 4.8: Figure showing the appearance of Cantor Preheating as the number of fields decrease. This is in accord with the argument that dephasing is responsible for the suppression of Cantor Preheating. a) shows Cantor Preheating for $\tilde{N} = 3$. (b) $\tilde{N} = 5$.

comoving occupation number n_k calculated for X_k is shown in Figure 4.7(b). Here we see that there is some amplification due to parametric resonances at around $\tau \sim 450$. Here and later on we find the occasional amplitude enhancement of a few orders of magnitude. For larger wavenumbers $k/am_0 \gtrsim 10^4$, n_k behaves differently. Since the overall amplitude of $\dot{\omega}_k/\omega_k^2$ is smaller, the resonance around $\tau \sim 450$ vanishes, but spikes at large τ are still present. As a result, the late time dynamics features a behavior akin to a random-walk. However, these resonance effects are not frequent or long enough to dominate preheating.

Increasing the width of the mass distribution, that is taking $\beta > 1/2$, does not change this conclusion, as can be seen in Figure 4.9, where we consider $\beta = 0.7$ and $\beta = 0.9$. If we decrease β, we approach the equal mass case, and resonances become more pronounced again.

If the number of inflatons that couple to a single matter field is decreased, we encounter more pronounced resonances again, see Figure 4.8, in accord with Cantor preheating.

4.3 Discussion

We saw that preheating is not due to explosive particle production in $\mathcal{N}$-flation if many axions couple to the same matter field; even though there is some weak amplification, it is much too feeble to compete with the dilution due to Hubble expansion. The physical reason for the suppression of parametric resonance is quite simple: the axions are all out of phase, averaging out each other's contribution to the matter fields effective mass, so that the driving term $\propto \sum \varphi_i^2$ in the equation of motion for χ_k decays quite smoothly

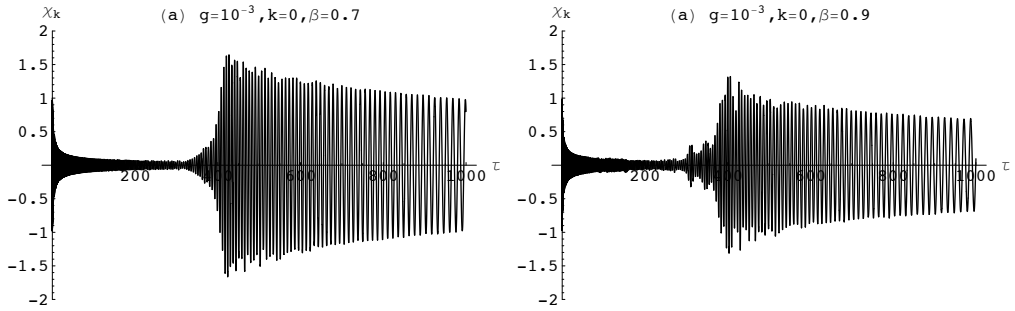

Figure 4.9: Increasing the value of β does not change the results. (a) $\beta = 0.7$. (b) $\beta = 0.9$.

$\propto a^{-3}$ after the first few oscillations, just like matter, since $\rho_{\varphi_i} \propto a^{-3}$. Hence, instead of an exponential increase, we observe power-law behavior $\chi_k \sim a^{-\gamma}$ where γ increases from 3/4 to 1 for increasing wavenumber. This is consistent with the conclusions of [58], where it was emphasized that a large "bare mass" of the matter field (bigger than the amplitude of the oscillations) suppresses resonances.

Our conclusion differs considerably from the common lore, namely, that parametric resonance effects are crucial for preheating [17]. For instance, it is argued in [57,66] that the oscillations of multiple inflatons (with irrational mass ratios) can enhance drastically the decay rate (Cantor preheating). This argument is based on two pillars: first, theorems in spectral theory indicate that stability bands vanish [56,57,66] in the case of more fields whose masses are not related by rational numbers. (Note that nothing is known about the magnitude of these instabilities). Second, numerical evidence in two field models indicate a slight enhancement of particle production for well chosen parameters [57]. In the latter study, dephasing of fields is unimportant, since only two fields are considered. Nevertheless, this effect is crucial if one considers many fields, say $\mathcal{O}(100)$ instead of 2, all coupled to a single matter field.

Of course, dephasing would be absent if each axion were coupled to a different matter field, in which case, stochastic resonance would indeed be important. Further, If only a few axions, say two or three, couple to a given matter field, we saw that Cantor preheating is indeed efficient (Figure 4.8). However, when hundreds of fields are coupled to the same matter field, it is the old theory of perturbative preheating which remains applicable. This may actually be desirable, since it is guaranteed that no unwanted relicts such as magnetic monopoles are produced. Of course, there is the danger of left over inflaton fields, which might disrupt nucleosynthesis.

At this point we would like to mention that to the best of our knowledge

no systematic (numerical or analytic) study of Cantor preheating with more than two fields exists in the literature. It would be interesting to investigate the efficiency of preheating if one increases the number of fields one by one: first, stability bands will dissolve, and an increase of resonant particle production is expected. However, at some critical field number the driving force of the matter field would become so erratic and out of phase, that resonances are diminished. We leave this topic for future studies.

Before concluding, we would like to comment on yet another effect. It has been shown in [114, 115] that noise on top of an oscillating driving force can also enhance resonant particle production. This phenomenon could also occur in multi-field inflation if a single field carries the majority of the energy, while the remaining fields provide only very little. Alternatively, all fields could carry the same energy but have wildly different coupling constants to the matter field. The oscillations of the many fields would then act similar to noise during the oscillations of the main field. However, this effect goes beyond the present study.

All in all, it is evident that preheating in multi-field scenarios is a lot more model dependent than in simple single field models. To make any concrete predictions, one needs to know precisely how the inflatons couple to matter. Unfortunately, this knowledge is usually unattainable in stringy models of inflation, at least for the time being.

4.4 Conclusions

In this chapter we studied preheating in $\mathcal{N}$-flation, a string motivated realization of assisted inflation, assuming the Marčenko-Pastur mass distribution (arising from random matrix theory) and equal-energy initial conditions at the onset of slow roll inflation. Using the analytic approximations of chapter 3 to set the initial stage for preheating, we consider only the lightest fields, which carry the majority of the energy.

To study preheating, we coupled a single bosonic matter field χ to the axions φ_i, assuming the same coupling constant g^2 between χ and any φ_i. Within this setup we solved for the evolution of the matter field numerically, including the expansion of the universe, and found a power-law like behavior in the parameter region that would otherwise give rise to stochastic resonance in single field models. In particular, the growth of the matter field is generically not strong enough to resist redshifting due to cosmic expansion. As a result, the old theory of perturbative preheating (see e.g. [46]) applies to this scenario and not parametric resonance models.

Our result differs considerably from the accepted view that parametric

resonance effects are crucial for preheating [17]. As argued in [57,66], Cantor preheating might be even more efficient than stochastic resonance. However, in these studies the relevance of fields running out of phase was not apparent. Nevertheless, this effect is crucial when considering many fields, provided they are all coupled to a single matter field. This is at the core of the weak amplification we observe. Indeed, instead of an exponential increase, we observe power-law behavior. Of course, dephasing would be absent if each axion was coupled to a different matter field, in which case stochastic resonance will be important. If only a few axions, say two or three, couple to a given matter field, we expect Cantor preheating to be the applicable model.

Besides assuming a single matter field, the analysis presented here depends upon several other assumptions. Firstly, we ignored backreaction and rescattering during preheating; modifications due to these two effects should be minor, since explosive particle production due to parametric resonance is suppressed in $\mathcal{N}$-flation, as argued above; in addition, their inclusion would only diminish resonance effects further. We further assumed that the axion-matter couplings are all set to be equal. Dropping this assumption might change the scenario. To illustrate, Cantor preheating cannot be excluded in $\mathcal{N}$-flation, especially if only a few axions couple strongly to a given matter field, while the vast majority has negligible coupling.

To summarize, preheating in multi-field models such as $\mathcal{N}$-flation can differ considerably from their effective single field analogs, as parametric resonance effects can be heavily suppressed. If this is the case, the old theory of perturbative preheating is the relevant one, a potentially desirable outcome given that unwanted relicts are not produced.

Chapter 5

Magnetogenesis via Rotating Cosmic String Loops

5.1 Introduction

In this chapter we consider the generation of primordial magnetic seed fields by a cosmic string network [2] (see section 1.6 for possible origins of cosmic strings as well as semi analytic network models). These seed fields are needed in order to account for observed magnetic fields in galaxies and clusters in the μG range (see section 1.7 for a review of magnetic fields at cosmological scales.)

Among the positive attributes of cosmic string networks for magnetogenesis is the fact that they span over the cosmological horizon giving rise to coherent effects over large length scales. Also, as the strings and loops pass through the primordial plasma, they generate vector-type perturbations, a necessary condition for magnetic field generation. These and other features of cosmic strings make them attractive candidates for magnetogenesis. Hence, magnetic field generation from long strings have indeed been considered in the past [136, 137, 151]. We will re-investigate this case, finding that cosmic string loops give the dominant contribution. Throughout this study, we average over small scale wiggles on the strings such that the effective mass per unit length μ does not match up with the tensions T, giving a net gravitational acceleration of the surrounding plasma towards the strings, see section 1.6.3.

In a nutshell, the magnetic field generation operates as follows: first, cosmic string loops generate vorticity in the primordial plasma via gravitational dragging (see section 5.3). This vorticity is in turn converted into a magnetic seed field through the Harrison-Rees mechanism, a process reviewed in

section 1.7.2. Once the seed field is produced, the magnetic field strength is diluted during the ensuing Hubble expansion, but amplified during the protogalactic collapse, though the correlation decreases drastically, section 1.7.3. From the time of protogalactic collapse till our present time fields can get amplified in spiral galaxies by means of a dynamo, such as the $\alpha\omega$-dynamo. It is then possible for the magnetic field to get amplified until its strength reaches today's observable value (see table 1.1 for possible amplification factors). If we assume very efficient dynamos with $\Gamma_{dy}^{-1} \simeq 0.3$Gyr, we obtain reasonable values for the magnetic field to account for today's magnetic fields in spiral galaxies.

We present analytic and numerical techniques to estimate the magnetic fields produced by the cosmic string network. Our analytic estimates show that loops give the dominant contribution to the total magnetic field produced by the network, and not long string encounters as was previously claimed in [136, 137]. Further, in addition to giving a prediction of the overall field strength, we compute the spectrum of field strength as a function of correlation length and fractional horizon volume coverage. We do this by considering two semi-analytic string network models, the velocity dependent one-scale model (VOS) and the one-scale model (OSM), which are briefly reviewed in section 1.6.2. We also incorporate the evolution of loops (changes in size, translational and rotational velocity) due to emission of gravitational waves, Hubble expansion and dragging of the plasma. To that end, we also provide approximate analytic solutions, which were used to test the numerical code.

The values we take for various constants as well as their sources are summarized in table 5.1.

5.2 Loop Dynamics

This section introduces an analytic study of loop dynamics and can be read independently of the succeeding ones. The equations of motion are integrated numerically within our code (our results are presented in section 5.4.2) and we tested that the analytic approximations below are recovered correctly.

Loops are acted upon by a variety of effects: dynamical friction forces, which are responsible for accreting matter around loops, slow the loops down, both in its translational as well as its rotational movement. On the other hand, the emission of gravitational waves can speed up the translational movement, whereas the rotational one always decreases. Also, the size of loops decreases as a result of gravitational wave emission. Further, redshifting due to the Hubble expansion slows loops down, but leaves the rotational

movement unscathed.

Based on these effects we derive the differential equations that govern the evolution of the translational velocity $v_t(t)$, rotational velocity $v_r(t)$ and length $\ell(t)$ of a loop.

Since we use a rigid loop approximation when we compute gravitational dragging of the plasma, we need that v_r, v_t and ℓ evolve much slower than the typical time-scale during which the plasma is affected by a loop whizzing by. This will indeed be the case for the study presented here so that the approximations we make in section 5.3 are valid.

5.2.1 Changes in Size and Shape

The length of the loop decreases due to gravitational radiation, so that

$$\begin{aligned} \ell(t) &= f_r \alpha L_H(t_F) - \Gamma_l G\mu_0 (t - t_F) && (5.1) \\ &\equiv \ell_0 - G\Gamma_l \mu_0 (t - t_F)\,, && (5.2) \end{aligned}$$

where $f_r \leq 1$ describes energy loss directly after formation, $\Gamma_l \approx 50$ controls the efficiency with which the loop emits gravitational radiation [128,130,131], $\ell_0 \equiv \tilde{\alpha} t_F = f_r \alpha L_H(t_F)$, and the time scale for loop shrinkage is

$$t_{shrink} \equiv \frac{\tilde{\alpha}}{G\Gamma_l \mu_0} t_F = 2000 t_F\,, \qquad (5.3)$$

for $\tilde{\alpha} = 0.01$ and $G\mu_0 = 10^{-7}$; so a loop with $\tilde{\alpha} > 10^{-5}$ remains large enough for magnetogenesis for many Hubble times. Further, large-scale loop oscillations change the shape of the loop. (Small scale oscillations of the string are averaged over to give the effective tension T and linear mass density μ). If the oscillation timescale is comparable to the rotation period, the rigid loop approximation does not apply. Since the initial velocity distribution on the loop has to be quite peculiar to yield a fast oscillation affecting the loop as a whole, we expect that these oscillations make only a small fraction of loops unsuitable.

5.2.2 Translational Movement

Three effects determine the drift velocity of a loop: redshifting from Hubble expansion, dynamical friction due to dragging of the plasma as computed in (5.34) below, and recoil from gravitational wave emission [166] (often refereed to as the *rocket effect*). The latter causes an acceleration of $\Gamma_p G\mu_0 \hat{n}/\ell$, where $\hat{n}$ is a unit vector in the direction of recoil and $\Gamma_p \approx 10$ [166]. (It is μ_0 and

not $\lambda = \mu - T = \mu(1 - \mu_0^2/\mu^2) \approx 0.56\mu_0$ which determines the emission of gravitational waves.) Incorporating these forces leads to

$$\dot{\mathbf{v}}_t = -H\mathbf{v}_t - \frac{\mathbf{v}_t \ln\theta_{min}^{-1}}{t_*} + \frac{\Gamma_p G\mu_0}{\ell}\hat{\mathbf{n}}, \tag{5.4}$$

where [167, 168] t_* is

$$t_* = \frac{v_t^3}{8\pi^2 G^2 R\lambda\rho}\,, \tag{5.5}$$

and

$$\theta_{min} = \frac{2G\lambda\ell}{v_t^2 r_{max}}\,, \tag{5.6}$$

and $r_{max} = \int v_t dt \simeq 3vt$. In the matter era, using $H = 2/(3t)$ and $8\pi G\rho = 3H^2$ gives

$$t_* \equiv \frac{v_t^3 t^2}{C_1}\,, \quad C_1 = \frac{2}{3}G\ell\lambda\,. \tag{5.7}$$

Since our arguments in the previous subsection show that the loop length ℓ decreases very little over the timescales we are interested in, we take ℓ to be a constant. Further, we ignore the time dependence in the logarithm and estimate this factor by [1]

$$\ln\theta_{min}^{-1} \;\approx\; \ln\left(\frac{3v_t^3(t_F)t_F}{2G\lambda\ell}\right) = \text{const}\,, \tag{5.8}$$

where the time of loop creation is

$$t_F = \ell/\tilde{\alpha}. \tag{5.9}$$

Different initial values can lead to large differences in the long-term behavior of v_t. The loop either slows rapidly, or accelerates quickly to relativistic velocities from the rocket effect. Below we integrate the dynamical equation (5.4) in each regime, and derive the limiting velocity v_{lim} that separates the two regimes. Without the rocket effect term, equation (5.4) becomes

$$\dot{v}_t = -\frac{2}{3t}v_t - \frac{C_1\ln(\theta_{min}^{-1})}{t^2 v_t^2}\,, \tag{5.10}$$

[1] We approximate $r_{max} = \int v_t\,\mathrm{d}t \approx 3v_t t \approx 3v_t(t_F)t_F$, anticipating $v_t \propto 1/a \propto 1/t^{2/3}$ initially, due to redshifting.

which has the solution

$$\begin{aligned} v_t^f(t) &= t^{-2/3}\left(-3C_1\ln(\theta_{min}^{-1})t + \frac{\ell}{\tilde{\alpha}^2}(3C_1\ln(\theta_{min}^{-1})\tilde{\alpha} + v_0^3\ell)\right)^{1/3} \\ &\approx v_0\left(\frac{\ell}{\tilde{\alpha}t}\right)^{2/3}\left(1-\frac{t}{t_f}\right)^{1/3} \end{aligned} \tag{5.11}$$

where the last step uses $v_t(t_F) = v_0$, neglects $3C_1\tilde{\alpha}\ln(\theta_{min}^{-1})$, and employs the time scale of dynamical friction defined by

$$t_f \equiv \frac{v_0^3\ell}{2\lambda G\tilde{\alpha}^2\ln(\theta_{min}^{-1})}\,. \tag{5.12}$$

When dynamical friction is irrelevant (5.4) becomes

$$\dot{v}_t = -\frac{2}{3t}v_t + C_2\,, \tag{5.13}$$

where $C_2 \equiv \Gamma_p G\mu_0/\ell$ and we assume that the recoil is collinear with the velocity. This has the solution

$$\begin{aligned} v_t^r(t) &= \frac{1}{5t^{2/3}}\left(3C_2t^{5/3} - \frac{\ell^{2/3}}{\tilde{\alpha}^{5/3}}\left(3\ell C_2 - 5v_0\tilde{\alpha}\right)\right) \\ &\approx v_0\left(\frac{\ell}{\tilde{\alpha}t}\right)^{2/3}\left(1+\left(\frac{t}{t_r}\right)^{5/3}\right)\,, \end{aligned} \tag{5.14}$$

where we neglect $3\ell C_2$ in the last step (this is justified for the parameters we are interested in, see Table 5.1) and introduce the relevant time scale t_r for the rocket effect

$$t_r \equiv \left(\frac{5v_0}{3\Gamma_p G\mu_0}\right)^{3/5}\frac{\ell}{\tilde{\alpha}^{2/5}}\,. \tag{5.15}$$

If t_r and t_f are of the same order of magnitude, both dynamical friction and the rocket effect are important, but if $t_r > t_f$ friction dominates and vice-versa. Thus, we can introduce a limiting initial velocity by setting $t_r = t_f$

$$v_{lim} = G^{1/6}\left(\frac{\lambda^5}{\mu_0^3}\right)^{1/12}\left(\frac{5}{3\Gamma_p}\right)^{1/4}2^{5/12}\tilde{\alpha}^{2/3}(\ln\theta_{min}^{-1})^{5/12}\,, \tag{5.16}$$

Hence, for $v_t \ll v_{lim}$ dynamical friction is more important, whereas for larger velocities, the rocket effect predominates in the long run. What is a reasonable initial value for v_t? If large loops are created in the matter era, we expect

their velocities to be comparable to the RMS velocity in the string network $v_{RMS} \sim 0.6$ [2]. If we average over the small scale wiggles, the RMS velocity drops down to $\bar{v}_{RMS} \sim 0.15$ [134], so the initial translational velocity of the loops should be smaller too. Rotating loops share kinetic energy between translation and rotation, so an initial value of $v_t \sim v_r$, say down to 0.4, may be reasonable. This velocity is still larger than the limit velocity (5.16), even for the largest loops produced in the network: for $\tilde{\alpha} = 0.01$ and the bound $G\lambda/0.56 = G\mu_0 \lesssim 10^{-7}$, the limiting velocity becomes $v_{lim} \lesssim 0.0072$, where we approximated $\ln \theta_{min}^{-1} \approx 19$, based on (5.8) with $v_t(t_F) = 0.4$. Hence, the translational velocity of loops which are created in the matter era is given by

$$v_t(t) \approx v_0 \left(\frac{\ell}{\tilde{\alpha} t}\right)^{2/3} \left(1 + \left(\frac{t}{t_r}\right)^{5/3}\right) , \tag{5.17}$$

for all relevant values of $\tilde{\alpha}$. The loop initially slows due to redshifting, even though the rocket effect dominates over dynamical friction. Indeed, for $\tilde{\alpha} \sim 0.01$, $v_0 = 0.4$ and $\Gamma\mu_0 = 10^{-7}$ we have $t_r \approx 197\ell/\tilde{\alpha} = 197\, t_F$. In this case, v_t drops down to the minimal value of $v_t \approx 0.024$ at $t \approx t_r 3/4$, and it increases linearly thereafter up until loop shrinking becomes important. Since it takes more than $1000\, t_F$ for a loop to accelerate so that it moves faster than v_0 again, we expect the majority of loops to have a translational velocities of order $v_t \sim \mathcal{O}(10^{-1})$, which we use as a rough estimate of v_t for loops created between t_{eq} and t_{dec}. Since $t_r < t_{shrink}$ from (5.3), our assumption of a fixed loop length ℓ is justified.

5.2.3 Rotational Movement

The rotational velocity v_r of a loop is influenced by three effects: dynamical friction from plasma drag, emission of gravitational radiation [3] which produces a torque [170]

$$\tau_{gr} = -\ell G \mu_0^2 \Gamma_{gr} , \tag{5.18}$$

where $\Gamma_{gr} \approx 5$ [170], and the shrinking of the loop from gravitational wave emission. The torque τ_{drag} from dynamical friction is computed using the

[2] Recent simulations and analytic arguments suggest two distinct classes of loops [123, 169]: small, highly relativistic loops, and large ones, which have the velocities we consider.

[3] There is no rocket effect for angular momentum: numerical studies show that the emission of gravitational waves always decreases the angular momentum [170], even though a rigorous mathematical proof is lacking. The fundamental mass density μ_0 determines this effect and not the effective mass density λ.

arguments of section 5.3, applied to a single loop rotation. During one rotation, spanning a time $\Delta t \sim \ell/v_r$, the surrounding plasma acquires an angular momentum of roughly

$$\Delta J \sim \ell \Delta p_{plasma} \sim \ell^4 \rho v_x \sim \frac{\ell^4 \rho v_y^2}{7 v_r} \tag{5.19}$$

which gives the torque

$$\tau_{drag} \approx -\frac{(2\pi)^2}{7}\frac{G^2\lambda^2}{v_r^2}\ell^3\rho. \tag{5.20}$$

Loop shrinkage enters via the expression for the total angular momentum J,

$$\dot{J} = \frac{\lambda}{4\pi}\left(2\ell\dot{\ell}v_r + \ell^2\dot{v}_r\right), \tag{5.21}$$

with $\ell(t)$ from (5.2). We neglect redshifting of the rotational velocity for loops well within the horizon. Unlike the translational velocity, it is possible to obtain analytic solutions for the rotational velocity with dynamical $\ell(t)$. Dynamical friction is negligible, since the ratio of torques is

$$\frac{\tau_{drag}}{\tau_{gr}} = \frac{(2\pi)^2}{7}\frac{\lambda^2\tilde{\alpha}^2}{\mu_0^2 v_r^2 \Gamma_{gr} 6\pi}\frac{t_F^2}{t^2} \approx 1.3\times 10^{-5}\frac{t_F^2}{t^2} \ll 1 \tag{5.22}$$

where we use $8\pi G\rho = 4/(3t^2)$ as well as $\lambda/\mu_0 \sim 0.6$, $\tilde{\alpha} \sim 0.01$, $v_r \sim 0.4$ and $\Gamma_{gr} \approx 5$. This leaves $\dot{J} = \tau_{gr}$, leading to

$$\dot{v}_r = \frac{2G\Gamma_l\mu_0 v_r(t) - C_{gr}}{\ell_0 - G\Gamma_l\mu_0(t-t_F)}, \tag{5.23}$$

where

$$C_{gr} = \frac{4\pi G\mu_0^2\Gamma_{gr}}{\lambda}, \tag{5.24}$$

and $\ell(t)$ is given by (5.2). Assuming the initial condition $v_r(t_F) = v_0$, then $v_r(t)$ is

$$v_r(t) = \frac{1}{2}\frac{C_{gr}f(t) + 2v_0\tilde{\alpha}^2}{G\Gamma_l\mu_0 f(t) + \tilde{\alpha}^2} \tag{5.25}$$

with

$$f(t) \equiv 2\tilde{\alpha}\left(1 - \frac{t}{t_F}\right) + G\Gamma_l\mu_0\left(1 - \frac{t}{t_F}\right)^2. \tag{5.26}$$

As with the translational velocity v_t, there is a critical initial rotational velocity that determines the future evolution of v_r, given by $v_{lim}^r \equiv C_{gr}/(2G\Gamma_l\mu_0)$. For the parameters in table 5.1 we get $v_{lim}^r > 1$, indicating that v_r decreases for all loops under consideration. What is then the initial velocity of a loop? Loops can be produced by self-intersections of a single string. In this case, we expect the intersecting pieces to move roughly in the same direction. As a consequence, most of the energy will go into translational movement and a loop with very little angular momentum but large momentum results, so that $v_r \ll v_t$. However, Loops can also be created when two strings, moving in opposite directions, intersect and chop off a loop. Loops formed in this way have very little momentum, but large angular momentum, so that initial rotational velocities comparable to the RMS velocity of the network result $v_r \approx v_{RMS}$, while $v_t \ll v_r$. An ideal loop for magnetogenesis lies somewhere in between. Optimally efficient loop magnetogenesis requires rotation to stir up the plasma, but also rapid translational motion to sweep over a large fraction of the universe. To account for kinetic energy in the form of the small scale wiggles and oscillations of the loop, as well as the angular momentum that is radiated away in gravitational waves immediately after its creation, we take $v_r \sim 0.4 < v_{RMS}$ to be a conservative initial value.

5.3 Accretion

In this section we focus entirely on the generation of vorticity by a rotating loop, since it is a precondition for the Harrison-Rees mechanism to create magnetic flux, see section 1.7.2. Based on the results of section 5.2. we use a rigid loop approximation, that is, we assume that loops do not drastically change their size, shape, rotational or translational velocity, while the plasma is affected by the loop. We also use a circular loop, not because we expect that loops are circular in real life, but because this simplifies our computations and should yield reasonable estimates.

Why do we expect loops, and the vortices they create, to be important in the first place? Before we delve into the computational aspects, lets contemplate this question: Since vortices are real astrophysical objects, they are subject to many physical processes [4]. For instance, though there might be a small vortical component to the plasma flow in the region between two widely separated cosmic string wakes, this vast distance will encompass many local over- and under-dense regions, complicating the physics. On the other hand, the length scales perturbed by string loops are somewhat smaller, and

[4] In this study we will not consider all of them, and our comparisons of the length scales and vortex velocities should be viewed in this light.

should thus be less subject to the whims of small plasma variations. Furthermore, the strings are doing more than generating vortical motions and magnetic fields: they are accreting matter. This adds to local over-densities, and makes the regions over-swept by strings somewhat more likely later to collapse and develop structure. We should also have string loops attracted to relatively overdense areas. We may thus expect regions that have been affected by string-loop magnetogenesis to be, preferentially, those regions which later form structure. Though small, we believe this phenomenon will help to increase the effective coverage of loop-sourced magnetic fields, since even if they fail to cover the whole universe, the parts that they do cover will likely be the parts that will eventually host galaxies.

5.3.1 Gravitational Dragging by Loops

We mentioned repeatedly that rotational velocity flows in the plasma can be sourced by a loop, but how does it work in detail? First, assume that a loop is in a typical state of motion, meaning it possesses a nonzero angular velocity ω and some translational velocity. Gravitational interaction causes a drag force from the loop which then transfers angular momentum to the plasma in a straightforward fashion. The correlation length of the rotational flow, and thus of the magnetic field, is set by the size of the loop.

To compute this effect, we follow the procedure introduced in section 1.6.3, that is we use the Newtonian approximation to compute the infall velocity and thereafter the drag velocity as a second order effect. Thus our first task is to compute the gravitational impulse exerted on a test particle by a passing rotating loop. We consider a rigid, circular loop of radius R, length $\ell = 2\pi R$, and linear (gravitationally relevant) mass density $\lambda = \mu - T = \mu(1 - \mu_0^2/\mu^2)$, with its angular velocity ω and translational velocity v_t oriented along the z-axis. This situation is illustrated in Figure 5.1.

Although analytic solutions to the loop equations of motion are known [171], in general the loop dynamics are quite complex, and certainly we do not expect cosmic string loops to act precisely as the rigid loops we study here. Nonetheless, we assume that the relevant physics operating on the largest loop length scales is effectively captured by the idealization of a rigid loop, and its "coarse-grained" properties such as velocity, angular momentum, mass and size. The parameters ℓ, v_r and v_t are all functions of time, thanks to the dynamical forces acting on the loop and its emission of gravitational radiation. We described the equations that govern these quantities in section 5.2, and find that ℓ, v_r and v_t change very little over the timescales associated with test particle encounters. While we take all of these dynamical forces into account when studying the long-term evolution of the loop

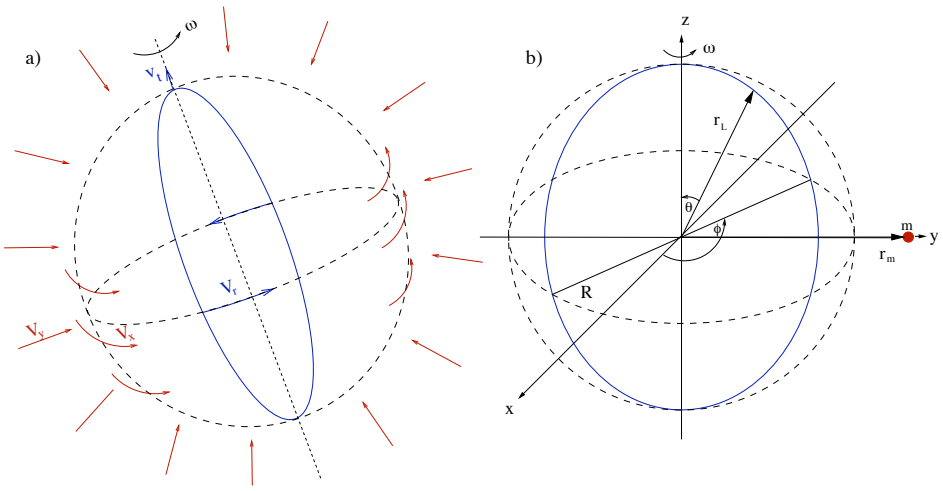

Figure 5.1: A rotating loop with angular velocity ω and drift velocity v_t attracts the surrounding plasma with a net velocity of order $v_\perp \sim G\lambda/v_t$, which in turn causes a vortex with rotational velocity of order $v_\parallel \sim v_\perp^2/v_r$ over the size of the loop. The resulting angular velocity of the plasma is of order $\omega_{pl} \sim \lambda^2 G^2/(R v_t^2 v_r)$.

population, for the purpose of estimating the drag on the plasma, we treat ℓ, v_r and v_t as constants.

Switching to the loop's rest frame, we consider a particle at $\mathbf{r}_m = \tilde{R}\hat{\mathbf{y}}$. At time t, we parameterise points $\mathbf{r}_L$ on the loop by

$$\mathbf{r}_L = R \begin{pmatrix} \sin\pi\sigma\, \cos\omega t \\ \sin\pi\sigma\, \sin\omega t \\ \cos\pi\sigma \end{pmatrix} \tag{5.27}$$

where σ ranges over $-1 \ldots 1$. We take the ratio

$$\mathcal{R} = \frac{\tilde{R}}{R} \tag{5.28}$$

to be larger than, but close to, unity. We further define the displacement $\mathbf{d} = \mathbf{r}_L - \mathbf{r}_m$ with magnitude

$$d = R\left(1 - \frac{2y_m}{R}\sin\pi\sigma\sin\omega t + \frac{y_m^2}{R^2}\right)^{1/2}. \tag{5.29}$$

Recalling that we have defined x as the direction parallel to the string's motion, we know that the acceleration component a_x vanishes to first order if we average over a full rotation. The net acceleration is in the y-direction,

toward the loop, and given by

$$a_y = \pi G\lambda R \int_0^1 \mathrm{d}\tau \int_{-1}^1 \mathrm{d}\sigma \frac{d_y}{d^3} = \mathcal{C}_1 \pi \frac{G\lambda}{R}, \tag{5.30}$$

where $\tau = t/T$, with T the loop rotation period $T = 2\pi/\omega$ and

$$\mathcal{C}_1 \equiv R^2 \int_0^1 \mathrm{d}\tau \int_{-1}^1 \mathrm{d}\sigma \frac{d_y}{d^3}\,, \tag{5.31}$$

which is of order one. (For example, one finds $\mathcal{C}_1 \approx -1/2$ for $\tilde{R} = 2R$). The net velocity toward the loop after one rotation is then

$$v_y \;\approx\; \frac{2\pi}{\omega}|a_y| = |\mathcal{C}_1| 2\pi^2 \frac{G\lambda}{v_r} \sim \pi^2 \frac{G\lambda}{v_r}\,. \tag{5.32}$$

Thanks to its drift velocity v_t, the loop undergoes roughly $4R\omega/(2\pi v_t) = 2v_r/(\pi v_t)$ rotations before it moves away from the test particle, so the total velocity acquired by the test particle during the encounter is

$$v_y \sim \frac{2\pi G\lambda}{v_t}\,, \tag{5.33}$$

which is similar to the straight string case in (1.106). Only the translational velocity v_t enters this expression, since the longer a particle experiences the gravitational attraction towards the loop, the faster they approach each other in the end.

The drifting loop drags the plasma behind it – just as a straight string does – but unlike the string encounter, the flow has a rotational component. The drag velocity in the x-direction is again of order $v_x \sim v_y^2/v_t$ (see below), resulting in a dynamical friction force on the loop of $F \sim R^2\rho v_y^2 \sim R^2\rho G^2\lambda^2/v_t^2$. This has two effects on the loop. First, it feels a net force due to dynamical friction of [167, 168]

$$\dot{v}_t = -\frac{v_t}{t_*} \ln \theta_{min}^{-1} \tag{5.34}$$

where θ_{min} and t_* are defined in (5.6) and (5.5) respectively. Second, because the loop rotates, the drag force generates a vortical flow. As in the long string case, this is a second-order effect. The acceleration in the x-direction due to an infinitesimal element of the loop $\mathrm{d}\sigma$ is

$$\mathrm{d}a_x \;=\; \frac{\pi G\lambda R^2}{d^3} \sin\pi\sigma \cos\omega t \; \mathrm{d}\sigma \tag{5.35}$$

Substituting the first-order trajectory of the test particle, given by

$$y_m(t) = \tilde{R} + v_y \left(t - \frac{\pi}{\omega}\right) \tag{5.36}$$

with $y_m(\pi/\omega) = \tilde{R}$, into (5.35), expanding in terms of $\varepsilon \equiv v_y(t - T/2)/R \ll 1$, computing the drag velocity by integrating the first order term over a single period (the zeroth order contribution vanishes due to symmetry), and replacing $G\lambda$ in terms of v_y results in

$$v_x \approx \frac{v_y^2}{v_r}|\mathcal{C}_2| \sim \frac{v_y^2}{7\, v_r}, \tag{5.37}$$

where

$$\begin{aligned} \mathcal{C}_2 \equiv\ & 12\pi \int_{-1}^{1} \mathrm{d}\,\sigma \int_0^1 \mathrm{d}\tau \sin\pi\sigma \cos 2\pi\tau \left(\tau - \frac{1}{2}\right) \\ & \times \frac{\mathcal{R} - \sin\pi\sigma \sin 2\pi\tau}{(1 + \mathcal{R}^2 - 2\mathcal{R}\sin\pi\sigma\sin 2\pi\tau)^{5/2}}\,. \end{aligned} \tag{5.38}$$

Numerical integration gives $\mathcal{C}_2 \approx -0.14$ for $\mathcal{R} = \tilde{R}/R = 2$, so we take $\mathcal{C}_2 = -1/7$. The drift velocity v_t enters (5.37) via $v_y \sim 2\pi G\lambda/v_t$, so as a result of the drag force, the plasma is stirred up with angular velocity

$$\omega_{pl} \sim \frac{v_x}{\ell} \sim \frac{v_y^2}{7\ell v_r} \sim \frac{(2\pi)^2\lambda^2 G^2}{7\,\ell v_t^2 v_r}\,, \qquad \text{(loops)} \tag{5.39}$$

where we take the vortex size to be given by the loop length $\ell = 2\pi R$.

As we have shown in section 5.2 $v_r(t)$ and $v_t(t)$ are comparable to the average velocity of straight strings, v_s. Therefore the ratio of vorticities is essentially controlled by the ratio ℓ/R of loop length to long string separation. Since the loop must linger in each region of space long enough to establish a vortex, vortices are only created when $v_r > v_t$.

5.3.2 Comparison: Vortices between Straight Strings

In section 1.6.3 we computed the flow behind a single long string; a simple superposition of the flow beyond two oppositely moving strings yields the flow depicted in Figure 5.2, which is not rotational.

A rotational flow can be created by vortices that build up due to turbulence in the string wake, as first proposed by Vachaspati and Vilenkin [134,135] (see also [151,172]). The authors of [151] argue that a two-string encounter creates a vortex whose size is comparable to the interstring distance,

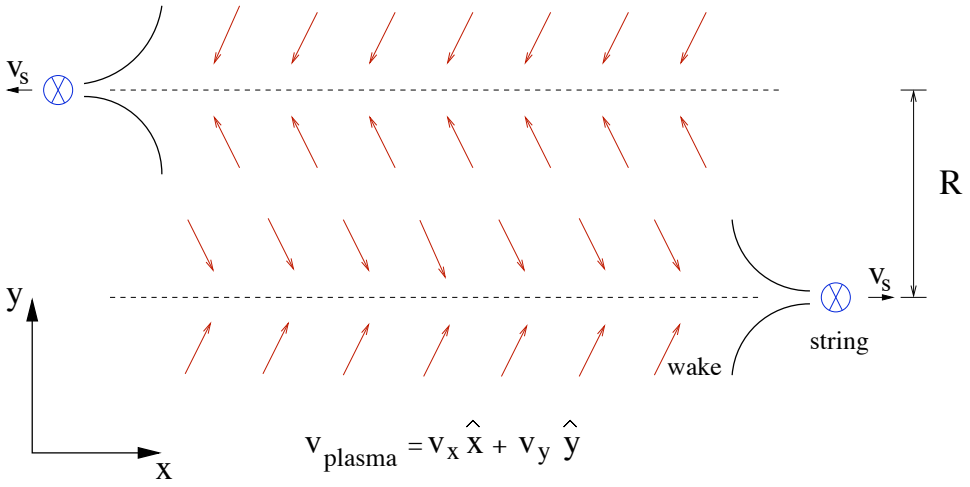

Figure 5.2: Two straight strings with effective Newtonian mass density $\lambda = \mu - T$ cause wakes in the surrounding plasma via gravitational interaction. After the encounter, the magnitude of the dragging component of the plasma flow velocity is approximately $v_y \sim G\lambda/v_s$ and $v_x \sim v_y^2/(v_s)$. The resulting plasma flow carries at most a rotational component of velocities up to $v_{rot} \sim v_x$ over interstring distances, so that an angular frequency of order $\tilde{\omega}_{pl} \sim \lambda^2 G^2/(R v_s^3)$ results, see (5.43).

with rotational velocities comparable to the infall velocity of the plasma $v_{rot} \sim v_y$. Dimopoulos and Davis [136, 137] later investigated the two-string encounter assuming the same plasma flow. The argument they employ runs essentially as follows: plasma of density ρ in a region of volume $V \sim R^2 v_s T$, with post-encounter net momentum $\Delta p \sim R^3 \rho v_x$, leads to a force on the string of $F \sim \Delta p/T \sim R^2 \rho v_y^2$. Applied over a distance R, the string does work $W_s \sim \rho R^3 v_y^2$. If we were to assume that the overall flow in the region V is rotational and were to set $E_{rot} \sim \rho R^3 v_{rot}^2$ equal to W_s, this would imply $v_{rot} \sim v_y$ [5]. The keystone of these proposals is the assumption that the vortex size is comparable to the interstring distance, and that it carries the majority of the total kinetic energy imparted to the plasma. However, such a vortex is not present immediately after the encounter as indicated in Figure 5.2. Indeed, the change in angular momentum of the strings due to the dragging of the plasma is roughly $\Delta J_s \sim R\Delta p \sim R^4 \rho v_x$. Conservation of angular momentum implies that the plasma may have, at most, a rotational compo-

[5] An additional factor of 2 in [137] stems from taking $v_{rot} \sim u \equiv 2v_y$, where u is the relative velocity of particles on opposite sides of the string.

nent in the volume $\sim R^3$ with angular momentum $J_{plasma} \sim R^4 \rho v_{rot} \sim \Delta J_s$. Therefore the net rotational velocity is closer to $v_{rot} \sim v_x$, which is much smaller than v_y. This is illustrated schematically in Figure 5.2.

These simple estimates can be improved as follows. The wake behind a single string, created at $t_F \gtrsim t_{eq}$, has a length l_w, width w_w and thickness d_w, given by the scaling relations [117, 173–175]

$$l_w \sim t_F \frac{z_F}{z} \ , \ w_w \sim v_s t_F \frac{z_F}{z} \ , \ d_w \sim v_y t_F \left(\frac{z_F}{z}\right)^2 \ , \tag{5.40}$$

which are valid for $z > z_F v_y / v_s$. Turbulent eddies arise within the wake shock [172], and could potentially lead to large rotational velocities of order v_y. However, the characteristic size associated with matter chunks due to fragmentation of the wake is comparable with the thickness of the wake d_w behind an individual string [117, 176, 177]. We expect turbulent, gravitationally supported vortices at this length scale. Comparing this thickness to the interstring distance $R(t) \sim P^\beta v_s t$ yields

$$\frac{d_w}{R} \ \sim \ \frac{v_y t_F \left(z_F/z\right)^2}{v_s P^\beta t} \sim 2\pi \sqrt{\frac{z_F}{z}} \frac{G\lambda}{v_s^2 P^\beta} \, , \tag{5.41}$$

where we use v_y from (1.106), P is the intercommutation probability [6], $1/2 \leq \beta \leq 1$ [178], and $t_F/t = (a_F/a)^{3/2} \sim (z/z_F)^{3/2}$. Considering mildly relativistic strings ($v_s \sim 0.1$ as an order of magnitude) and the largest possible $G\lambda \sim 10^{-7}$, we are left with

$$\frac{d_w}{R} \ \sim \ 2\pi \sqrt{\frac{z_F}{z}} \frac{10^{-5}}{P^\beta} \, . \tag{5.42}$$

The vorticies relevant for magnetogenesis are created toward the end of the radiation era, so the redshifting factor is of order unity and vortices due to turbulence in the string wake are much smaller than the interstring distance. The seed fields necessary to initiate plausible galactic dynamos should be coherent over distances of at least $\xi_{seed} \sim 5 - 50\,\mathrm{pc}$ at decoupling, but $d_w \sim 1\,\mathrm{pc}$ for turbulent eddies created around t_{dec}. We reviewed the relevant length scales in more detail in chapter 1.7.3.

Since the magnetic field is directly proportional to the angular velocity of the plasma, our new estimate greatly reduces the expected strength of magnetic fields produced by the long strings. Our arguments indicate that

[6] $P \approx 1$ for cosmic strings, $10^{-1} \leq P \leq 1$ for D-strings and $10^{-3} \leq P \leq 1$ for F-strings [120].

the drag velocity v_x is the relevant velocity for magnetic fields that are coherent over interstring distances, not the infall velocity v_y. This gives a plasma vorticity

$$\omega_{pl} \sim \frac{v_x}{R} \sim \frac{v_y^2}{2Rv_s} \sim \frac{(2\pi)^2\lambda^2 G^2}{2Rv_s^3}\,. \qquad \text{(long strings, this thesis)} \tag{5.43}$$

This is in contrast with [136, 137] which obtains the estimate

$$\omega_{pl} \sim \frac{v_y}{R} \sim \frac{2\pi\lambda G}{v_s R}\,. \qquad \text{(long strings, previous)} \tag{5.44}$$

We find that while rotational velocities $\sim v_y$ are possible within the string wake, by (5.42) their correlation length is much smaller than the interstring distance R.

To summarize: vortices due to turbulence in the string wake are confined to small scales, much smaller than the interstring distance R. Even though these vortices may have large rotational velocities, their small size makes them far less appealing for magnetogenesis.

5.4 Magnetic Fields

We have seen how vorticity can arise in a string network. Here, we present our analytic and numerical finding of the magnetic fields created within a string network.

5.4.1 Analytic Estimates Near Decoupling

Straight string encounters near decoupling produce vorticity given by ω_{pl} from (5.43), which by the Harrison-Rees mechanism creates a seed field of

$$B_s \sim 10^{-4}(2\pi)^2\frac{(\mu-T)^2G^2}{2v_s^3R} \lesssim 1.6P^{-\beta}\times 10^{-26}\,\mathrm{G}\,, \tag{5.45}$$

where we use $G(\mu - T) \leq 10^{-7}$, $v_s \geq 0.1$ and an interstring distance of $R = P^\beta v_s t_{dec}$. These fields have a correlation length at decoupling of

$$\xi_s \sim 12\,P^\beta\,\mathrm{kpc}\,. \tag{5.46}$$

The field strength in (5.45) is several orders of magnitude smaller than the corresponding one in [137], since our estimates of the vorticity on large scales generated by a two-string encounter is much lower than that in [137]. Cosmic

strings with $P^\beta \sim 1$ and the largest possible string tension produce fields that are just strong enough to seed the most efficient dynamos. This improves somewhat for F and D-strings, which can have a lower P^β. In either case the coherence length is larger than the minimal one in (1.119).

The vorticity from rotating loops with ω_{pl} from (5.39) results in seed fields of

$$B_\ell \;\sim\; 10^{-4}\frac{(2\pi)^2}{7}\frac{(\mu-T)^2G^2}{\ell v_t^2 v_r}\,. \tag{5.47}$$

Taking $G(\mu - T) \leq 10^{-7}$, $v_t \geq 0.1$, $v_r \approx 0.4$ and defining a new parameter $\tilde{\alpha}$ such that the loop length ℓ at formation is

$$\ell = \tilde{\alpha} t_F = \frac{f_r \alpha}{H(t_F)}\,, \tag{5.48}$$

at $t_F = t_{dec}$ we obtain

$$B_\ell \lesssim \frac{2.9\times 10^{-29}}{\tilde{\alpha}}\,\mathrm{G}\,. \tag{5.49}$$

We use $v_t \geq 0.1$ since even a large initial velocity of $v_t \sim v_{RMS}$ decreases due to redshifting in the matter era, before it speeds up again due to the rocket effect (see section 5.2.2). Because redshifting is absent for the rotational movement, the rotational velocity decreases only very slowly due to the emission of gravitational waves, which is also counterbalanced by loop shrinking to some extend (see section 5.2); hence we use use $v_r \approx 0.4$ (section 5.2.3). Since $\tilde{\alpha} < P^\beta v_s$, we can achieve a larger field strength than for a straight string encounter. Consequently, less efficient dynamos work, but not all galaxies are so lucky as to have had a loop sweeping over them in the past. The coherence length

$$\xi_l \sim 117\tilde{\alpha}\,\mathrm{kpc}\,. \tag{5.50}$$

is large enough to seed the dynamo for $\tilde{\alpha} \geq 10^{-5}$, so that both the largest loops and many of the smaller ones contribute to magnetogenesis. The smaller the loops, the stronger the resulting seed field. The analytic estimates suggest similar contributions in magnetic field flux from long strings and loops. In fact, the results of the numerical estimates presented in section 5.4.2, which include more details of the loop dynamics and population characteristics, show that loops produce much stronger magnetic field fluxes than long strings. Partly this is because the loop length spectrum peaks at lengths much smaller than αL_H, which effectively lowers the value of $\tilde{\alpha}$ and greatly increases the fields they create. In addition, redshifting slows the loops, which then create stronger magnetic fields.

5.4.2 Numerical Estimates

After combining the analytical results of section 5.3 with the semi-analytic string network models introduced in section 1.6.2 and the loop dynamics of section 5.2 into a numerical code (see the appendix of [2] for more details on the code), we obtain the magnetic fields shown in Figures 5.3-5.4. We wish to determine the dependence of the magnetic field on the following:

1. $G\mu_0$, the string's bare tension;
2. our model for string network evolution (OSM/VOS);
3. whether or not string loops are allowed to undergo dynamics;
4. the initial velocity at which a loop moves after formation;
5. α, the average length of a new loop after it has formed.

This last parameter is under active study at present from both analytical [123, 179, 180] and numerical [124, 181–183] perspectives. The average length is important to understand because large loops live much longer than small loops. Loops lose their length by generating gravitational radiation, which will be, in the near future, under observational limits; since longer loops emit gravity waves later, they are more tightly constrained (see ref. [169] for much more detail). For the discussion of our numerical results, we will first treat the above parameters as free and independent parameters so as to study how each affects magnetogenesis. On the other hand, we will take our test values for $G\mu_0$ from observational constraints: a fiducial value of 2×10^{-7} [118, 119], an optimistic value of 7×10^{-7} [184], and the most constrained value of 2×10^{-8} [185]; the former two come from combining CMB data with other cosmological observations, while the latter one is from pulsar timing and the worst case scenario. At the end, we present constraints on what we consider to be the best motivated combination of parameters, which differs slightly from our fiducial model. Our fiducial model, used wherever nothing else is specified, includes: the VOS model for long strings; loop dynamics turned on; $G\mu_0 = 2 \times 10^{-7}$; $\alpha = 0.01$; and $v_t(t = t_F) = 0.1$. Where relevant, we have drawn a line demarcating the minimum correlation length necessary to seed galactic dynamos and a line indicating the minimum magnetic field strength necessary, given a particular dynamo amplification time, Γ_{dy}^{-1}.

In Figure 5.3a we show the scaling of the magnetic field spectrum with $G\mu_0$. In this plot, it is shown that as $G\mu_0$ decreases each loop becomes less effective at generating magnetic fields; as a result, the magnetic flux is reduced. In addition, the loop length spectrum peaks at a characteristic

length determined by $G\mu_0$ as derived in (1.6.2) for the OSM/VOS model. Reducing $G\mu_0$ causes the characteristic loop size to fall, shifting the magnetic field spectrum to smaller correlation lengths.

For several values of α the magnetic field strength as a function of correlation length is given in Figure 5.3b. The magnetic field is weakly dependent on α due to two effects: firstly, even though α sets the size of the largest loops, at any fixed time, the greatest number of loops have a characteristic length set by $G\mu_0$, as described by the OSM model (see section 1.6.2). Hence the magnetic field flux and the peak correlation length depend weakly on α. Second, loops will always decrease to smaller sizes even if they are created in models with much larger α, thus mimicking models with smaller α. The slight dependence of magnetic field strengths on α is evident. Note that the peak magnetic flux grows only slightly with α. This can be understood heuristically in the following way: as α decreases, the network must give off energy to an ever growing number of smaller loops, as a result, the fraction of the loops capable of creating magnetic fields at the peak correlation length, grows slowly as α decreases.

Figures 5.3c, 5.3d and 5.4a show, for different values of $G\mu_0$, α, and translational velocity v_t at the time of formation, the fraction of the universe covered with different magnetic field strengths. For viable magnetogenesis to occur, cosmic string loops must not only produce sufficiently strong magnetic fields, but must be produced over nearly the entire volume of the universe. Figure 5.3c shows a fall in peak magnetic field strength with decreasing $G\mu_0$ like in Figure 5.3a. As $G\mu_0$ decreases, the magnetic field strength decreases, although the overall shape of the curves looks almost the same. It can be heuristically argued that as the value of $G\mu_0$ diminishes, the loop network has about the same size and number of loops, thus producing the same volume coverage, though at much lower magnetic field values. Along the same lines, Figure 5.3d shows a similar weak dependence of the magnetic field strength on α as we saw in Figure 5.3b. The fraction of the volume swept out decreases with every lower value of α, the reasoning behind this relationship is that the network is saturated with a large number of of smaller loops. Strictly speaking, the volume swept out by a single loop is proportional to α^2, while that of the number of loops being produced is proportional to α^{-1}. Combining these two scaling gives an approximate linear scaling with α. In Figure 5.4a we note that decreasing the loop's translational velocity decreases the fraction of volume swept out, giving larger magnetic field strengths. This makes sense since slower loops sweep out less volume making them more prone to remain in a specific area for a longer period of time. Thus the loops have more time to produce stronger magnetic field strengths than if the loop translational velocity is greater as is evident in the plot.

Now we want to explore the effect of loop dynamics and the network model on our conclusions. A plot of the fraction of the horizon volume swept out versus the magnetic field strength is shown in Figure 5.4b. Note that the inclusion of loop dynamics increases the strength of the magnetic field, but decreases the volume swept out. This is so since loop dynamics decrease the loop translational velocity over time, thus leading to stronger magnetic fields. The model with the best physical motivation is the velocity-dependent-one-scale model with loop dynamics. In this model, string loops are produced at 10% of the horizon size, and we assume that only 10% of the energy which goes into loops is injected into loops of this size. The remaining 90% goes into loops created near the gravitational radiation back-reaction scale, through loop fragmentation, among other effects. Figure 5.4c shows a comparison of magnetic field strengths generated from loops and long straight strings encounters. For long string encounters, the vortices generated are spread over large length scales, leading to much weaker magnetic field strengths than those generated by rotating string loops. Thus, cosmic string loops give the dominant contribution to the total magnetic field on present-day galactic scales, and not long string encounters as it was previously claimed in [136,137]. Finally Figure 5.4d shows a relationship between the fraction of the horizon volume swept out and the correlation length for the five models discussed above.

5.5 Conclusion

We computed magnetic fields generated by the loop population within a cosmic string network. Our results give strong evidence that it is cosmic string loops and not long string encounters (which we re-evaluated yielding drastically different results as those previously claimed in the literature) that give the dominant contribution to the total magnetic field. Coherence length and field strength are large enough to account for magnetic fields observed in spiral galaxies, given that the dynamo amplification during the galactic rotations is reasonably strong. These magnetic fields are created by cosmic strings with a tension $G\mu_0 \gtrsim 10^{-8}$, a value still allowed by cosmological observations. If cosmic strings with the relevant tensions are discovered in the next few years, and if galactic dynamos turn out to be as efficient as we assumed, our mechanism for magnetic field magnetogenesis is viable. On the other hand, if cosmic strings are observed but the tensions are much smaller than we assume, or if the dynamo efficiency is small, then our mechanism is ruled out.

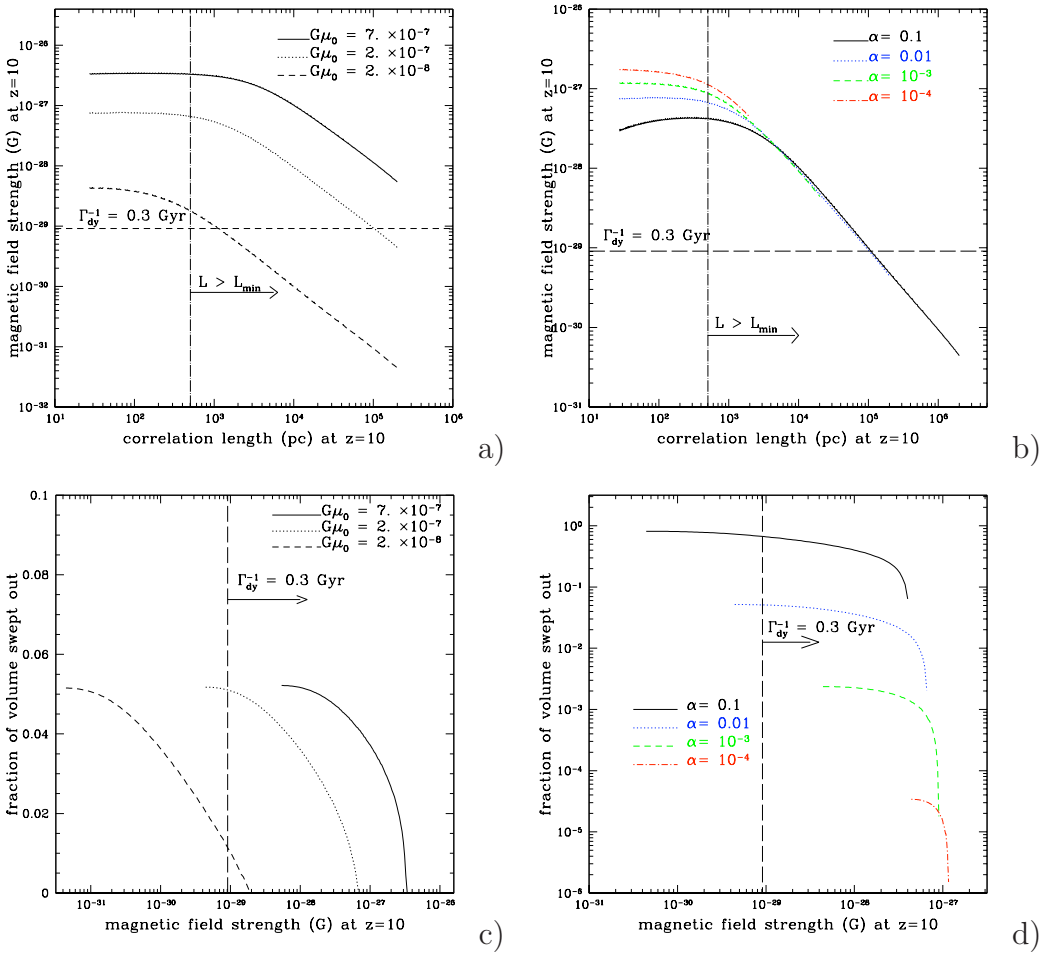

Figure 5.3: For all plots we assume the VOS model with loop dynamics, $G\mu_0 = 2 \times 10^{-7}$, $\alpha = 0.01$ and $v_t(t = t_F) = 0.1$. The horizontal axis gives the magnetic field strength at z=10, and the vertical axis shows the fraction of the volume of the universe immersed with a magnetic field of that flux or greater. **a)** represents a plot for different test values of the bare string mass per unit length μ_0; we plot the magnetic field strength as a function of the magnetic field's correlation length. **b)** shows a variation of magnetic field strength as a function of string formation length fraction α. In **c)** we again vary the mass density. Here we plot the volume of the universe imbued with a seed field as a function of the magnitude of the seed field flux. Finally, in **d)** we vary the initial loop size and show its effects on magnetic field strength and volume coverage.

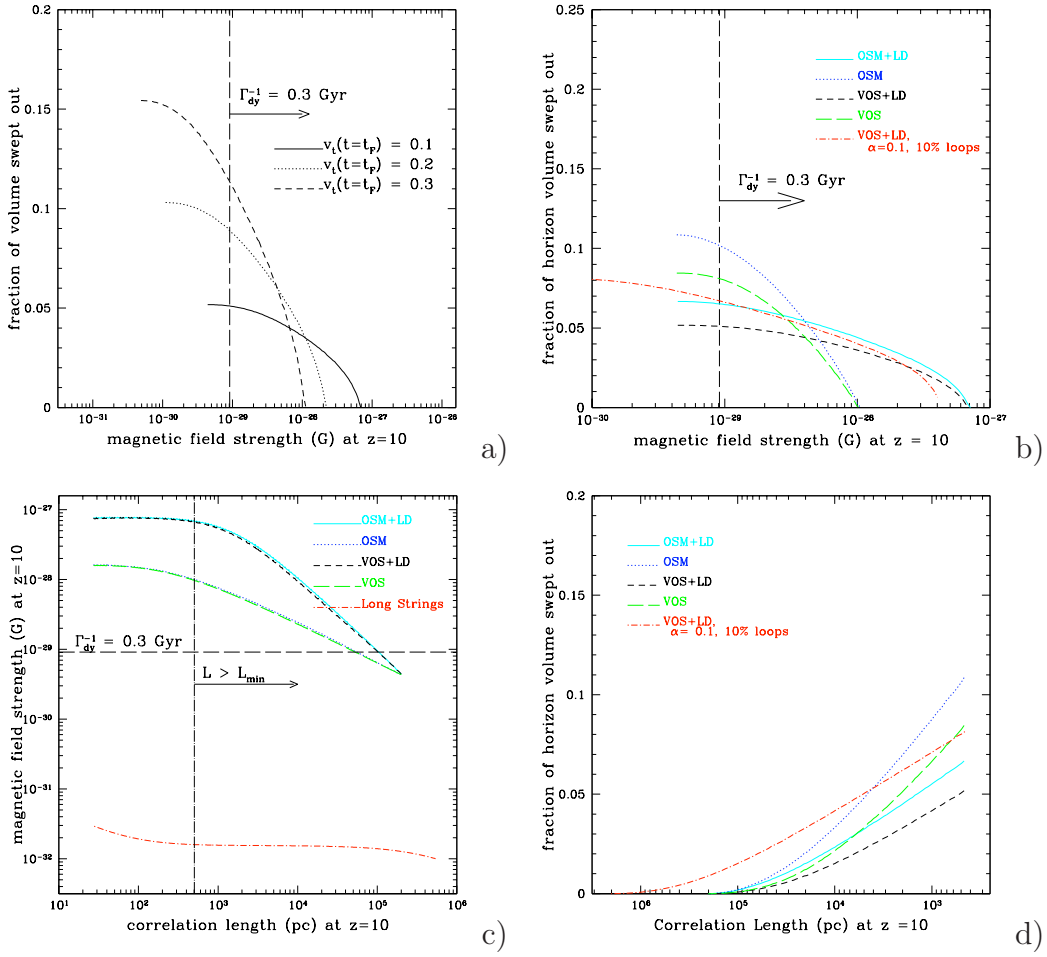

Figure 5.4: a) shows a variation of the initial translational velocity. **b)** shows the relationship between network model, OSM/VOS and loop dynamics (with or without). Since loops change their size over time, different volumes of space will be endowed with seed fields of differing magnitudes. Example to read the plot: the red line crosses 8% is at a magnetic field strength of approximately 10^{-30} G. What this means is that 8% of the volume of the universe at the time of galaxy formation was saturated with a seed field whose magnitude was equal to, or larger than, 10^{-30} G. Only fields whose correlation lengths are sufficiently large ($L_{corr} > 500$pc at $z = 10$) are included. We have also included what we believe to be the best motivated model: the VOS model for the long strings, loop dynamics, and $\alpha = 0.1$, but with only 10% of the string network's energy loss going into loops that large, with the rest lost to very small loops. **c)** shows a comparison between magnetic fields strengths from loops and strings. **d)** shows the fraction of the volume covered versus the correlation length for all models considered.

Param.	Value	Source	description, first used in (eqn.)
$G\mu_0$	2×10^{-7}	[118, 119]	string mass/length
μ	$1.9\mu_0$	[117], rad. era	effective mass/length (1.102)
	$1.5\mu_0$	[117], mat. era	
α	0.01	[117, 128]	size of large loop/horizon (1.88)
f_r	0.7	[128, 186]	loop redsh. energy loss (1.88)
$\tilde{\alpha}$	$f_r \alpha H^{-1}(t_F)/t_F$	Def. in (5.48)	new loop length over formation time
Γ_ℓ	50 $(\star)$		eff. of grav. wave em. [129] (1.88)
	$50 \lesssim \Gamma_\ell \lesssim 100$	[130]	
	$45 \lesssim \Gamma_\ell \lesssim 55$	[131]	
	50, 80	[128, 170, 187]	
Γ_{gr}	5	[170]	grav. wave em. $\rightarrow$ torque (5.18)
Γ_p	10	[166, 170]	rocket effect (5.4)
Γ_{dy}	0.2 Gyr $(\star)$		dynamo efficiency (1.115)
	$0.2 < \Gamma_{dy}^{-1}/\mathrm{Gyr} < 0.8$	[155, 188]	
	$\Gamma_{dy}^{-1} \gtrsim (1.1 - 1.4)\,\mathrm{Gyr}$	[141]	
	$\Gamma_{dy}^{-1} = 0.3\,\mathrm{Gyr}$	[161]	
	$\Gamma_{dy}^{-1} = 0.5\,\mathrm{Gyr}$	[159]	
	$\Gamma_{dy}^{-1} = 2.2\,\mathrm{Gyr}$	[162]	
z_{dec}	1089	[6]	redshift at decoupling
z_{gf}	6	[136]	redshift of galaxy formation
	10 $(\star)$		
t_{eq}	1.6×10^{12} s = 51 kyr		time of matter-radiation equality
t_{dec}	1.2×10^{13} s = 380 kyr		time of decoupling (5.45)
t_0	13.7 Gyr	[6]	age of the universe
v_{RMS}	0.60	[134], mat. era	RMS vel. in network
$\bar{v}_{RMS}$	0.15	[134], mat. era	RMS vel. avg. over corr. length
$\Omega_m h^2$	0.1277	[6]	mat. fraction (1.117)
h	0.732	[6]	Hubble parameter (1.117)
β	$1/2 \leq \beta \leq 1$	[137]	(5.41)
P	1 $(\star)$	cosmic strings	intercommutation probability
	$10^{-1} \leq P \leq 1$	D-Strings [120]	
	$10^{-3} \leq P \leq 1$	F-Strings [120]	
c_1	0.21 (0.2475)	[132, 133]	VOS parameters
c_2	0.18 (0.3675)		in radiation (matter) era
c_3	0.28		

Table 5.1: Our parameters. When several values are given, we select the one marked by a $(\star)$.

Chapter 6

Conclusions

The focus of this thesis was devoted to two distinct, major topics: non-Gaussianities and preheating in multi-field inflationary models, using $\mathcal{N}$-flation as a concrete example, and magenetogenesis from rotating cosmic string loops.

To evaluate whether non-Gaussianities are possible in $\mathcal{N}$-flation, we considered the non-linearity parameters f_{NL}, τ_{NL} and g_{NL} (characterizing the bi- and tri-spectrum) in the horizon crossing approximation. In this limit, $\mathcal{N}$-flation and simple single field inflationary models were found to be indistinguishable, with unobservable small non-Gaussianities. In order to lift this degeneracy, the evolution of the comoving curvature perturbation after horizon crossing was considered. This evolution is due to isocurvature perturbations, which can in turn cause additional non-Gaussianities. Thus, this evolution can provide the possibility to differentiate between models. To make the calculation concrete, we assumed the Marcěnko-Pastur mass distribution and equal energy initial conditions at the beginning of slow roll. Based on this, we computed the magnitude of f_{NL} for narrow and generic mass distributions (including broad ones, as favored in $\mathcal{N}$-flation). Even though additional contributions were found, they constitute only a few percent of the horizon crossing result, leading to the conclusion that they are unobservable. The apparent insignificance of the additional terms stems from the application of the slow roll approximation. For fast rolling fields, we expect larger contributions to f_{NL}, which may be present in models other than $\mathcal{N}$-flation. To illustrate, if a field suddenly begins to evolve faster, even as inflation continues, the trajectory in field space makes a sharp turn, inducing isocurvature perturbations to incite the adiabatic mode, generating non-Gaussianities.

Next, we constructed two distinct effective single field models, to investigate $\mathcal{N}$-flation in the era after the slow roll condition is violated for one

or more fields, but before preheating commences; the first one consists of the continued application of the slow roll result (beyond its domain of applicability) yielding a lower bound of the potential energy up until preheating starts. We then found an upper bound by holding subsequently fixed fields whenever their slow roll parameter η_i became of order one. Since the fields are still rolling slowly up until preheating starts and the trajectory in field space remains smooth, we conclude that additional non-Gaussianities are not produced in $\mathcal{N}$-flation during this era. Subsequently, preheating starts and non-Gaussianities may still be sourced – a topic that needs further investigation.

We followed with a study of preheating in $\mathcal{N}$-flation, coupling all axions to a single, scalar matter field. Employing our analytic approximations as well as numerical calculations we found that most of the energy is concentrated in a few light fields at the end of inflation. As a consequence, we focussed on these fields as the ones responsible for preheating. Our results differ considerably from those obtained in the literature in that we find parametric resonance effects to be largely absent during preheating. The reason why parametric resonance is suppressed in $\mathcal{N}$-flation is that the axions are out of phase, thus conspiring to average out each other's contributions to the matter field's effective mass. As a result, instead of an exponential increase of the amplitude during the matter fields oscillations, we find power law behavior. Thus, the old theory of perturbative preheating remains applicable in multi-field models of inflation such as $\mathcal{N}$-flation. For the sake of simplicity we made a few assumptions that include the consideration of only one matter field, while backreaction and rescattering were ignored during preheating. We expect that incorporating these effects leads to minor effects only, since explosive particle production due to parametric resonance is unimportant in $\mathcal{N}$-flation already. Indeed, the inclusion of these effects would cause a further decrease of resonance effects. Additionally, we assumed axion matter couplings to be equal to each other. Relaxing this assumption might in principle change the scenario quantitatively, however, qualitative changes are not expected.

We then shifted gears and focussed on the problem of seeding large scale magnetic fields. We proposed a mechanisms by which the primordial plasma is first stirred up by rotating, cosmic string loops within a string network in the early matter era before decoupling. Subsequently, ions and electrons are slowed down differently by interaction with the CMBR, causing currents which in turn seed magnetic fields (the Harrison-Rees mechanism). We used semi-analytic string network models as well as detailed loop dynamics to model the loop population realistically in a numerical code. Our results give strong evidence that it is cosmic string loops and not long string encoun-

ters which give the dominant contribution to the total magnetic field. We found that coherence length, field strength and horizon coverage are sufficient to account for magnetic fields observed in spiral galaxies, given that the dynamo amplification during the galactic rotations is reasonably strong. The magnetic fields so produced are created by cosmic strings with a tension $G\mu_0 \gtrsim 10^{-8}$, a value still allowed by cosmological observations. If cosmic strings with the relevant tensions are discovered in the next few years, and if galactic dynamos turn out to be as efficient as we assumed, our mechanism for magnetic field magnetogenesis is viable. On the other hand, if cosmic strings are observed but the tensions are much smaller than we assume, or if the dynamo efficiency is small, then our mechanism is ruled out.

Bibliography

[1] D. Battefeld and T. Battefeld, Non-Gaussianities in N-flation, JCAP **0705**, 012 (2007) [arXiv:hep-th/0703012].

[2] D. Battefeld, T. Battefeld, D. H. Wesley and M. Wyman, "Magnetogenesis from Cosmic String Loops," JCAP **0802**, 001 (2008) arXiv:0708.2901 [astro-ph].

[3] D. Battefeld, S. Kawai, "Preheating after N-flation," Phys. Rev. D **77**, 123507, (2008) arXiv:0803.0321 [astro-ph].

[4] T. Battefeld and R. Easther, "Non-gaussianities in multi-field inflation," JCAP 03 (2007) 020, [arXiv:astro-ph/0610296].

[5] E. Hubble, "A relation between distance and radial velocity among extra–galactic nebulae," Proc. Nat. Acad. Sci. **15**, 168 (1929).

[6] D. N. Spergel *et al.*, "Wilkinson Microwave Anisotropy Probe (WMAP) three year results: Implications for cosmology," arXiv:astro-ph/0603449.

[7] S. Perlmutter *et al.* [Supernova Cosmology Project Collaboration], "Measurements of Omega and Lambda from 42 High-Redshift Supernovae," Astrophys. J. **517**, 565 (1999) [arXiv:astro-ph/9812133].

[8] A. G. Riess *et al.* [Supernova Search Team Collaboration], "Observational Evidence from Supernovae for an Accelerating Universe and a Cosmological Constant," Astron. J. **116**, 1009 (1998) [arXiv:astro-ph/9805201].

[9] A. A. Penzias and R. W. Wilson, "A Measurement of excess antenna temperature at 4080-Mc/s," Astrophys. J. **142**, 419 (1965).

[10] G. F. Smoot *et al.*, "Structure in the COBE differential microwave radiometer first year maps," Astrophys. J. **396**, L1 (1992).

[11] R. A. Alpher, H. Bethe and G. Gamow. "The Origin of Chemical Elements," Physical Review, **73**, 803 (1948).

[12] M. Tegmark *et al.*, "Cosmological Constraints from the SDSS Luminous Red Galaxies," Phys. Rev. D **74**, 123507 (2006) [arXiv:astro-ph/0608632].

[13] W. J. Percival *et al.* [The 2dFGRS Collaboration], "The 2dF Galaxy Redshift Survey: The power spectrum and the matter content of the universe," Mon. Not. Roy. Astron. Soc. **327**, 1297 (2001) [arXiv:astro-ph/0105252].

[14] A. H. Guth, "The Inflationary Universe: A Possible Solution To The Horizon And Flatness Problems," Phys. Rev. D **23**, 347 (1981).

[15] A. Linde, "Inflationary Cosmology," Lect. Notes Phys. **738**, 1 (2008) [arXiv:0705.0164 [hep-th]].

[16] V. Mukhanov, "Physical foundations of cosmology," *Cambridge, UK: Univ. Pr. (2005) 421 p*

[17] B. A. Bassett, S. Tsujikawa and D. Wands, "Inflation dynamics and reheating," Rev. Mod. Phys. **78**, 537 (2006) [arXiv:astro-ph/0507632].

[18] D. H. Lyth and A. Riotto, "Particle physics models of inflation and the cosmological density perturbation," Phys. Rept. **314**, 1 (1999) [arXiv:hep-ph/9807278].

[19] A. D. Linde, "Chaotic Inflation," Phys. Lett. B **129**, 177 (1983).

[20] V. F. Mukhanov, H. A. Feldman and R. H. Brandenberger, "Theory of cosmological perturbations. Part 1. Classical perturbations. Part 2. Quantum theory of perturbations. Part 3. Extensions," Phys. Rept. **215**, 203 (1992).

[21] J. M. Bardeen, P. J. Steinhardt and M. S. Turner, "Spontaneous Creation Of Almost Scale - Free Density Perturbations In An Inflationary Universe," Phys. Rev. D **28**, 679 (1983).

[22] M. Sasaki and E. D. Stewart, "A General Analytic Formula For The Spectral Index Of The Density Perturbations Produced During Inflation," Prog. Theor. Phys. **95**, 71 (1996) [arXiv:astro-ph/9507001].

[23] A. A. Starobinsky, JETP Lett. **42**, 152 (1985) [Pis. Hz. Esp. Tor. Fizz. 42, 124 (1985)].

[24] D. Seery and J. E. Lidsey, "Primordial non-gaussianities from multiple-field inflation," JCAP **0509**, 011 (2005) [arXiv:astro-ph/0506056].

[25] F. Vernizzi and D. Wands, "Non-Gaussianities in two-field inflation," JCAP **0605**, 019 (2006) [arXiv:astro-ph/0603799].

[26] L. E. Allen, S. Gupta and D. Wands, "Non-Gaussian perturbations from multi-field inflation," JCAP **0601**, 006 (2006) [arXiv:astro-ph/0509719].

[27] D. H. Lyth, K. A. Malik and M. Sasaki, "A general proof of the conservation of the curvature perturbation," JCAP **0505**, 004 (2005) [arXiv:astro-ph/0411220].

[28] D. H. Lyth and Y. Rodriguez, "The inflationary prediction for primordial non-gaussianity," Phys. Rev. Lett. **95**, 121302 (2005) [arXiv:astro-ph/0504045].

[29] D. H. Lyth and D. Wands, "Conserved cosmological perturbations," Phys. Rev. D **68**, 103515 (2003) [arXiv:astro-ph/0306498].

[30] G. I. Rigopoulos and E. P. S. Shellard, "The separate universe approach and the evolution of nonlinear superhorizon cosmological perturbations," Phys. Rev. D **68**, 123518 (2003) [arXiv:astro-ph/0306620].

[31] A. R. Liddle and D. H. Lyth, "Cosmological inflation and large-scale structure," *Cambridge, UK: Univ. Pr. (2000) 400 p*

[32] R. H. Brandenberger, "Challenges for inflationary cosmology," arXiv:astro-ph/0411671.

[33] F. C. Adams, K. Freese and A. H. Guth, "Constraints on the scalar field potential in inflationary models," Phys. Rev. D **43**, 965 (1991).

[34] J. Martin and R. H. Brandenberger, "The trans-Planckian problem of inflationary cosmology," Phys. Rev. D **63**, 123501 (2001) [arXiv:hep-th/0005209].

[35] R. H. Brandenberger and J. Martin, "The robustness of inflation to changes in super-Planck-scale physics," Mod. Phys. Lett. A **16**, 999 (2001) [arXiv:astro-ph/0005432].

[36] A. Borde and A. Vilenkin, "Eternal Inflation And The Initial Singularity," Phys. Rev. Lett. **72**, 3305 (1994) [arXiv:gr-qc/9312022].

[37] R. Allahverdi, K. Enqvist, J. Garcia-Bellido and A. Mazumdar, "Gauge invariant MSSM inflaton," Phys. Rev. Lett. **97**, 191304 (2006) [arXiv:hep-ph/0605035].

[38] R. Allahverdi, K. Enqvist, J. Garcia-Bellido, A. Jokinen and A. Mazumdar, "MSSM flat direction inflation: slow roll, stability, fine tunning and reheating," JCAP **0706**, 019 (2007) [arXiv:hep-ph/0610134].

[39] K. Enqvist, L. Mether and S. Nurmi, "Supergravity origin of the MSSM inflation," JCAP **0711**, 014 (2007) [arXiv:0706.2355 [hep-th]].

[40] S. Kachru, R. Kallosh, A. Linde and S. P. Trivedi, "De Sitter vacua in string theory," Phys. Rev. D **68**, 046005 (2003) [arXiv:hep-th/0301240].

[41] S. Kachru, R. Kallosh, A. Linde, J. M. Maldacena, L. P. McAllister and S. P. Trivedi, "Towards inflation in string theory," JCAP **0310**, 013 (2003) [arXiv:hep-th/0308055].

[42] S. Dimopoulos, S. Kachru, J. McGreevy and J. G. Wacker, "N-flation," arXiv:hep-th/0507205.

[43] K. Becker, M. Becker and A. Krause, "M-theory inflation from multi M5-brane dynamics," Nucl. Phys. B **715**, 349 (2005) [arXiv:hep-th/0501130].

[44] L. F. Abbott, E. Farhi and M. B. Wise, "Particle Production In The New Inflationary Cosmology," Phys. Lett. B **117**, 29 (1982).

[45] A. D. Dolgov and A. D. Linde, Sov. J. Nucl. Phys. **51**, 172 (1990)

[46] L. Kofman, A. D. Linde and A. A. Starobinsky, "Towards the theory of reheating after inflation," Phys. Rev. D **56**, 3258 (1997) [arXiv:hep-ph/9704452].

[47] J. H. Traschen and R. H. Brandenberger, "Particle production during out of equilibrium phase transitions," Phys. Rev. D **42**, 2491 (1990).

[48] A. D. Dolgov and D. P. Kirilova, "Production of particles by a variable scalar field," Sov. J. Nucl. Phys. **51**, 172 (1990) [Yad. Fiz. **51**, 273 (1990)].

[49] Y. Shtanov, J. H. Traschen and R. H. Brandenberger, "Universe reheating after inflation," Phys. Rev. D **51**, 5438 (1995) [arXiv:hep-ph/9407247].

[50] P. B. Greene, L. Kofman, A. D. Linde and A. A. Starobinsky, "Structure of resonance in preheating after inflation," Phys. Rev. D **56**, 6175 (1997) [arXiv:hep-ph/9705347].

[51] D. I. Podolsky, G. N. Felder, L. Kofman and M. Peloso, "Equation of state and beginning of thermalization after preheating," Phys. Rev. D **73**, 023501 (2006) [arXiv:hep-ph/0507096].

[52] N. W. MacLachlan, "Theory and Application of Mathieu Functions," (Dover, New York 1961).

[53] I. I. Gihman, A. V. Skorohod, "Theory of Stochastic Processes, I, II, III," (Springer-Verlag Berlin, Heidelberg New York, 1979).

[54] Joseph E. Avron, Barry Simon, "Almost Periodic Hill's equation and the Rings of Saturn," Phys. Rev. Lett **46**, 1166 (1981)

[55] Joseph. A. Avron, Barry. Simon, "Almost Periodic Schoredinger Spectrum," J. Functional Analysis **43**, 1-31 (1981).

[56] J Moser, "Integrable Hamiltonian Systems and Spectral Theory," Lezioni Fermiane, (1981)

[57] B. A. Bassett and F. Tamburini, "Inflationary reheating in grand unified theories," Phys. Rev. Lett. **81**, 2630 (1998). [arXiv:hep-ph/9804453].

[58] I. Zlatev, G. Huey and P. J. Steinhardt, "Parametric resonance in an expanding universe," Phys. Rev. D **57**, 2152 (1998) [arXiv:astro-ph/9709006].

[59] L. Kofman, A. Linde, X. Liu, A. Maloney, L. McAllister and E. Silverstein, "Beauty is attractive: Moduli trapping at enhanced symmetry points," JHEP **0405**, 030 (2004) [arXiv:hep-th/0403001].

[60] G. N. Felder, L. Kofman and A. D. Linde, "Instant preheating," Phys. Rev. D **59**, 123523 (1999) [arXiv:hep-ph/9812289].

[61] G. N. Felder, L. Kofman and A. D. Linde, "Inflation and preheating in NO models," Phys. Rev. D **60**, 103505 (1999) [arXiv:hep-ph/9903350].

[62] G. N. Felder, J. Garcia-Bellido, P. B. Greene, L. Kofman, A. D. Linde and I. Tkachev, "Dynamics of symmetry breaking and tachyonic preheating," Phys. Rev. Lett. **87**, 011601 (2001) [arXiv:hep-ph/0012142].

[63] G. N. Felder, L. Kofman and A. D. Linde, "Tachyonic instability and dynamics of spontaneous symmetry breaking," Phys. Rev. D **64**, 123517 (2001) [arXiv:hep-th/0106179].

[64] G. N. Felder, J. Garcia-Bellido, P. B. Greene, L. Kofman, A. D. Linde and I. Tkachev, Phys. Rev. Lett. **87**, 011601 (2001) [arXiv:hep-ph/0012142].

[65] L. Kofman, "Tachyonic preheating," arXiv:hep-ph/0107280.

[66] B. A. Bassett, "Inflationary reheating classes via spectral methods," Phys. Rev. D **58**, 021303 (1998) [arXiv:hep-ph/9709443].

[67] B. A. Bassett and S. Liberati, "Geometric reheating after inflation," Phys. Rev. D **58**, 021302 (1998) [Erratum-ibid. D **60**, 049902 (1999)] [arXiv:hep-ph/9709417].

[68] Juergen Baacke, Katrin Heitmann, and Carsten patzold, "Nonequilibrium dynamics of fermions in a spatially homogeneous scalar background field," Phys. Rev. D **58**, 125013 (1998).

[69] D. Wands, "Multiple field inflation," Lect. Notes Phys. **738**, 275 (2008) [arXiv:astro-ph/0702187].

[70] A. D. Linde, "Hybrid inflation," Phys. Rev. D **49**, 748 (1994) [arXiv:astro-ph/9307002].

[71] C. Gordon, D. Wands, B. A. Bassett and R. Maartens, "Adiabatic and entropy perturbations from inflation," Phys. Rev. D **63**, 023506 (2001) [arXiv:astro-ph/0009131].

[72] G. Rigopoulos, "On second order gauge invariant perturbations in multi-field inflationary models," Class. Quant. Grav. **21**, 1737 (2004) [arXiv:astro-ph/0212141].

[73] S. Groot Nibbelink and B. J. W. van Tent, "Scalar perturbations during multiple field slow-roll inflation," Class. Quant. Grav. **19**, 613 (2002) [arXiv:hep-ph/0107272].

[74] J. M. Maldacena, "Non-Gaussian features of primordial fluctuations in single field inflationary models," JHEP **0305**, 013 (2003) [arXiv:astro-ph/0210603].

[75] L. Alabidi and D. H. Lyth, "Inflation models and observation," JCAP **0605**, 016 (2006) [arXiv:astro-ph/0510441].

[76] C. T. Byrnes, M. Sasaki and D. Wands, "The primordial trispectrum from inflation," Phys. Rev. D **74**, 123519 (2006) [arXiv:astro-ph/0611075].

[77] D. Seery and J. E. Lidsey, "Non-gaussianity from the inflationary trispectrum," JCAP **0701**, 008 (2007) [arXiv:astro-ph/0611034].

[78] C. T. Byrnes, K. Koyama, M. Sasaki and D. Wands, "Diagrammatic approach to non-Gaussianity from inflation," JCAP **0711**, 027 (2007) [arXiv:0705.4096 [hep-th]].

[79] P. Creminelli, A. Nicolis, L. Senatore, M. Tegmark and M. Zaldarriaga, "Limits on non-Gaussianities from WMAP data," JCAP **0605**, 004 (2006) [arXiv:astro-ph/0509029].

[80] P. Creminelli, L. Senatore, M. Zaldarriaga and M. Tegmark, "Limits on f_NL parameters from WMAP 3yr data," arXiv:astro-ph/0610600.

[81] A. P. S. Yadav and B. D. Wandelt, "Detection of primordial non-Gaussianity (fNL) in the WMAP 3-year data at above 99.5 confidence," arXiv:0712.1148 [astro-ph].

[82] E. Jeong and G. F. Smoot, "Probing Non-Gaussianity In The Cosmic Microwave Background Anisotropies: One Point Distribution Function," arXiv:0710.2371 [astro-ph].

[83] E. Komatsu *et al.* [WMAP Collaboration], arXiv:0803.0547 [astro-ph].

[84] E. Komatsu and D. N. Spergel, "Acoustic signatures in the primary microwave background bispectrum," Phys. Rev. D **63**, 063002 (2001) [arXiv:astro-ph/0005036].

[85] C. Hikage, E. Komatsu and T. Matsubara, "Primordial Non-Gaussianity and Analytical Formula for Minkowski Functionals of the Cosmic Microwave Background and Large-scale Structure," Astrophys. J. **653**, 11 (2006) [arXiv:astro-ph/0607284].

[86] http://www.rssd.esa.int/index.php?project=Planck

[87] A. Cooray, "21-cm Background Anisotropies Can Discern Primordial Non-Gaussianity from Slow-Roll Inflation," arXiv:astro-ph/0610257.

[88] N. Kogo and E. Komatsu, "Angular Trispectrum of CMB Temperature Anisotropy from Primordial Non-Gaussianity with the Full Radiation Transfer Function," Phys. Rev. D **73**, 083007 (2006) [arXiv:astro-ph/0602099].

[89] A. R. Liddle, A. Mazumdar and F. E. Schunck, "Assisted inflation," Phys. Rev. D **58**, 061301 (1998) [arXiv:astro-ph/9804177].

[90] K. A. Malik and D. Wands, "Dynamics of assisted inflation," Phys. Rev. D **59**, 123501 (1999) [arXiv:astro-ph/9812204].

[91] P. Kanti and K. A. Olive, "On the realization of assisted inflation," Phys. Rev. D **60**, 043502 (1999) [arXiv:hep-ph/9903524].

[92] P. Kanti and K. A. Olive, "Assisted chaotic inflation in higher dimensional theories," Phys. Lett. B **464**, 192 (1999) [arXiv:hep-ph/9906331].

[93] R. Easther and L. McAllister, "Random matrices and the spectrum of N-flation," JCAP **0605**, 018 (2006) [arXiv:hep-th/0512102].

[94] A. Ashoorioon and A. Krause, "Power spectrum and signatures for cascade inflation," arXiv:hep-th/0607001.

[95] A. Krause, "Large Gravitational Waves and Lyth Bound in Multi Brane Inflation," arXiv:0708.4414 [hep-th].

[96] G. Calcagni and A. R. Liddle, "Stability of multi-field cosmological solutions," Phys. Rev. D **77**: 023522 (2008) arXiv:0711.3360 [astro-ph].

[97] S. A. Kim and A. R. Liddle, "Nflation: Multi-field inflationary dynamics and perturbations," Phys. Rev. D **74**, 023513 (2006) [arXiv:astro-ph/0605604].

[98] T. T. Nakamura and E. D. Stewart, "The spectrum of cosmological perturbations produced by a multi-component inflaton to second order in the slow-roll approximation," Phys. Lett. B **381**, 413 (1996) [arXiv:astro-ph/9604103].

[99] N. Kaloper and A. R. Liddle, "Dynamics and perturbations in assisted chaotic inflation," Phys. Rev. D **61**, 123513 (2000) [arXiv:hep-ph/9910499].

[100] F. Oravecz and D. Petz, "On the eigenvalue distribution of some symmetric random matrices", Acta. Sci. Math. Szeged. **63**, 383 (1997).

[101] J. O. Gong, "End of multi-field inflation and the perturbation spectrum," Phys. Rev. D **75**, 043502 (2007) [arXiv:hep-th/0611293].

[102] S. A. Kim and A. R. Liddle, "Nflation: observable predictions from the random matrix mass spectrum," Phys. Rev. D **76**, 063515 (2007) [arXiv:0707.1982 [astro-ph]].

[103] S. Yokoyama, T. Suyama and T. Tanaka, "Primordial Non-Gaussianity in Multi-Scalar Inflation," Phys. Rev. D **77**, 083511 (2008) arXiv:0711.2920 [astro-ph].

[104] R. Kallosh, N. Sivanandam and M. Soroush, "Axion Inflation and Gravity Waves in String Theory," Phys. Rev. D **77**:043501 (2008) arXiv:0710.3429 [hep-th].

[105] J. O. Gong, "Sustainability of multi-field inflation and bound on string scale," arXiv:0708.2045 [hep-th].

[106] D. Green, "Reheating Closed String Inflation," Phys. Rev. D **76**, 103504 (2007) [arXiv:0707.3832 [hep-th]].

[107] J. O. Gong, "Generation of perturbation after multi-field inflation," Phys. Lett. B **657**, 165 (2007) [arXiv:0706.3599 [astro-ph]].

[108] M. E. Olsson, "Inflation Assisted by Heterotic Axions," JCAP **0704**, 019 (2007) [arXiv:hep-th/0702109].

[109] M. M. Anber and L. Sorbo, "N-flationary magnetic fields," JCAP **0610**, 018 (2006) [arXiv:astro-ph/0606534].

[110] Y. S. Piao, "On perturbation spectra of N-flation," Phys. Rev. D **74**, 047302 (2006) [arXiv:gr-qc/0606034].

[111] S. A. Kim and A. R. Liddle, "Nflation: Non-gaussianity in the horizon-crossing approximation," Phys. Rev. D **74**, 063522 (2006) [arXiv:astro-ph/0608186].

[112] L. Pastur and A. Figotin, "Spectra of Random and Almost-Periodic Operators" (Springer-Verlag, 1992).

[113] Barry Simon, Advances. Appl. Math., **3**, 463 (1982)

[114] V. Zanchin, A. . J. Maia, W. Craig and R. H. Brandenberger, "Reheating in the presence of inhomogeneous noise," Phys. Rev. D **60**, 023505 (1999) [arXiv:hep-ph/9901207].

[115] V. Zanchin, A. . J. Maia, W. Craig and R. H. Brandenberger, "Reheating in the presence of noise," Phys. Rev. D **57**, 4651 (1998) [arXiv:hep-ph/9709273].

[116] M. Ishihara, "Effects of white noise on parametric resonance in lambda phi**4 theory," Prog. Theor. Phys. **114**, 157 (2005) [arXiv:hep-th/0410130].

[117] Vilenkin, A. & Shellard, E.P.S. 2000, Cosmic Strings and Other Topological Defects (Cambridge:CUP)

[118] M. Wyman, L. Pogosian and I. Wasserman, "Bounds on cosmic strings from WMAP and SDSS," Phys. Rev. D **72**, 023513 (2005) [Erratum-ibid. D **73**, 089905 (2006)] [arXiv:astro-ph/0503364].

[119] U. Seljak, A. Slosar and P. McDonald, "Cosmological parameters from combining the Lyman-alpha forest with CMB, galaxy clustering and SN constraints," JCAP **0610**, 014 (2006) [arXiv:astro-ph/0604335].

[120] J. Polchinski, "Introduction to cosmic F- and D-strings," arXiv:hep-th/0412244.

[121] A. Vilenkin, "Cosmic strings: progress and problems," arXiv:hep-th/0508135.

[122] T. W. B. Kibble, "Topology Of Cosmic Domains And Strings," J. Phys. A **9**, 1387 (1976).

[123] J. Polchinski and J. V. Rocha, "Cosmic string structure at the gravitational radiation scale," arXiv:gr-qc/0702055.

[124] K. D. Olum and V. Vanchurin, "Cosmic string loops in the expanding universe," Phys. Rev. D **75**, 063521 (2007) [arXiv:astro-ph/0610419].

[125] S. Sarangi and S. H. H. Tye, "Cosmic string production towards the end of brane inflation," Phys. Lett. B **536**, 185 (2002) [arXiv:hep-th/0204074].

[126] K. Becker, M. Becker and A. Krause, "Heterotic cosmic strings," Phys. Rev. D **74**, 045023 (2006) [arXiv:hep-th/0510066].

[127] E. Witten, "Cosmic Superstrings," Phys. Lett. B **153**, 243 (1985).

[128] Caldwell "Cosmological constraints on cosmic-string gravitational radiation", R.R. & Allen, B. 1992, PhysRevD, 45, 3447

[129] M. B. Hindmarsh and T. W. B. Kibble, "Cosmic strings," Rept. Prog. Phys. **58**, 477 (1995) [arXiv:hep-ph/9411342].

[130] B. Allen and P. Casper, "A Closed form expression for the gravitational radiation rate from cosmic strings," Phys. Rev. D **50**, 2496 (1994) [arXiv:gr-qc/9405005].

[131] P. Casper and B. Allen, "Gravitational radiation from realistic cosmic string loops," Phys. Rev. D **52**, 4337 (1995) [arXiv:gr-qc/9505018].

[132] C. J. A. P. Martins and E. P. S. Shellard, "Quantitative String Evolution", Phys. Rev. **D54** 2535 (1996), hep-ph/9602271;
"String Evolution with Friction", Phys. Rev. **D53** R575 (1996), hep-ph/9507335;
"Extending the Velocity-dependent One-scale String Evolution Model", Phys. Rev. **D65** 043514 (2002), hep-ph/0003298.

[133] S. H. Tye, I. Wasserman and M. Wyman, "Scaling of multi-tension cosmic superstring networks," Phys. Rev. D **71**, 103508 (2005) [Erratum-ibid. D **71**, 129906 (2005)] [arXiv:astro-ph/0503506].

[134] T. Vachaspati and A. Vilenkin, "Large scale structure from wiggly cosmic strings," Phys. Rev. Lett. **67**, 1057 (1991).

[135] T. Vachaspati, "The Structure of wiggly cosmic string wakes," Phys. Rev. D **45**, 3487 (1992).

[136] K. Dimopoulos, "Primordial magnetic fields from superconducting cosmic strings," Phys. Rev. D **57**, 4629 (1998) [arXiv:hep-ph/9706513].

[137] A. C. Davis and K. Dimopoulos, "Cosmic superstrings and primordial magnetogenesis," Phys. Rev. D **72**, 043517 (2005) [arXiv:hep-ph/0505242].

[138] D. N. Vollick, "Small scale structure on cosmic strings and galaxy formation," Phys. Rev. D **45**, 1884 (1992).

[139] M. Giovannini, "Magnetic fields, strings and cosmology," arXiv:astro-ph/0612378.

[140] D. Grasso and H. R. Rubinstein, "Magnetic fields in the early universe," Phys. Rept. **348**, 163 (2001) [arXiv:astro-ph/0009061].

[141] L. M. Widrow, "Origin of Galactic and Extragalactic Magnetic Fields," Rev. Mod. Phys. **74**, 775 (2003) [arXiv:astro-ph/0207240].

[142] C. L. Carilli and G. B. Taylor, "Cluster Magnetic Fields," Ann. Rev. Astron. Astrophys. **40**, 319 (2002) [arXiv:astro-ph/0110655].

[143] P. J. Peebles, Astrophys. J. 147 (1967) 859.

[144] M.J. Rees and M. Rheinhardt, Astr. Ap. 19, (1972) 189.

[145] I. Wasserman, Astrophys. J. 224 (337) 1978.

[146] T. Kobayashi, R. Maartens, T. Shiromizu and K. Takahashi, "Cosmological magnetic fields from nonlinear effects," Phys. Rev. D **75**, 103501 (2007) [arXiv:astro-ph/0701596].

[147] V. B. Semikoz and D. D. Sokoloff, "Large-scale cosmological magnetic fields and magnetic helicity," Int. J. Mod. Phys. D **14**, 1839 (2005).

[148] A. Brandenburg, K. Enqvist and P. Olesen, "Large-scale magnetic fields from hydromagnetic turbulence in the very early universe," Phys. Rev. D **54**, 1291 (1996) [arXiv:astro-ph/9602031].

[149] E. R. Harrison, "Generation of Magnetic Fields in the Radiation Era," Mon. Not. astr. Soc **147**, 279 (1970).

[150] Martin J. Rees, "The Origin and Cosmogonic Implications of Seed Magnetic Fields," Q. Jl R. astr. Soc **28**, 197 (1987).

[151] P. P. Avelino and E. P. S. Shellard, "Dynamical Friction On Cosmic String Motion And Magnetic Field Generation," Phys. Rev. D **51**, 5946 (1995).

[152] H. Lesch and M. Chiba, "Protogalactic evolution and magnetic fields," arXiv:astro-ph/9411072.

[153] R. M. Kulsrud, R. Cen, J. P. Ostriker and D. Ryu, "The Protogalactic Origin for Cosmic Magnetic Fields," Astrophys. J. **480**, 481 (1997) [arXiv:astro-ph/9607141].

[154] M. S. Turner and L. M. Widrow, "Inflation Produced, Large Scale Magnetic Fields," Phys. Rev. D **37**, 2743 (1988).

[155] A. C. Davis, M. Lilley and O. Tornkvist, "Relaxing the Bounds on Primordial Magnetic Seed Fields," Phys. Rev. D **60**, 021301 (1999) [arXiv:astro-ph/9904022].

[156] I. McIvor "The inertial range of weak magnetohydrodynamic turbulence in the interstellar medium," MNRAS **178**, 85 (1977).

[157] J. C. Higdon Ap. J. **285**, 109 (1984).

[158] E. N, Parker, "Cosmological Magnetic fields," Clarendon, Oxford (1979).

[159] Ya.B. Zeldovich, A.A. Ruzmaikin and D.D. Sokolov, *Magnetic Fields in Astrophysics* (Gordon and Breach, New York, 1983).

[160] H. K, Moffatt, "Magnetic Field Generation in Electrically Conducting fluids," Cambridge University Press, Cambridge, England (1978).

[161] A.A. Ruzmaikin, D.D. Sokolov and V.I. Turchaninov, Astron. Zh. **57**, 311 (1980) [Sov. Astron. **24**, 182 (1980)].

[162] K. Ferriere and D. Schmitt, "Numerical models of the galactic dynamo driven by supernovae and superbubbles," Astronomy and Astrophysics, **358**, p.125-143 (2000).

[163] [Planck Collaboration], "Planck: The scientific programme," arXiv:astro-ph/0604069; http://www.rssd.esa.int/index.php?project=Planck

[164] X. Chen, M. x. Huang, S. Kachru and G. Shiu, "Observational signatures and non-Gaussianities of general single field inflation," JCAP **0701**, 002 (2007) [arXiv:hep-th/0605045].

[165] M. Majumdar and A. C. Davis, Phys. Rev. D **69**, 103504 (2004) [arXiv:hep-th/0304226].

[166] T. Vachaspati and A. Vilenkin, "Gravitational Radiation From Cosmic Strings," Phys. Rev. D **31**, 3052 (1985).

[167] S. Chandrasekhar, "Dynamical Friction. I. General Considerations: The Coefficient Of Dynamical Friction," Astrophys. J. **97**, 255 (1943).

[168] J. Silk and A. Vilenkin, "Cosmic Strings And Galaxy Formation," Phys. Rev. Lett. **53**, 1700 (1984).

[169] J. Polchinski, "Cosmic String Loops and Gravitational Radiation," arXiv:0707.0888 [astro-ph].

[170] R. Durrer, "Gravitational Angular Momentum Radiation of Cosmic Strings," Nucl. Phys. B **328**, 238 (1989).

[171] E. J. Copeland and N. Turok, Phys. Lett. **B173** (1986) 129.

[172] D. N. Vollick, "Cosmic String Shocks, Magnetic Fields, And Microwave Anisotropies," Phys. Rev. D **48**, 3585 (1993).

[173] T. Vachaspati, "Cosmic Strings and the Large-Scale Structure of the Universe," Phys. Rev. Lett. **57**, 1655 - 1657 (1986).

[174] A. Stebbins, S. Veeraraghavan, R. H. Brandenberger, J. Silk and N. Turok, "Cosmic String Wakes," Astrophys. J. **322**, 1 (1987).

[175] L. Pogosian and A. Vilenkin, "Early reionization by cosmic strings revisited," Phys. Rev. D **70**, 063523 (2004) [arXiv:astro-ph/0405606].

[176] T. Hara, P. Mahonen, and S. Miyoshi, Ap. J. **412**, 22 (1993).

[177] P. P. Avelino and E. P. S. Shellard, Phys. Rev. D **51**, 369 (1995).

[178] A. Avgoustidis and E. P. S. Shellard, "Effect of reconnection probability on cosmic (super)string network density," Phys. Rev. D **73**, 041301 (2006) [arXiv:astro-ph/0512582].

[179] J. Polchinski and J. V. Rocha, "Analytic study of small scale structure on cosmic strings," Phys. Rev. D **74**, 083504 (2006) [arXiv:hep-ph/0606205].

[180] F. Dubath and J. V. Rocha, "Periodic gravitational waves from small cosmic string loops," Phys. Rev. D **76**, 024001 (2007) [arXiv:gr-qc/0703109].

[181] V. Vanchurin, K. D. Olum and A. Vilenkin, "Scaling of cosmic string loops," Phys. Rev. D **74**, 063527 (2006) [arXiv:gr-qc/0511159].

[182] C. J. A. Martins and E. P. S. Shellard, "Fractal properties and small-scale structure of cosmic string networks," Phys. Rev. D **73**, 043515 (2006) [arXiv:astro-ph/0511792].

[183] C. Ringeval, M. Sakellariadou, and F. Bouchet, JCAP **0702**, 023 (2007), astro-ph/0511646.

[184] N. Bevis, M. Hindmarsh, M. Kunz and J. Urrestilla, "Fitting CMB data with cosmic strings and inflation," arXiv:astro-ph/0702223.

[185] X. Siemens, V. Mandic and J. Creighton, "Gravitational wave stochastic background from cosmic (super)strings," Phys. Rev. Lett. **98**, 111101 (2007) [arXiv:astro-ph/0610920].

[186] D. Bennett and F. Bouchet, Phys. Rev. Lett. **60** 257 (1988); Astrophys. J. **354** L41 (1990); in *The Formation and Evolution of Cosmic Strings*, proceedings of the Symposium, Cambridge, England 1989, edited by G. W. Gibbons, S. W. Hawking, and T. Vachaspati (Cambridge University Press, Cambridge England 1989); Phys. Rev. D **41** 2408 (1990)

[187] C. J. Hogan and M. J. Rees, "Gravitational Interactions Of Cosmic Strings," Nature **311** (1984) 109.

[188] A. A. Ruzmaikin, D. D. Sokolov, and V. I. Turchaninov, "The turbulent dynamo in a disk," Astron. Zh. **57**, 311 (1980).

[189] W. Kirsch, "Lyapunov Exponents," Proc., Eds. L. Arnold and V. Wilhstutz (Springer-Verlag, Berlin 1986).

[190] J. H. Traschen and R. H. Brandenberger, Phys. Rev. D **42**, 2491 (1990)

[191] Y. Shtanov, J. H. Traschen and R. H. Brandenberger, Phys. Rev. D **51**, 5438 (1995)

[192] S. Y. Khelbnikov and I. I. Tkachev, Phys. Rev. Lett. **77**, 219 (1996)

[193] S. Y. Khelbnikov and I. I. Tkachev, Phys. Lett. B **390**, 80 (1997)

[194] S. Y. Khelbnikov and I. I. Tkachev, Phys. Rev. Lett. **79**, 80 (1997)

[195] T. Prokopec and T. G. Roos, Phys. Rev. D **55**, 3768 (1997)

[196] Joseph E. Avron, Barry Simon, "Almost Periodic Schroedinger Operators," Commun. Math. Phys **82**, 101-120 (1981)

[197] Joseph E. Avron, Barry Simon, "Transient and Recurrent Spectrum," J. functional Analysis **43**, 1-31 (1981)

[198] E. J. Copeland, A. Mazumdar and N. J. Nunes, "Generalized assisted inflation," Phys. Rev. D **60**, 083506 (1999) [arXiv:astro-ph/9904309].

[199] H. Singh, "The N-tachyon assisted inflation," Mod.Phys.Lett.A22:2737-2748, (2007) arXiv:hep-th/0608032.

[200] G. I. Rigopoulos, E. P. S. Shellard and B. W. van Tent, "Quantitative bispectra from multifield inflation," Phys.Rev.D76:083512, (2007) arXiv:astro-ph/0511041.

[201] W. Kirsch,in "Lyapunov Exponents" Proc., Eds. L. Arnold and V. Wilhstutz, (Springer-Verlag, Berlin, 1986).